

Conductive Resists for Nanofabrication on Insulating Substrates

by

Farhan Hasan

**A thesis submitted to the University of
Birmingham for the degree of
DOCTOR OF PHILOSOPHY**

**School of Chemical Engineering
College of Engineering and Physical Sciences
University of Birmingham
March 2017**

UNIVERSITY OF
BIRMINGHAM

University of Birmingham Research Archive

e-theses repository

This unpublished thesis/dissertation is copyright of the author and/or third parties. The intellectual property rights of the author or third parties in respect of this work are as defined by The Copyright Designs and Patents Act 1988 or as modified by any successor legislation.

Any use made of information contained in this thesis/dissertation must be in accordance with that legislation and must be properly acknowledged. Further distribution or reproduction in any format is prohibited without the permission of the copyright holder.

Abstract

The purpose of this work is to support the demand for ongoing miniaturization of microelectronic devices, in particular focusing on low-volume high-value market sectors (such as III-V semiconductor devices), which present a unique combination of economic and technical challenges. As miniaturization proceeds towards the nano scale, photolithography (the industrial micro-patterning technique of choice) has been able to meet the required lithographic feature sizes through the use of increasingly complex optical engineering techniques, which has allowed 20 nm optical patterning. However, this requires very expensive device-specific optical mask-sets, which are not economically viable for the low-volume fabrication seen in the III-V arena. The most promising technique in this latter case is electron beam lithography (EBL), which allows patterning of arbitrary patterns with sub-20 nm resolution. Unfortunately whilst EBL is a widely used lithography technology on poorly conductive (and insulating) substrates, such as found in III-V devices, charging of the substrate by the electron beam leads to pattern distortion and resolution is limited to feature size above 100 nm. A number of charge mitigation strategies exist, such as the use of thin metal layers on the substrate, but these typically introduce their own problems such as process complexity, substrate poisoning, and resolution limits.

A new approach to address the problem has therefore been investigated. Presented in this work is a new triphenylene derivative based electron beam resist that has conductive characteristics, which allow the resist film to simultaneously act as the dissipation layer. Triphenylene derivatives form well-ordered hexagonal columnar discotic liquid crystals that show fast hole mobility (e.g. $10^{-3} \text{ cm}^2 \text{V}^{-1} \text{s}^{-1}$) along columns. The triphenylene derivative based chemically amplified resist investigated

here has demonstrated conductivity around 10^{-6} S/m at room temperature, when spin coated on a glass substrate. Besides its conductivity characteristics, it also has demonstrated a high sensitivity to electron beam exposure, requiring a patterning dose of $\sim 14 \mu\text{C}/\text{cm}^2$ on silicon and $\sim 10 \mu\text{C}/\text{cm}^2$ on fused silica substrates at 50 keV exposure. The resist has also demonstrated high-resolution patterning including 20 nm half pitch lines on silicon, and 55 nm width lines on a 200 nm pitch on glass at 30 keV exposure.

Acknowledgements

I would like express my gratitude to my supervisors Dr. A. P. G. Robinson and Prof. J. A. Preece who guided me throughout the project. I would like to thank Greg O'Callaghan for his knowledge and support on triphenylene chemistry and synthesis.

I am also grateful to Dr. A. Frommhold and Dr. D. Yang for their support and training in the Cleanroom at the Nanoscale Physics Research Laboratory; and Dr. E. Tarte for conductivity measurement support at Electrical and Electronic Engineering School in University of Birmingham.

I am especially thankful to our collaborators Dr. Mark Rosamond at University of Leeds, Dr. Wilkinson's group at University of Cambridge, and to Mr. Bengt Nilsson, Dr. Göran Alestig and Dr. Ulf Södrvall in the MC2 laboratory in Chalmers University of Technology for their support and vast knowledge in electron beam lithography and conductivity measurements.

I am also thankful to Engineering and Physical Sciences Research Council (EPSRC) for financial support of my research.

And finally, I am very much thankful to my parents for their encouragement and love throughout of my studies.

Contents

Abstract	i
Acknowledgements	iii
Chapter 1	
Introduction	1
1.1 History of lithography	1
1.1.1 Micro-nano electronics and lithography	2
1.1.2 Aim of this project	4
1.2 Lithography	5
1.3 Photo Lithography	6
1.3.1 Contact Lithography	10
1.3.2 Proximity Lithography	12
1.3.3 Projection Lithography	12
1.3.4 Advanced Photolithography	14
1.3.4.1 Immersion Lithography	14
1.3.4.2 Double patterning lithography	15
1.3.5 Other techniques	18
1.3.5.1 Extreme ultraviolet lithography	18
1.3.5.2 Nanoimprint lithography	19
1.4 Electron beam lithography	21
1.4.1 How an ebeam tool works	23
1.4.2 Next generation EBL tool	25
1.4.2.1 MAPPER	25
1.4.2.2 Projection Maskless Lithography	26
1.4.2.3 Reflective electron beam tool	27
1.4.3 Scattering effects in ebeam lithography	29

1.5 Photoresist	33
1.5.1 Resist Characteristics	34
1.5.1.2 Sensitivity and Contrast.....	34
1.5.1.2 Resolution	36
1.5.1.3 Line-Edge and Line-Width Roughness	37
1.5.1.4 Etch resistance	38
1.5.2 Resist mechanism.....	40
1.5.2.1 Non-chemically amplified resist.....	40
1.5.2.2 Chemically Amplified Resists	41
1.5.3 Electron beam resists	44
1.5.3.1 Positive electron beam resists.....	45
1.5.3.2 Negative electron beam resists	47
1.6 Charge dissipation in ebeam lithography	48
1.7 Why Triphenylene derivatives	53
Chapter 2	
Experimental Techniques	56
2.1 Thin film processing.....	56
2.2 Measuring Conductivity	60
2.2.1 Two and Four Point probe techniques	61
2.2.2 Van der Pauw Technique	64
2.3 Equipment.....	67
2.3.1 Scanning Electron Microscope	67
2.3.1.1 Electron Beam Lithography.....	69
2.3.1.2 Pattern Design.....	70
2.3.1.3 Steps before the Exposure	71
2.3.1.4 Exposure	71
2.3.2 Etcher	71

2.3.3	Sputter Coater	73
2.3.4	Plasma Asher.....	75
2.3.5	Surface Profiler	76
2.3.6	Keithley source measure unit.....	77
2.4	Conductivity Approaches	80
2.5	Measurement error handling.....	85
Chapter 3		
Conductivity tests		87
3.1	Sample preparation	87
3.2	C5C5 - thickness vs. conductivity.....	88
3.3	Conductivity tokens	93
3.5	PMMA, C5C5 and doped C5C5	95
3.6	PMMA.....	97
3.7	CAR – Conductivity vs. Temperature.....	98
3.8	C5C5, C5OH and C5EPX.....	100
3.9	CAR in toluene.....	103
3.10	CAR (in toluene) – age test.....	106
3.11	Conductivity tests in Cambridge.....	107
3.12	Conductivity tests at Chalmers University.....	108
Chapter 4		
Lithography tests		111
4.1	Resist preparation	111
4.2	Substrate cleaning.....	112
4.3	Film processing	113
4.4	Lithographic Performance: Sensitivity and Contrast	114
4.4.1	Pure C5C5	115
4.4.2	Chemically amplified resist	116

4.4.2.1	CAR in PGMEA.....	116
4.4.2.2	CAR in chloroform.....	117
4.4.2.3	Optimizing film formation.....	119
4.4.2.4	CAR on glass	121
4.5	Resolution.....	124
4.5.1	Pure C5C5	124
4.5.2	CAR.....	126
4.5.2.1	CAR in chloroform on silicon	126
4.5.2.2	CAR in chloroform on glass.....	128
4.5.2.3	Comparing PMMA on glass.....	131
4.6	Lithography at Chalmers	132
4.6.1	Sensitivity of pure C5C5.....	133
4.6.2	Sensitivity of CAR.....	134
4.6.3	High resolution Patterning of CAR at 100 keV	137
4.7	Lithography in Leeds.....	140
4.8	Conclusion.....	140
Chapter 5		
Conclusions and Future work		
5.1	Conclusions	141
5.2	Future Work.....	144
References		
		148

List of Figures

1.1	ITRS resist road map 2013.....	4
1.2	Triphenylene with epoxide and C5OH.....	5
1.3	Photolithography process.....	6
1.4	Lithography steps.....	9
1.5	Schematic diagram of contact, proximity and projection lithography.....	10
1.6	Schematic diagram of contact lithography.....	11
1.7	Schematic diagram of proximity lithography.....	12
1.8	Schematic diagram of projection lithography.....	13
1.9	Schematic diagram of the immersion systems.....	15
1.10	Schematic diagram of LELE process.....	16
1.11	Schematic diagram of SADP process.....	17
1.12	Schematic diagram of EUVL optics.....	19
1.13	Schematic diagram of nanoimprint lithography.....	20
1.14	Scanning Electron Microscope (SEM) lithography.....	22
1.15	A typical EBL system.....	24
1.16	Schematic diagram of MAPPER system.....	25
1.17	Schematic diagram of PML2 system.....	27
1.18	Schematic diagram of REBL.....	28
1.19	Schematic diagram of forward and backward scattering.....	30
1.20	Electron scattering angle with atom and nucleus.....	31
1.21	Schematic diagram of electron–solid interactions.....	32
1.22	Scattering effects at lower to higher energy.....	33
1.23	Response curve of positive and negative tone resist.....	34
1.24	Resolution by pitch and the linewidth.....	36
1.25	Random fluctuations on a pattern’s edge.....	37
1.26	Si etching.....	39
1.27	Chemical Amplification.....	42
1.28	De-protection reaction.....	43
1.29	Acid generation and epoxy crosslinking.....	44
1.30	Surface charging deflects the incoming ebeam.....	49
1.31	Example of pattern displacement.....	50
1.32	Pattern distortion due to substrate charging.....	50

1.33	Image charging at 5 keV.....	51
1.34	Conductivity vs. temperature for a pure and doped Triphenylene.....	53
1.35	Triphenylenes' discharge mechanism.....	54
1.36	Pure triphenylene and Triphenylene with functional groups.....	55
2.1	Film formation stages by spin coater.....	58
2.2	Conductivity scale for various materials at room temperature.....	60
2.3	Two point and Four point probe test setup.....	61
2.4	Schematic of two and four-point probe configuration.....	62
2.5	Sample geometries for Van der Pauw resistivity measurement.....	65
2.6	The VdP characteristic resistances.....	66
2.7	The SEM used in this study	68
2.8	Oxford Instruments PlasmaPro 80 ICP.....	72
2.9	Edwards FL400 sputter coater.....	73
2.10	Schematic diagram of Sputtering Chamber.....	74
2.11	Deposition process by atom bombardment.....	75
2.12	TePla 100-E.....	75
2.13	Dektak ³ ST Surface Profiler.....	76
2.14	Schematic of working mechanism of Dektak ³ ST.....	77
2.15	Keithley 236 SMU.....	77
2.16	Diagram of supplying and measuring I-V.....	78
2.17	Linear Stair program LS v8.3.....	80
2.18	I-V Box and chip holder.....	81
2.19	Schematic of I-Vbox and the connection	81
2.20	Four point probe station with Copper probes.....	82
2.21	Copper probes with silver paint on a glass substrate.....	82
2.22	Four point probe station with Tungsten probes.....	83
2.23	Tungsten probes without silver paint.....	83
2.24	Four probe token.....	84
2.25	Tow probe token.....	84
2.26	A two-probe token is mounted on a heater with silver paint.....	85
2.27	Heater inside Faraday cage and a thermocouple setup.....	85
3.1	Thickness vs. Conductivity C5C5.....	89
3.2	Speculated molecular layers of Triphenylene depend on thickness.....	90
3.3	C5C5 on silicon under a polarizing microscope.....	91

3.4	Slow measurement loop.....	92
3.5	Fast measurement loop.....	92
3.6	Around 110nm gold on glass substrates	93
3.7	Conductivity tokens for two-probe and four-probe measurements.....	94
3.8	Hysteresis test on the 2-probe system, applying current.....	94
3.9	Hysteresis test on the 2-probe system, applying voltage.....	95
3.10	Experimental setup with copper probes with silver paint.....	96
3.11	Current supplied on baked and not baked PMMA.....	98
3.12	Sample on a heater, placed inside a Faraday cage.....	99
3.13	Temperature vs. Conductivity (S/m) of CA resists.....	99
3.14	Comparing heater and thermocouple's reading.....	100
3.15	Thermocouple in contact with the gold-pad.....	100
3.16	Temperature vs. Conductivity tests of glass.....	101
3.17	Temperature vs. conductivity tests of gold pads.....	101
3.18	Temperature vs. Conductivity tests of C5OH.....	102
3.19	CAR in Toluene on two-probe token.....	103
3.20	I-V curve of CA, at 0 – 0.1V at 18 – 105 °C.....	103
3.21	I-V curve of CA at 0 – 10V and 0 – 100V at 105 °C.....	104
3.22	I-V curve of CAR at 0-10 V at 18 °C.....	105
3.23	I-V curve of CAR at 0-100V at 18 °C.....	105
3.24	I-V curve of CAR at -100V to +100V at 20 °C.....	106
3.25	I-V measurement tools in Cambridge.....	107
3.26	I-V measurement tools in Chalmers.....	108
4.1	Sensitivity of pure C5C5.....	115
4.2	Sensitivity of (-) tone CAR.....	116
4.3	Film condition after spin coating.....	117
4.4	Uneven top surface of a exposed pattern.....	118
4.5	Sensitivity of CAR in different baking conditions.....	118
4.6	Samples after spin coating and after developing.....	119
4.7	Sensitivity of CAR in different developers.....	120
4.8	Au on glass - for focusing under SEM.....	121
4.9	After sputtering ~4 nm gold on top (1 st sample).....	122
4.10	After sputtering ~4 nm gold on top (2 nd sample).....	122
4.11	Before gold sputtered on top.....	123

4.12	After gold sputtered on top.....	124
4.13	14.1 nm pattern in a 28 nm C5C5 film at 32nC/cm dose.....	125
4.14	20 nm half pitch lines in a 28 nm C5C5 film at 62 nC/cm dose.....	125
4.15	100 nm half pitch lines in a 28 nm CA film at 0.24 nC/cm dose.....	126
4.16	80 nm half pitch lines in a 28 nm CA film at 0.34 nC/cm dose.....	127
4.17	60 nm half pitch lines in a 28 nm CA film at 0.34 nC/cm dose.....	127
4.18	50 nm half pitch lines in a 28 nm CA film at 0.34 nC/cm dose.....	127
4.19	At 20 $\mu\text{C}/\text{cm}^2$ dose, 76 nm features on a pitch of 200 nm on glass.....	128
4.20	At 50 $\mu\text{C}/\text{cm}^2$ dose, 55 nm features on a pitch of 150 nm on glass.....	129
4.21	Area dose 116 $\mu\text{C}/\text{cm}^2$ and line dose 1.16 nC/cm on glass.....	130
4.22	200 nm half pitch and 200 nm line at 360 $\mu\text{C}/\text{cm}^2$ on glass.....	130
4.23	PMMA at dose 345 $\mu\text{C}/\text{cm}^2$ and pitch 200on glass.....	131
4.24	Sensitivity of pure C5C5 on Si, at 50 keV with 10 nA.....	134
4.25	Sensitivity of CAR on Si, at 100 keV with 10 nA on 130 nm film.....	134
4.26	Sensitivity of CAR on Si, at 100 keV with 10 nA on 90 nm film.....	135
4.27	Sensitivity of CAR on Si, at 100 keV and 50 keV on 70 nm film.....	136
4.28	Sensitivity of CAR on Si, QZ, BS, FS and AFG at 50 keV.....	136
4.29	250 nm line/space patterns on CAR,100 keV at 120 $\mu\text{C}/\text{cm}^2$ dose.....	137
4.30	500 nm line/space patterns on CAR, 100 keV at 120 $\mu\text{C}/\text{cm}^2$ dose.....	138
4.31	250 nm line/space patterns on CAR, 100 keV at 39 $\mu\text{C}/\text{cm}^2$ dose.....	138
4.32	500 nm line/space patterns on CAR, 100 keV at 39 $\mu\text{C}/\text{cm}^2$ dose.....	139
4.33	2 um line/space patterns on CAR, 50 keV at 52 $\mu\text{C}/\text{cm}^2$ dose.....	139
4.34	Discharge during exposure at 100 keV with 2nA on glass.....	139
4.35	C5C5 on QZ after 50kV exposure and development.....	139
4.36	Pattern exposed at 100keV in Pure C5EPX film.....	140
5.1	Proposed four-probe station with heating stage.....	144
5.2	Schematic of new four-probe token.....	145
5.3	Mask 1, for creating gold pads.....	146
5.4	Mask 2, for creating opening widows.....	147

List of Tables

3.1	C5C5 conductivity measurements as a function of film thickness.....	89
3.2	VdP measurements of PMMA, C5C5 and Doped C5C5.....	96
3.3	Conductivity of PMMA.....	97
3.4	Conductivity of CAR (in toluene) at 18 °C.....	104
3.5	Conductivity of CAR (in toluene) at 20 °C.....	106
3.6	Conductivity of C5C5 and CAR at MC2, Chalmers.....	109
4.1	Sensitivity and Contrast at 50 keV Si, QZ, BS, FS and AFG.....	137

Chapter 1

Introduction

1.1 History of lithography

In 1796 a German author named Alois Senefelder wanted to publish his theatrical works [1, 2] in a cheaper way, which led him to devise a method called Lithography. This word is derived from two Greek words *Litho* that means stone and *Graphein* that means to write.[3] Thus Lithography means to write something on stone.

Alois Senefelder's lithography process was a purely chemical process that was able to create any image on any suitable material – paper, stone or metal. These materials are known as the substrate and the chemicals used to pattern the substrate were as ink with oil mixture.[3]

Thirty years after Senefelder developed his lithography process, Joseph Niepce of France developed a new photolithography method in 1826. This photolithography method involved shining ultraviolet (UV) light through a pre-designed mask (a chrome coated quartz glass with a pattern engraved into the chrome) to expose a light-sensitive resist underneath the chrome-mask. The resist that he used was mixture of lavender oil with mineral spirits and he used it to produce one of the first photographs.

Although it was possible to produce photographs using this oil based resist, the image quality wasn't good and it had problem of etch stability. To address this Louis Minsk of Eastman Kodak developed the first synthetic photopolymer, poly(vinyl cinnamate), a negative resist, in 1935. Following the success of the poly(vinyl cinnamate) negative resist Otto Suessof Kalle Div. of Hoechst AG developed a new diazoquinone based positive resist in 1940.

As technology has advanced and photolithography demands have increased, it has been necessary to continuously improve the materials used for the process. This chapter will review the recent and current requirements state-of-the-art.

1.1.1 Micro-nano electronics and lithography

The ongoing focus for microelectronic devices is towards ever greater miniaturization. By using nanofabrication techniques packaging density is continuously increasing. Nanofabrication techniques are essential for making devices in electronics and bio applications.[4] In many cases quantum effects are being studied in the sub-100 nm region.[5, 6] Quantum dot lasers,[7] quantum light emitting diodes,[8] and single electron transistors [9, 10] are some notable applications.

For the last decade gallium nitride (GaN) has been of increasing interest for microwave and power electronics [11, 12] and other high value areas (such as – aerospace, defense and communications) due to its wide band gap and heat tolerance ability. Other materials such as zinc oxide (ZnO) are also under investigation for radiation resistant electronics for extreme environments and also ultra-bright LEDs.

ZnO also has lower toxicity and lower material cost than indium tin oxide (ITO) and is being considered for use in solar cells and OLED displays.[13] In the area of non-linear optics and acousto-optical devices [14] lithium niobate (LiNbO_3) is of interest, and for making high power, frequency and temperature tolerant electronics [15] diamond is being investigated.

From the beginning of 1990s the first blue LEDs were produced with GaN.[16] Since then this material has found wide application and its market was estimated around to be \$4.6billion in 2008.[17] This material is in use by many semiconductor industries from high efficiency to ultra-high frequency electronics, and for power handling applications.

Microelectronic devices are formed by the process of lithography, wherein photoresist, also known as resist, is patterned by exposure to light, or to electrons. The resist film is then used to mask the substrate for subsequent fabrication steps. The resist material therefore forms an important part of the lithography.

The figure 1.1 show the past and future resist roadmap based on current and future resist resolution requirements. Resist sensitivity is also an important parameter. According to the International Technology Roadmap for Semiconductors (ITRS) resist sensitivity set to for the high voltage ebeam lithography should be $5\text{--}10 \mu\text{C}/\text{cm}^2$ and for low voltage ebeam Lithography $0.2\text{--}1.0 \mu\text{C}/\text{cm}^2$.

Additionally, as the feature sizes have become smaller with time, line width roughness (LWR) has also become an important parameter.

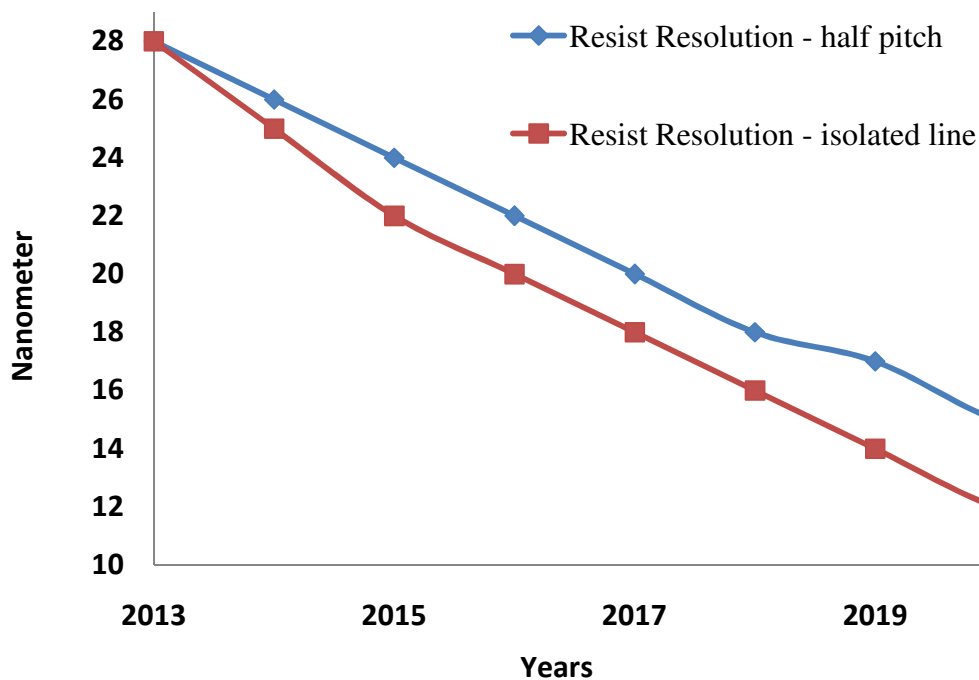


Figure 1.1: ITRS resist road map 2013

1.1.2 Aim of this project

The aim of this project is to develop photoresist materials to improve the fabrication capability of ebeam on poorly conductive substrates, e.g. – Glass, Gallium Nitride, Zinc Oxide etc.

This ebeam resist should be highly sensitive, very high resolution and at the same time conductive. It should have the ability to reduce pattern distortion, on insulating substrates due to charging, by dissipating electrons through the resist layer.

A triphenylene based derivative which can be chemically amplified (CA) using a photo-acid generator (PAG), triphenylene-epoxide and triphenylene-OH (see figure 1.2) in order to increase sensitivity will be used. The pattern resolution will be increased by integrating charge dissipation, controlling acid diffusion and avoiding

phase separation. High proportions of carbon will be maintained in order to make the resist highly etch durable. In order to dissipate charge and prevent pattern distortion the target conductivity is above 10^{-2} S/m,[18] which may require additional doping.

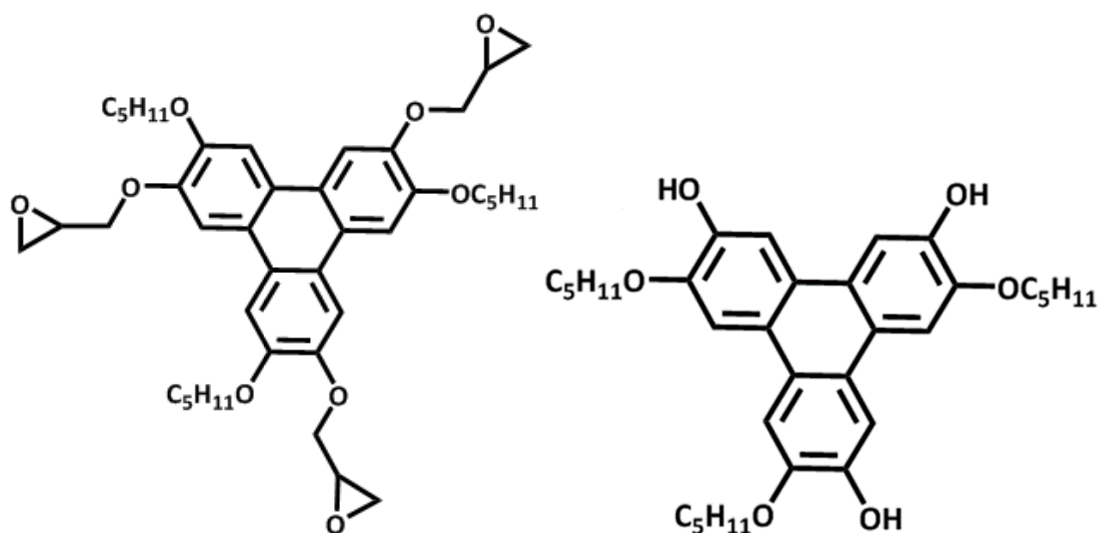


Figure 1.2: C5EPX - Triphenylene with epoxide (left). C5OH (right)

1.2 Lithography

As mentioned, for lithography, a mask is required. In photolithography, a transparent substrate, such as quartz, is coated with chrome patterns. For “mask-less” techniques, such as ebeam lithography, a computer file is used to control the motion of the beam using electrostatic deflectors – in effect a software “mask”.

To create a photolithography mask, the quartz is coated in chromium and then coated with a negative photo resist. The photoresist is then patterned with EBL. After exposure, the resist is developed, removing the unexposed areas of the resist. The sample is then treated with an etchant, which removes chromium in areas that are no longer protected with the photo resist.

1.3 Photo Lithography

The modern semiconductor industry almost exclusively uses photolithography with ultraviolet or deep ultraviolet light to fabricate integrated circuits (IC).[19] The required pattern is transferred from the mask and to a suitable photoresist. Resists materials are sensitive to certain wavelengths of light.

The lithography process starts by coating the substrate with resist. A quantity of resist solution is deposited on the substrate, which is then spun at an appropriate rotational speed, whilst the resist dries, in order to form a smooth thin film. The thickness of the resist depends on the spin speed during the coating process, the viscosity of the resist solution, and the evaporation rate of the resist solvent. Figure 1.3, illustrates a simple photolithography system where projection lenses are placed in-between the mask and the substrate. These lenses de-magnify the mask pattern four or five times before projecting it onto the resist.

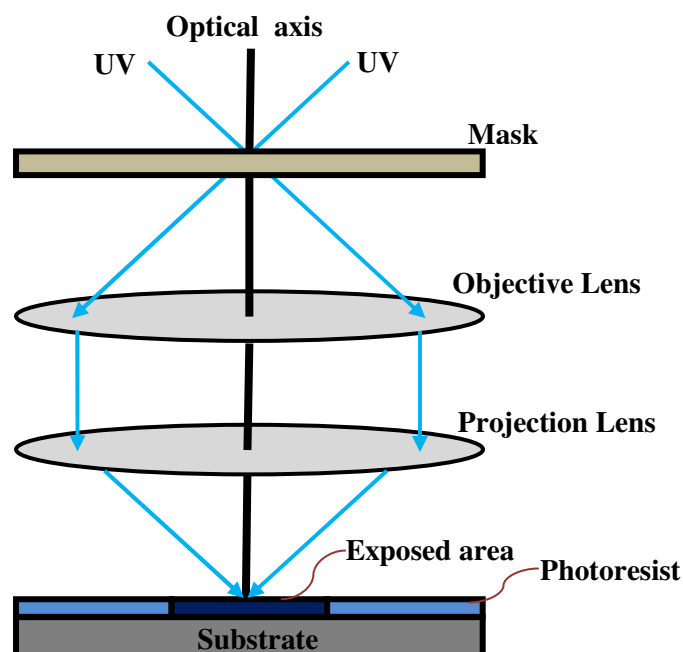


Figure 1.3: Photolithography process [20]

Before projecting light onto the resist, a pattern has been drawn on a mask. This mask can be virtual (i.e. computer generated) or physical (e.g. quartz mask) depending on which lithography technique is going to be used. The resist coated sample is then placed under the mask.

By shining light through the mask for a certain amount of time, the resist film is exposed in certain areas. After that the exposed sample is ready to develop. The development process involves dipping the exposed sample in a developer solution for a certain amount of time.

For developing a pattern it is important to use the correct developer and development-time. By using a suitable developer the unexposed areas of negative tone resist, and the exposed areas of positive tone resist, will be removed (see figure 1.4). Longer development processes can thin the residual resist film in the patterned area, which is undesirable. Therefore, it is advisable to start with a short development time and further development steps can be added if necessary.

A positive tone photoresist is a material in which its solubility increases upon exposure, whilst the solubility of a negative tone resist is reduced upon exposure, see figure 1.4.

In every photolithography or EBL process (i) resolution and (ii) depth of focus are important in determining the lithography tool's performances, which are described below.

Resolution is the smallest feature that can be imaged onto the resist and determines the performance of the lithography tool. The resolution is limited by the diffraction phenomenon of light. The resolution, R , of an optical projection system is

derived from the Rayleigh criterion,[21] and expressed as

$$R = k_1 \left(\frac{\lambda}{NA} \right) \quad (1.1)$$

where, NA is the numerical aperture of the final projection lens, λ is the wavelength of the light source and k_1 is a parameter determined by the resist exposure and development conditions and typically has a value of between 0.3 and 1.[22]

The NA of a lens is defined as

$$NA = n \sin \theta \quad (1.2)$$

where, θ is the half-angle of the maximum light cone which can enter or exit the final lens, and n is the refractive index of the surrounding medium.[21]

Depth of Focus (DOF) describes the virtual range over which an optical image is in focus. It limits the thickness of the film which can be exposed and the tolerance in positioning the sample to maintain an image in focus. The general form of DOF is also derived from the Rayleigh criterion [23] and expressed as

$$DOF = k_2 \left(\frac{\lambda}{NA^2} \right) \quad (1.3)$$

where k_2 is a experimental constant.

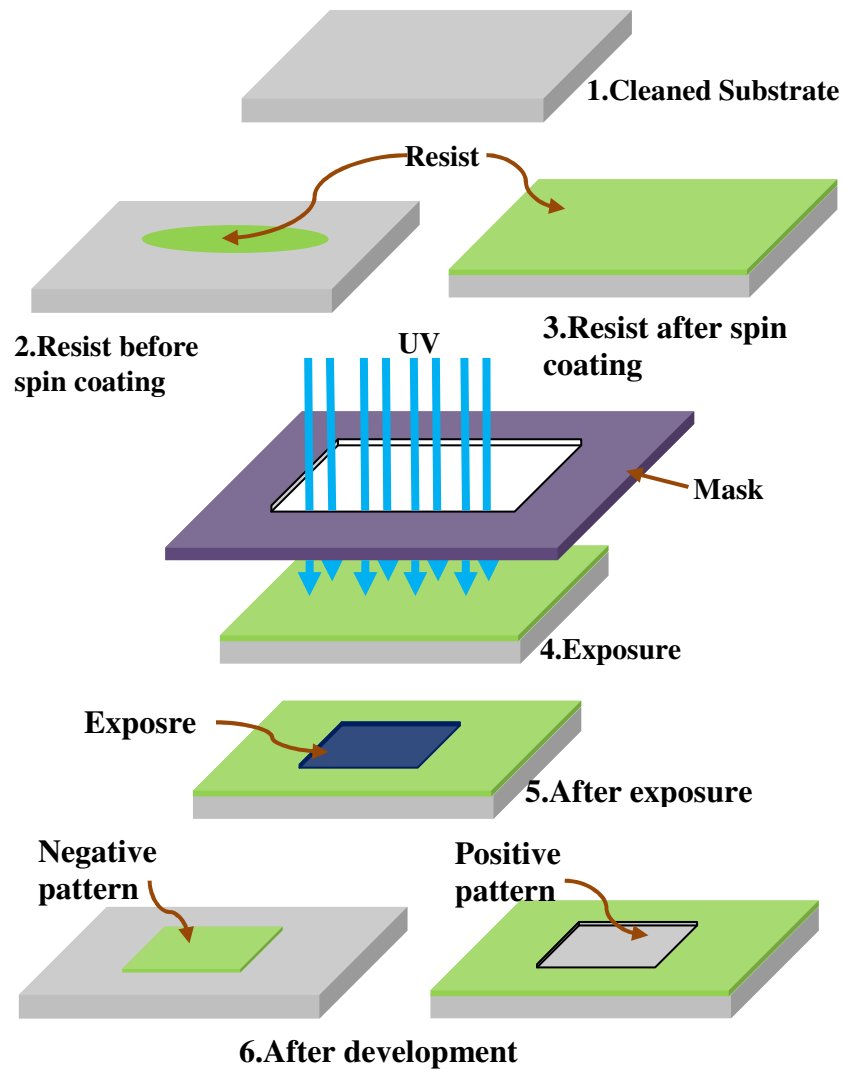


Figure 1.4: Lithography steps from exposure until development of the pattern.

From Equations (1.1) and (1.3) it is clear that the resolution R and DOF depend on the λ (wavelength), NA (numerical aperture), and constants (k_1 and k_2). These parameters guide how to approach a higher resolution lithography system.

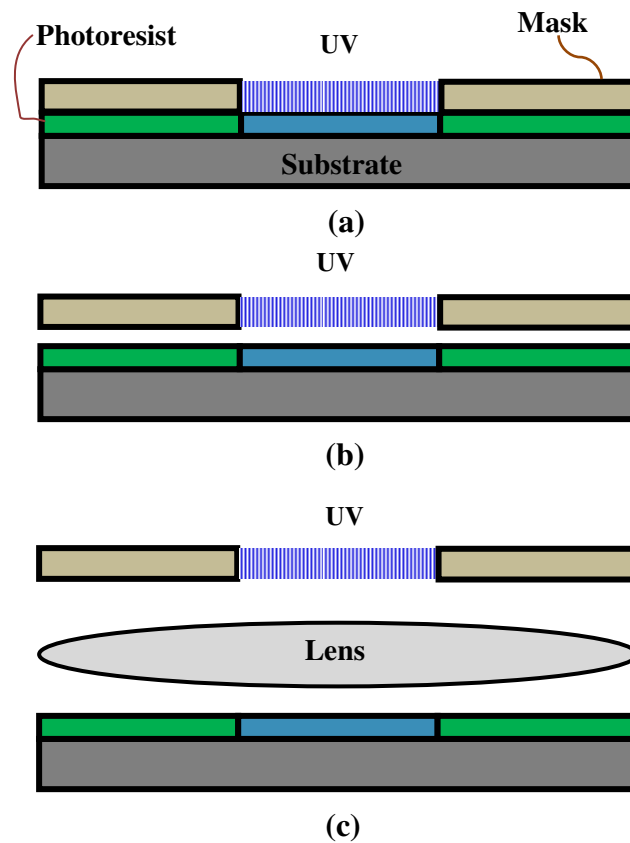


Figure 1.5: Schematic diagram of (a) contact lithography, where the mask is in contact with her photoresist, and (b) proximity lithography, where the mask is $\sim 10 - 50 \mu\text{m}$ from the photoresist surface, and (c) projection lithography, where the mask image is projected onto the resist through a series of lenses.

Depending on the distance between the mask and the sample, there are three types of photolithography process, shown figure 1.5, these are – contact, proximity and projection lithography. Each of these systems has advantages and disadvantages over the other.

1.3.1 Contact Lithography

This is the best process to get the latent image onto resist without diffraction effects, as there is no gap between the mask and the resist-substrate, see figure

1.5(a). However, the magnification ratio of the pattern on the mask and the pattern on the exposed substrate is unity (i.e. 1:1), which means that higher resolution is required to make the mask. More importantly in this process, there is a risk of damage to the mask by contact with the resist material during exposure.

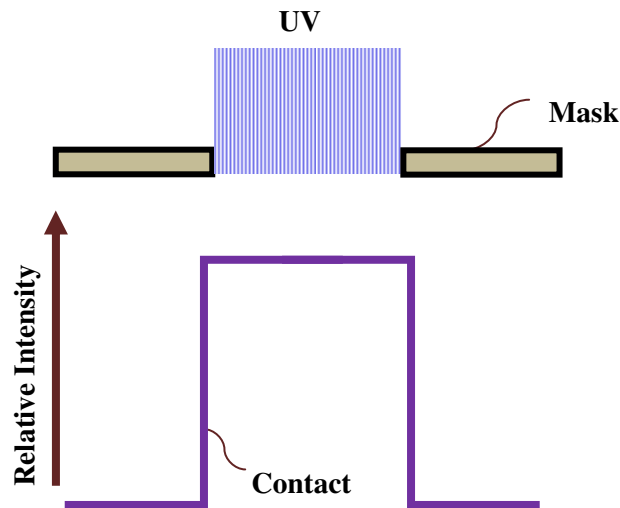


Figure 1.6: Schematic diagram of the projected intensity profile in the resist for the contact lithography, which shows the light intensity at the resist surface of a resolved feature, which has sharp profile at the edges.

Even a single induced fault on a mask may require the mask's replacement. An industrial beam tool can produce approximately one mask per week, with high-resolution masks (e.g. at 1:1 magnification ratio) typically taken longer. Mask production costs are directly proportional to exposure time and thus the frequent requirement for mask replacement in contact lithography can significantly increase the cost of manufacturing.

The big advantage of this method is its simplicity. It needs very simple equipment – a mask and a large UV light is enough to start. It is easy to do exposures on large areas simultaneously. The big disadvantage is the mask should be the same size as the final pattern. This means, the minimum feature size is limited by the resolution of whatever technology created the masks.

1.3.2 Proximity Lithography

In this process, there is approximately $10\ \mu\text{m}$ gap between the mask and the resist as shown in figure 1.5(b). This process prevents damage to the mask by the resist. However, the magnification ratio is still 1:1 and due to the gap and Fresnel (i.e. near field) diffraction, the resolution is not as good as contact lithography. In proximity lithography, the resolution is approximately given by the square root of the product of the wavelength and the gap between the wafer and the resist.

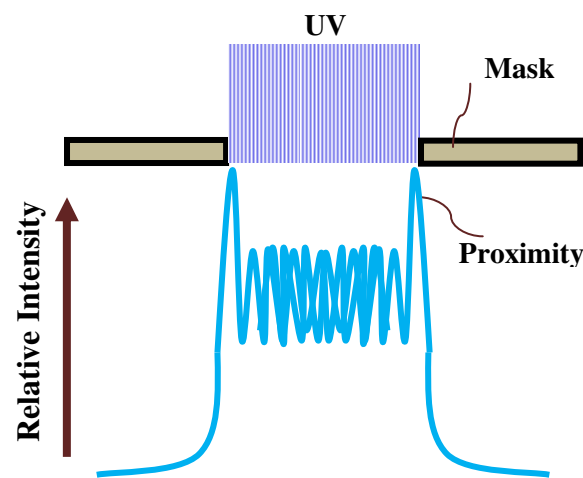


Figure 1.7: Schematic diagram of the projected intensity profile in the resist for the proximity lithography.

Figure 1.7 shows the light intensity at the resist surface of a resolved feature, demonstrating the non-uniform intensity due to Fresnel diffraction.

1.3.3 Projection Lithography

In this process a magnifying lens is introduced between the mask and the resist, which significantly de-magnifies the pattern (4 or 5 times), see figure 1.5(c). This protects the mask from damage by the resist. However, with this process Fraunhofer (far field) diffraction effects occur, due to the large separation distance between the mask and resist. This is illustrated by figure 1.8 (a).

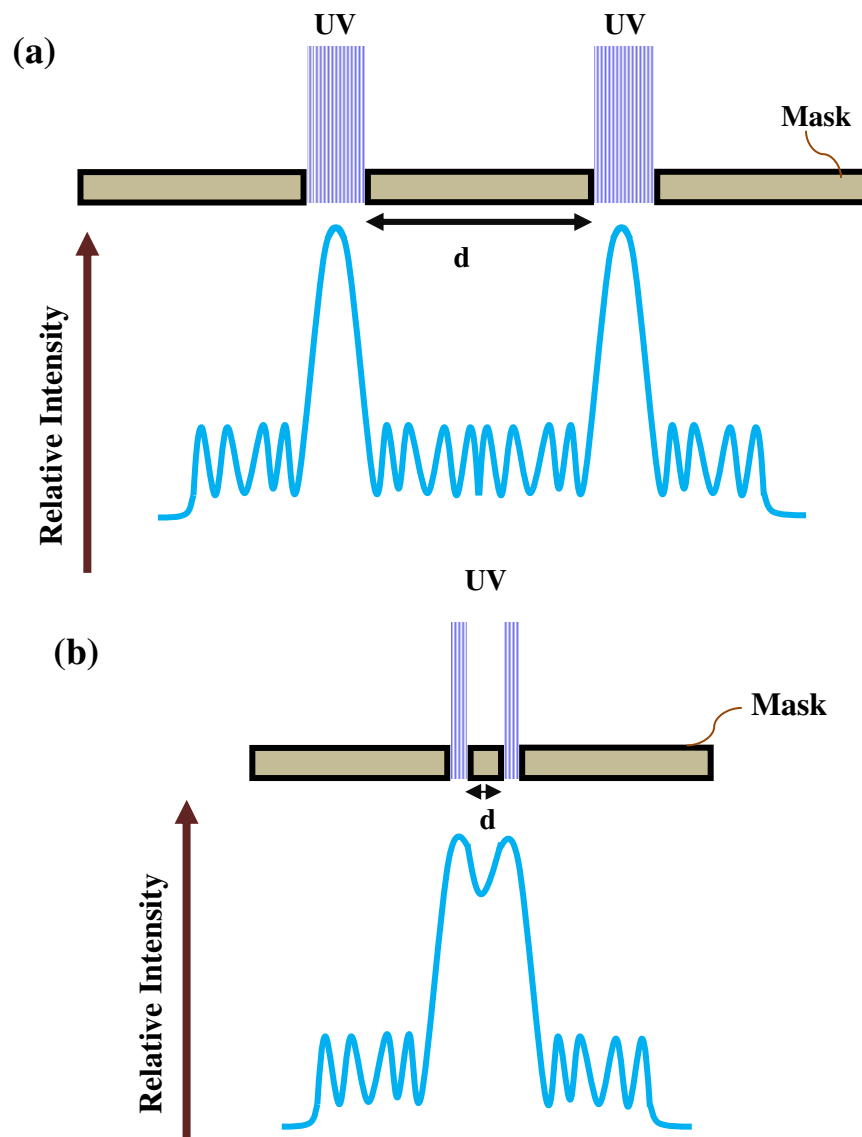


Figure 1.8: The final resolution of projection photolithography is limited by the diffraction effect of the illuminating light, where (a) if the distance, d , between two adjacent mask features is large enough, the aerial image projected onto the resists do not interfere, and (b) when the distance, d , approaches the wavelength of light, the aerial images interfere and degrade the image contrast at the resist surface.

By reducing the distance, d , the blurring of the aerial image can be improved, see figure 1.8 (b). The Rayleigh criteria,[24] for diffraction limits the minimum feature separation as shown by equation (1.1) the image edge resolution can be improved. Typically the value of k will be between 0.5 and 1.[25] The theoretical minimum value of k_1 is 0.25, but realistically minimum of about 0.3 can be achieved.

Projection lithography is one of the widely used industrial methods for making IC (integrated circuits). The primary disadvantage of this method is that the minimum feature size is limited by the diffraction limit of the exposing light. However, it is a very fast technique for high-volume manufacturing as it allows one to pattern entire wafers simultaneously. Projection systems do not suffer contact damage the photo-mask but the image intensity at the resist is degraded slightly.

1.3.4 Advanced Photolithography

1.3.4.1 Immersion Lithography

For more than hundred years immersion has been used to improve the resolving power of optical microscopes, increasing the resolution and depth of focus (DOF).[26] Using a high refractive index (~ 1.44) liquid, such as purified water, between the lens and the sample is sufficient to increase the NA . [27] When the light travels from a lens (refractive index n_1) in to air (refractive index n_2) it is typically refracted through an angle θ . However, when θ exceeds a value of $\arcsin(n_2/n_1)$, known as the critical angle, the light will instead undergo total internal refraction. This limits the maximum NA of a lens system as shown in figure 1.9. By replacing the air with a higher refractive index fluid the NA can be increased. By reducing θ_2 the DOF gets increased for a given NA value. Furthermore, by increasing NA it is possible to increase the resolution of the system without moving to a shorter wavelength. For example, in 193 nm lithography the achievable half pitch pattern will be ~ 90 nm, however, this can be improved to ~ 32 nm half pitch pattern, by using water instead of air in immersion lithography. This is equivalent to moving to a wavelength of 134nm.

The main problems of this technique are: bubble formation and particle

trapping, in the immersion liquid between the resist and the lens, which ultimately increase the process complexity.[27, 28]

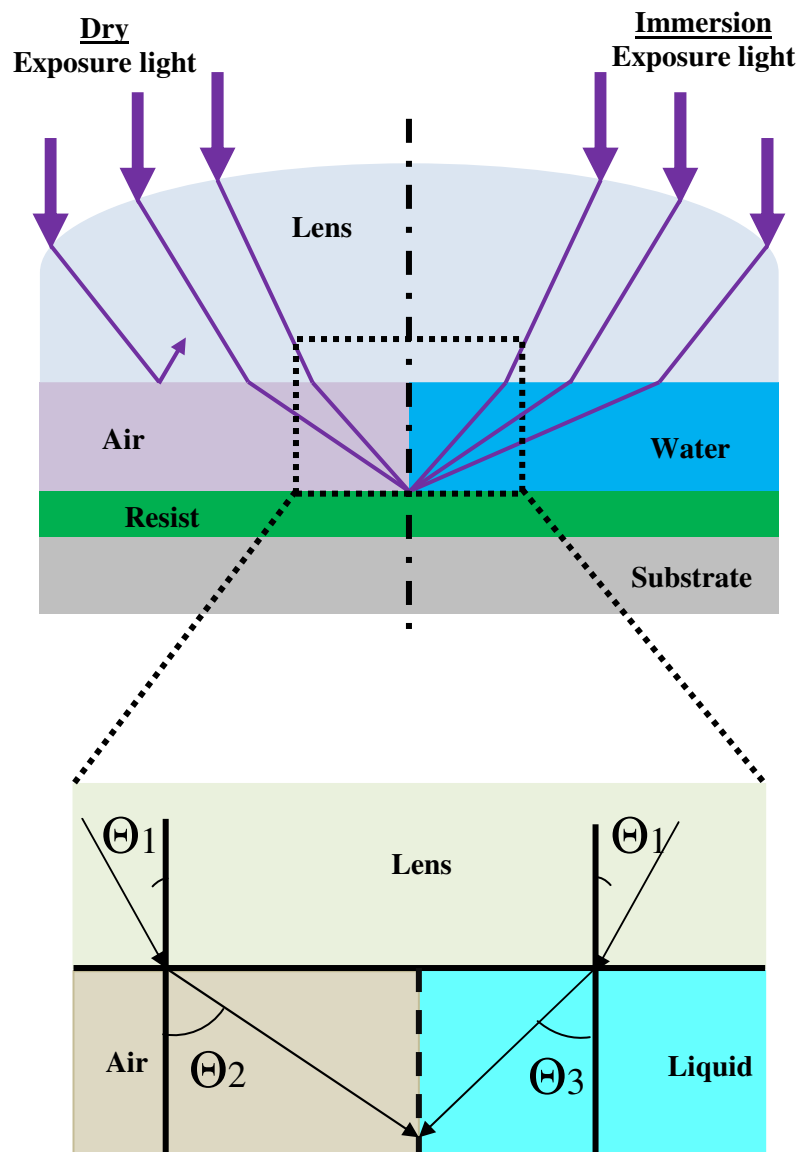


Figure 1.9: Schematic representations of the optical paths between dry and immersion systems.

1.3.4.2 Double patterning lithography

Double Patterning (DP) lithography is a technique that splits the pattern into two steps, in such a way as to separate adjacent features onto separate masks this allows

for higher resolution to be achieved. The most common DP technique is Litho-Etch-Litho-Etch (LELE), which requires in two steps, [29, 30, 31], see figure 1.10.

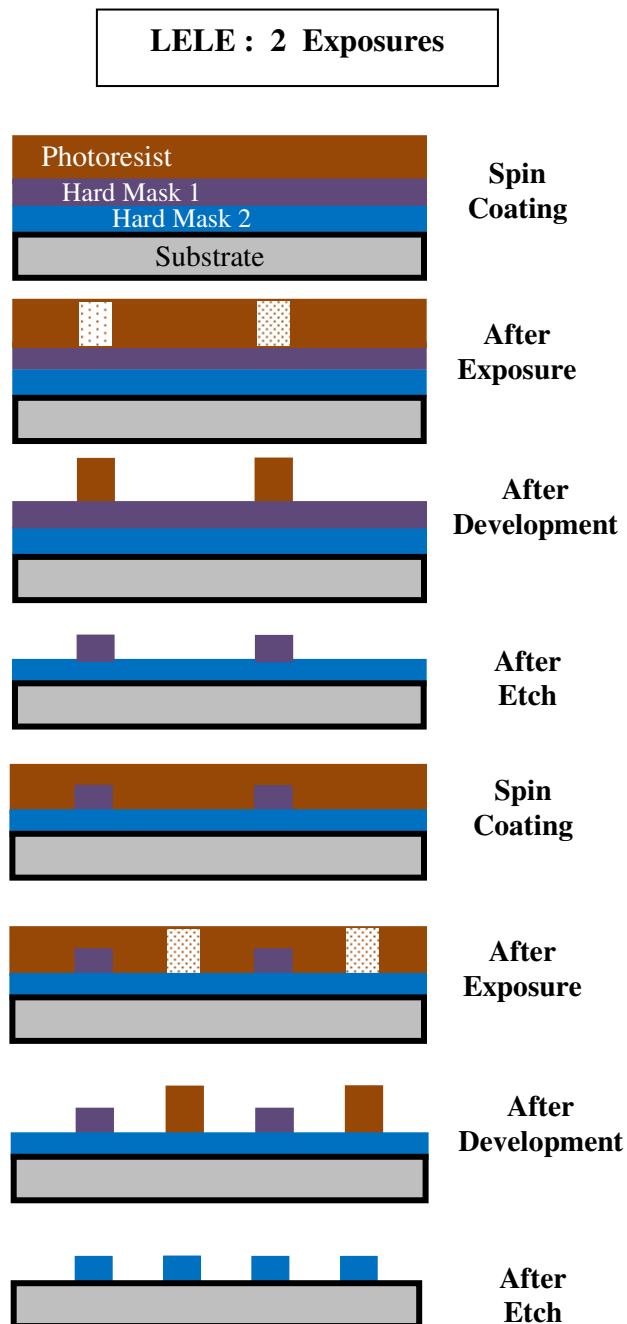


Figure 1.10: Schematic representations of LELE process: spin coat first resist onto hard masks, then expose and etch; spin coat second resist and then expose and etch.

The first step is to transfer half of the pattern onto a hard mask, and the second step transfers the other half of the pattern into the hard mask. Afterwards the whole

pattern can be transferred to the substrate by using an etching process. For each step a separate photoresist is required.

This process increases the mask design complexity and hence the cost. Besides the cost there is another serious concern about this process is the effect of feature due to feature positioning errors. Achieving good overlay alignment is important, and progressively more difficult for patterning below 22 nm.

Another DP technique is Self-Aligned Double Patterning (SADP) [32, 33] see figure 1.11.

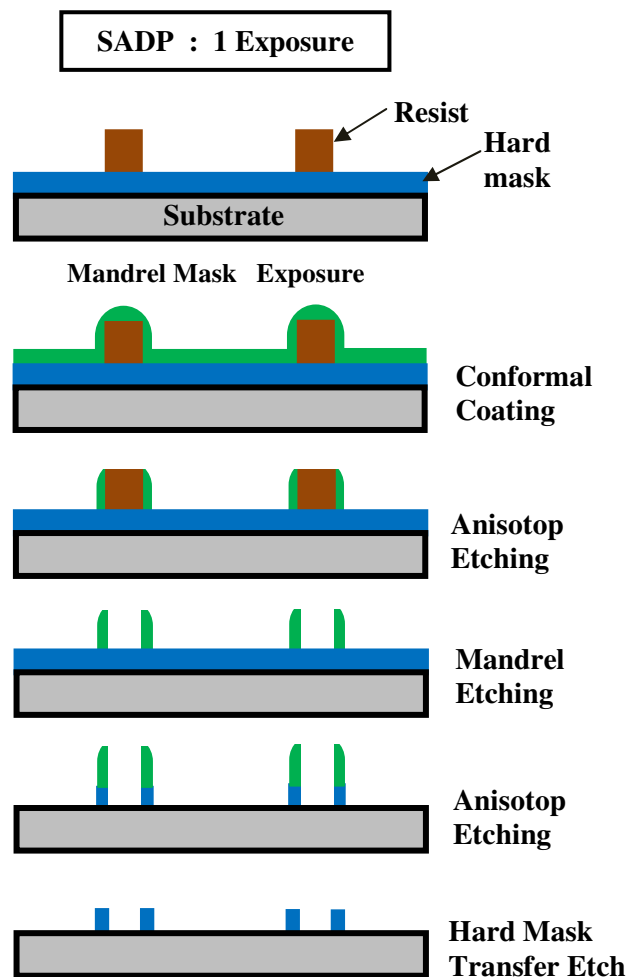


Figure 1.11: Schematic representations of SADP process.

At first, the resist layer is patterned and then a conformal layer of spacer material is deposited on top. An anisotropic etch is then used to remove horizontal section of the spacer material. A selective etch is then used to remove the mandrel and finally the remaining spacer material pattern is etched into the hard mask. By repeating the deposition of space material and etching steps multiple patterns can be formed.[34]

The big advantage of this process is that pitch reductions can be achieved, it inherently solves the overlay issue seen in LELE, and additionally only one critical exposure is needed. It has better line-edge and linewidth roughness and also better critical dimension uniformities than LELE. However, this process has more difficulties and can have manufacturing costs due to the requirement for design modification, particularly for 2D device layouts which require extra processing steps.

1.3.5 Other techniques

1.3.5.1 Extreme ultraviolet lithography

Extreme ultraviolet lithography (EUVL) works in the soft x-ray region, between 11 – 14 nm wavelengths, in a vacuum environment using reflection optics and mirrors (figure 1.12). EUV photons with a wavelength of 13.5 nm [35] are highly absorbed by most materials.

After generating EUV light it is focused on a condenser lens which reflects the light onto a positioning mirror then to a reflection mask, and by using four reduction mirrors finally onto the sample for exposure.

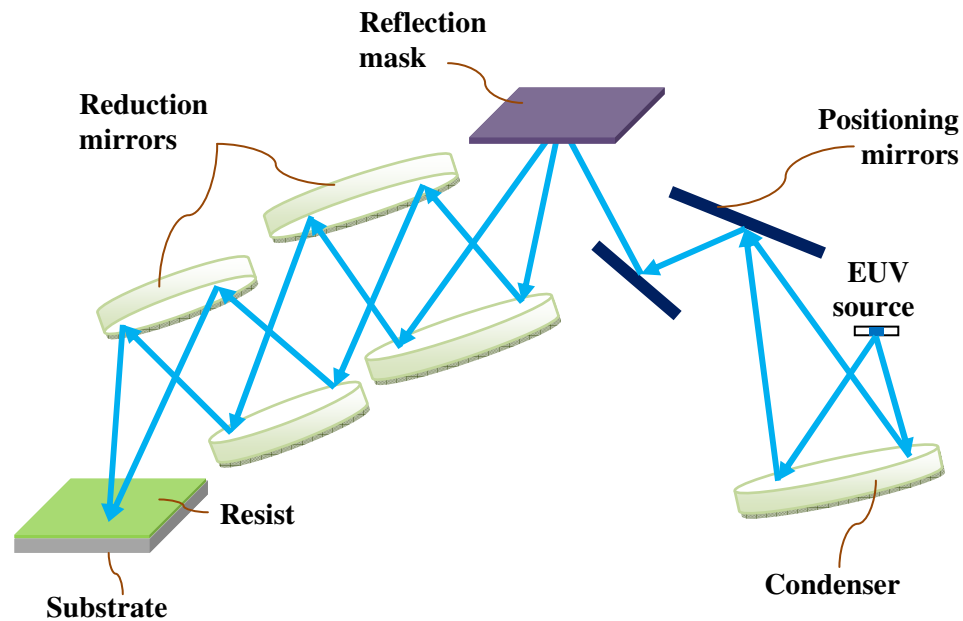


Figure 1.12: Schematic representation of EUVL optics

The main requirements for EUVL are – a high power and long life source, a defect-free mask, a defect inspection method, and a novel resist material.[36, 37] Due to EUV source power limitations, this system is much slower than other lithography.

1.3.5.2 Nanoimprint lithography

Nanoimprint Lithography was first introduced by Stephen Chou in 1996.[38] The main feature of Nanoimprint Lithography is high resolution at low cost. The high resolution patterns are created on a mold by a standard lithography process such as electron beam, and can subsequently be easily transferred onto a resist film at 1:1 scale by mechanical contact. After removing the mold the samples are transferred to a plasma etcher in order to remove unwanted resist residuals from the pattern, see figure 1.13.

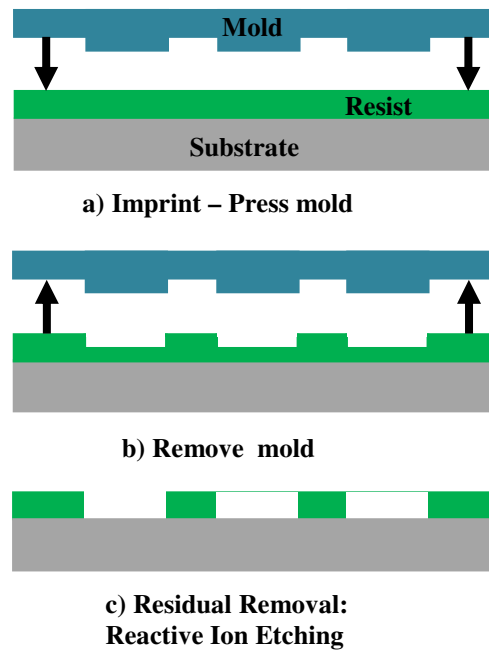


Figure 1.13: Schematic representation of nanoimprint lithography

There are two main processes; in thermal input a polymer is heated above its glass transition temperature to soften it after which the mould is pressed into the polymer to imprint the pattern.[39] In UV imprint a transparent mould is pressed into a liquid resist. UV light is then used to crosslink and solidify the resist.[40]

This technique is primarily used in research, but is not yet ready for commercial IC industries due to high defectivity levels. The smallest feature that can be produced in photolithography depends on the wavelength of light that is used. Using UV light in photolithography the maximum resolution that can be achieved is around 30 nm using a wavelength of 193 nm.[41] However, for other applications where very high resolution is needed, i.e. sub 30 nm resolution,[42, 43] then there is another lithography technology that has been used, and that is ebeam Lithography (EBL).

1.4 Electron beam lithography

Electron Beam Lithography (EBL) is more than 50 years old and widely used by IC industries for small volume production.[44] EBL has a finely focused ebeam, which can be steered to any position on a sample for a controllable duration. By using electrostatic or electromagnetic lenses, the beam is controlled and moved to draw any shape. The biggest advantage of EBL is that it's maskless lithography and software is used to define the required pattern. The first EBL tool was a modified Scanning Electron Microscope (SEM), see figure 1.14.

In an EBL system, the wavelength of the electrons are much smaller than light and EBL is therefore not diffraction limited, which gives EBL a very high resolution. The ability of an EBL tool to focus the electron beam to a tight spot is the primary factor limiting resolution.

The main advantage of EBL over photolithography is the ebeams can be focused to a spot whose position on the substrate can be controlled with electron optics and can thus expose only those areas that need to be exposed without the need for a physical mask.

Ebeam lithography can be undertaken with a dedicated tool, or by modifying a Scanning Electron Microscope (SEM) to allow arbitrary control of the beam position. Dedicated tools typically utilize a beam energy of 50 – 100 keV in modified SEMs 30 keV is more common.

EBL allows for very high resolution patterning with sub 10 nm features,[45] because the beam can be focused to a spot of 1nm diameter. This highly focused beam of electrons is then scanned across a surface using electrostatic and electromagnetic

lenses – so called direct-writing.[46 – 48] The electron beam is focused on to an electron sensitive resist, which is chemically modified by expose to the electrons.

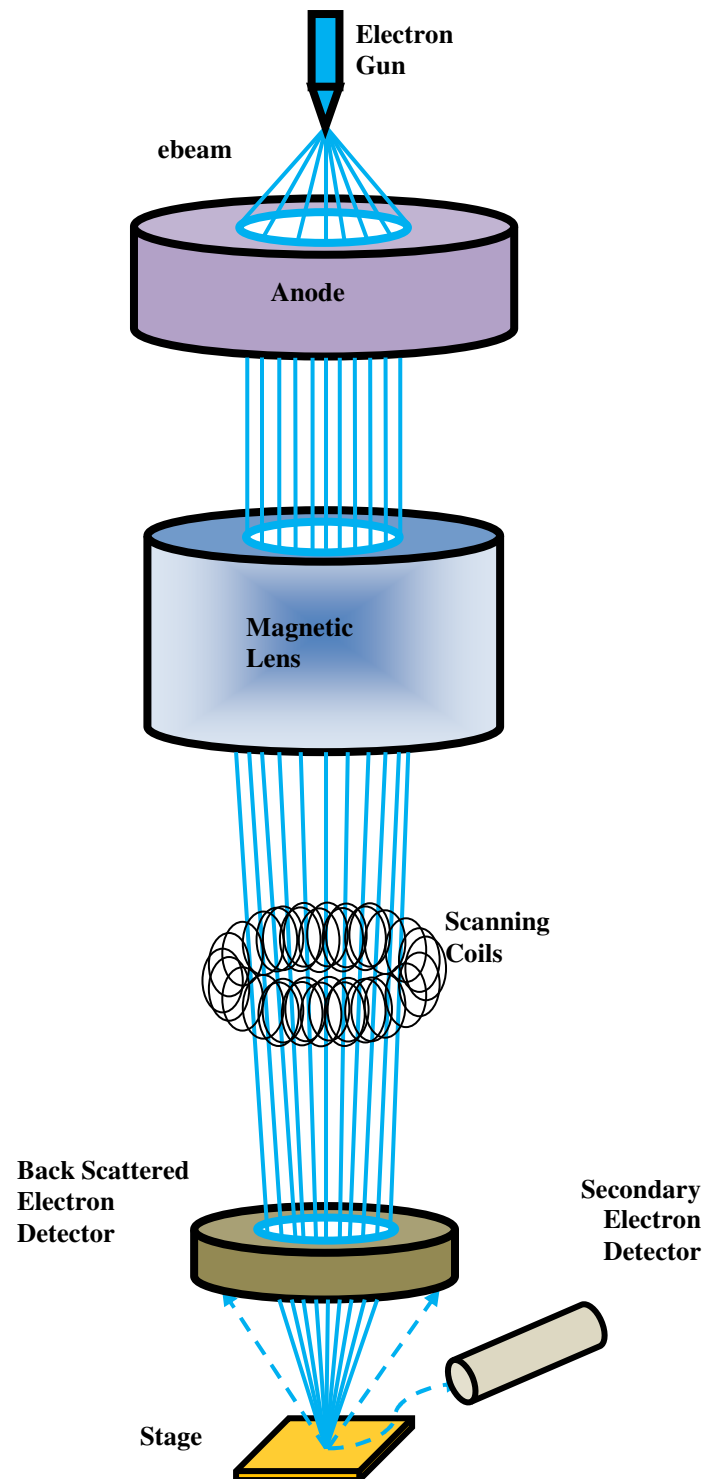


Figure 1.14: Scanning Electron Microscope (SEM) lithography

EBL is widely used in low volume high resolution fabrication processes, but pattern distortion on insulating substrates is a challenging problem. Even for new ebeam technology resist charging is a major problem during the ebeam exposure process.[49 – 51] Normally resists are made with insulating materials (e.g. polymers), however as the films are thin the electrons can travel through the resist to the substrate and then to ground. However, if the substrate is also insulating the charges are trapped and as the substrate charge increases it will increasingly deflect the electron beam's path and lead to pattern distortion. Both systematic and fluctuating beam placement errors can result which are difficult to compensate for and introduce lots of error.

1.4.1 How an ebeam tool works

The operation of a typical ebeam tool is in principle relatively simple, and similar to photolithography. Figure 1.15 shows a schematic of an EBL tool, which consists of a column, chamber and electron gun.

By using a suitable pump, the chamber and the column are maintained at a very high vacuum. Inside the column several functions occur, including creating a beam of electrons, acceleration of the electrons to the working voltage, turn the beam on and off (i.e. beam blanking) and most importantly to deflect the beam according to the pattern required to expose the sample. Typically, the samples are loaded into the chamber's interferometric stage, which is controlled by an accurate positioning electronic system that can be handled manually or by computer software.

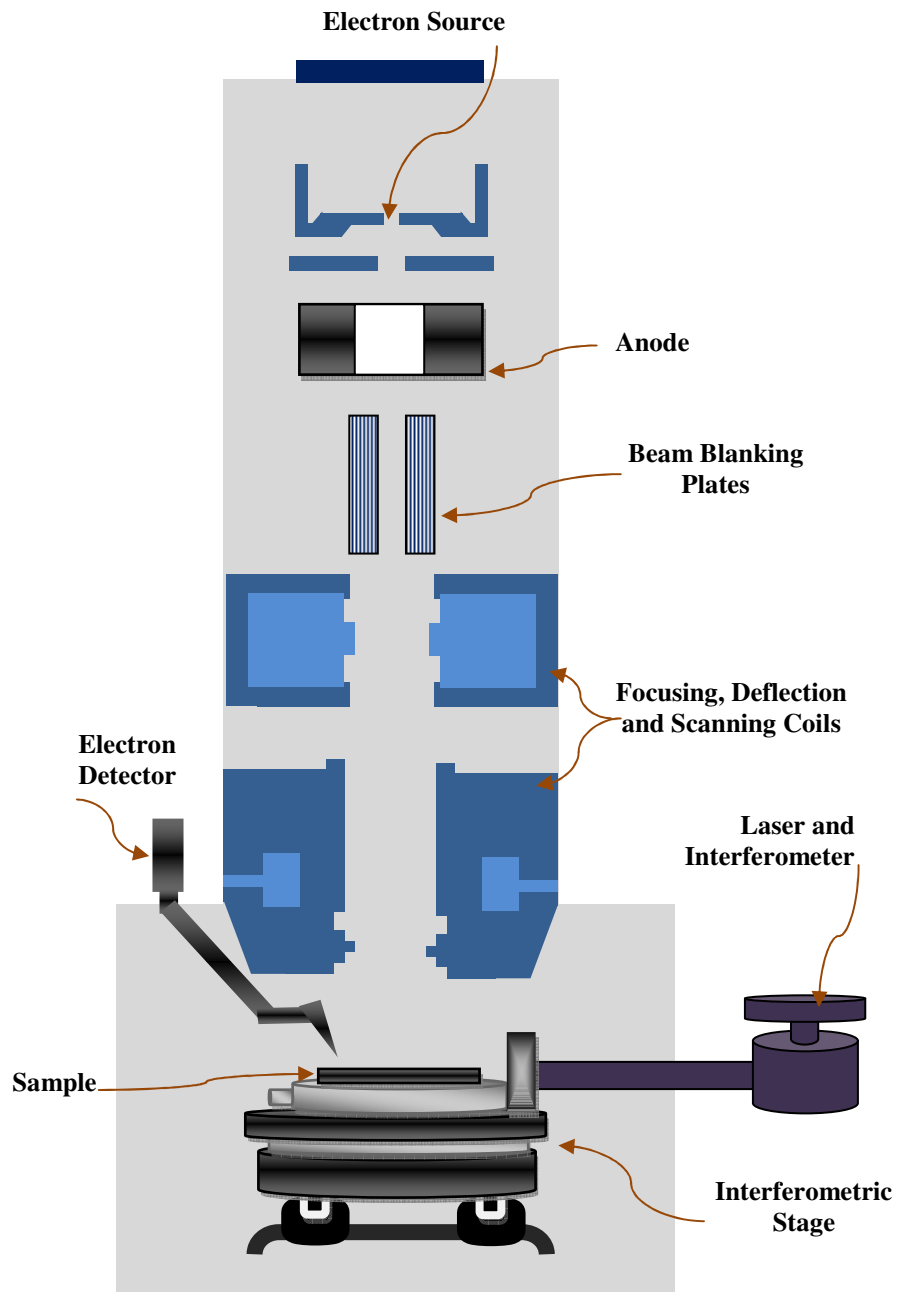


Figure 1.15: A typical EBL system.

Professional electron beam lithography tools typically operate with an electron beam voltage of 50 – 100 keV. Research tools, which are frequently based on modified scanning electron microscopes (SEM) typically, have a maximum voltage of 30 keV. However, these modified SEMs are significantly cheaper than a dedicated EBL tool.

1.4.2 Next generation EBL tool

1.4.2.1 MAPPER

Because of the serial nature of EBL patterning, it is much slower than photolithography. To address this limitation Multiple Aperture Pixel by Pixel Enhancement of Resolution (MAPPER) has been proposed which is a parallel patterning technique as shown in figure 1.16.

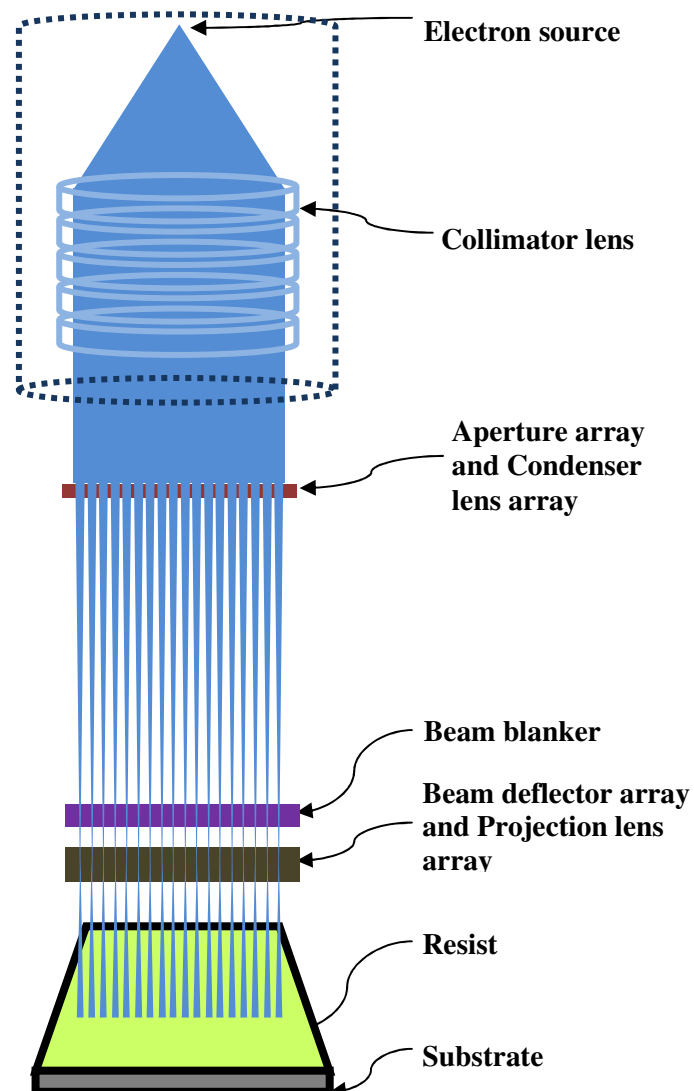


Figure 1.16: Schematic of MAPPER system.

By using an electrostatic lens array MAPPER can generate ~13,000 ebeams by splitting up a single electron beam from a single electron source. To avoid a central cross-over each beam has its own optical column.[52] It has been reported by MAPPER Lithography that it can expose more than 10 wafers an hour with resolution of less than 32 nm half pitch. It uses 5 keV electron beams, which reduce wafer heating.[52]

Each beam can deflect over 2 μm in one axis whilst the wafer stage moves in an orthogonal direction. The beams are blended according to computerized patterns in a bitmap format, which are divided over 13,000 data channels.[52]

1.4.2.2 Projection Maskless Lithography

The IMS Nanofabrication Company has developed an alternative multi-beam EBL technology, which is known as Projection Maskless Lithography (PML). Pattern can be produced simultaneously by PML by using 2,300 individually controllable parallel beams.[53] It has been shown 16 nm half pitch resolution patterns can be produced on hydrogen silsesquioxane (HSQ) resist.[54]

PML2 (figure 1.17) has a programmable Aperture Plate System (APS), which is a combination of an aperture array at the top plate and deflection arrays at the bottom, that allows the collimated 5 keV beam to be split into thousands of beamlets.[55] These beamlets are then accelerated up to 50 keV, and then magnified 200 times by condenser lenses.[55] Finally, these beamlets are projected through the aperture at the beam cross-over plane onto a wafer to perform spot exposure. This exposure can be performed whether the wafer-stage is moving or stayed still.

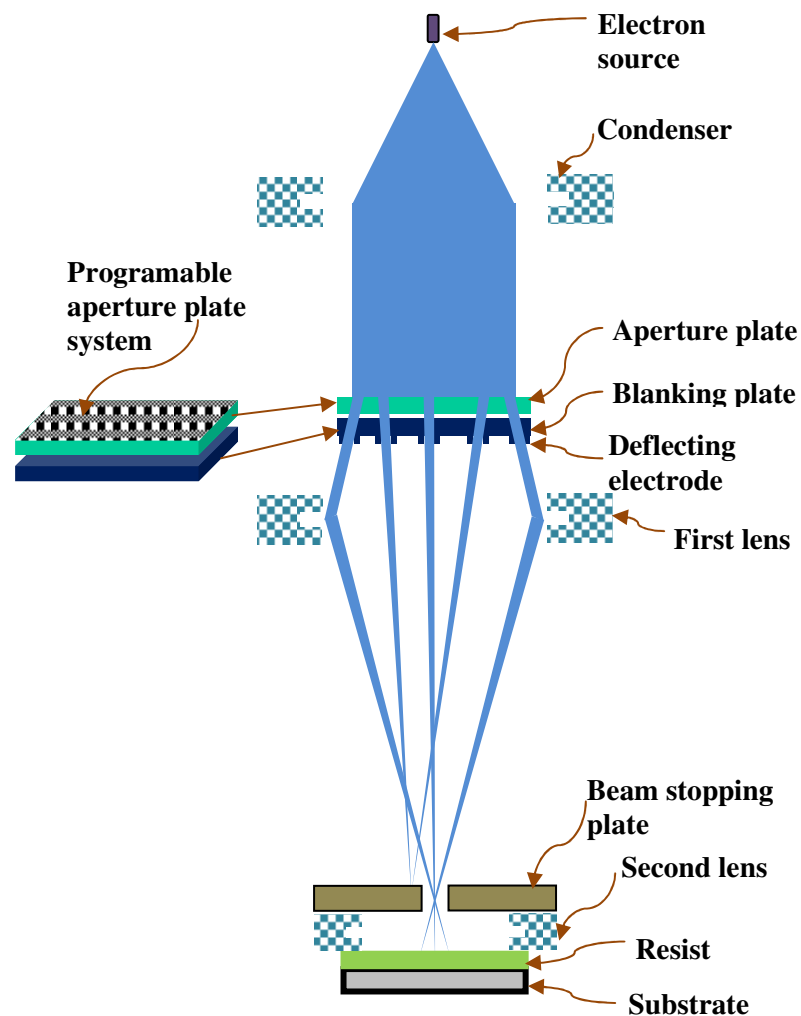


Figure 1.17: Schematic representation of PML2 system.

1.4.2.3 Reflective electron beam tool

The reflective electron beam lithography (REBL) nanowriter is another novel approach for mask-less lithography technology, see figure 1.18. It can expose 5 – 7 wafers per hour. REBL incorporates several novel technologies to generate and expose lithographic patterns.[56] It uses a time domain integration (TDI) technique [56] to scroll data across the digital pattern generator (DPG) and synchronize with the motion of the wafer stage.

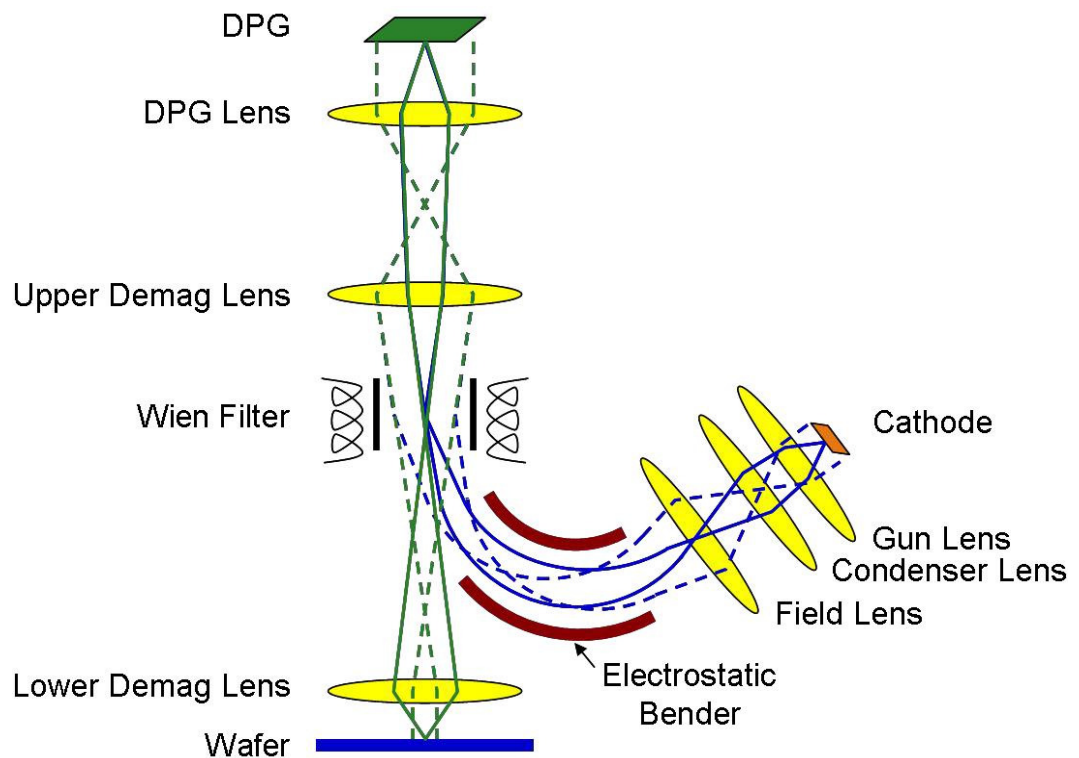


Figure 1.18: Schematic representation of REBL [56]

This DPG is one of the important parts of REBL Nanowriter. The DPG is primarily a complementary metal-oxide semiconductor (CMOS) chip with over one million controllable electron mirrors, which programmatically splits the primary beam into a patterned array of beamlets. These beamlets are parallel and reflect from DPG to the wafer providing a high-speed mask-less pattern generation capability.

The source is a large area cathode, with condenser lenses placed in the center of the beam crossover. These condenser lenses form the source image at the center of the field lens. By using an electrostatic beam bender the illuminating ebeams get bent about 110 degrees. This beam bender acts as a weak lens and forms an image of the cathode in the virtual center of the Wien filter. This filter is used to separate the illuminating beam from the projection beam.[56]

The Wien filter is constructed with electric and magnetic deflectors to bend the beam coming from the gun to the DPG. The projection beam which is reflected from the DPG and traveling in the opposite direction through the Wien-filter travels on a straight path through the filter from the DPG to the wafer.[56]

Finally, the upper demagnification lens forms a crossover at the back focal plane of the lower demagnification lens and the lower demagnification lens focuses the DPG image onto the wafer plane.[56]

1.4.3 Scattering effects in ebeam lithography

Scattering effects are a significant issue in beam lithography that makes it difficult to achieve nano-size features in the resist.[57] When electrons strike the resist, they can undergo two kinds of scattering event: forward and backward scattering, as shown in figure 1.19.

Different ebeam tools can utilize electrons with energies in the range 1 – 150 keV to expose a resist. Depending on the energy range chosen, the scattering distributions are different. When the ebeams hit the resist, the electrons can be deflected through a small angle, which tends to enlarge the beam diameter. This is known as forward scattering. Other electrons can undergo large angle scattering, known as back scattering. When this occurs in the resist film the electrons are scattered back out of the resist generally without significant effect. However, if electrons, which have travelled through the resist and into the substrate are back scattered, they can travel back into the resist at a significant distance to the original entry point leading to electron dose in the resist far away from the required position.

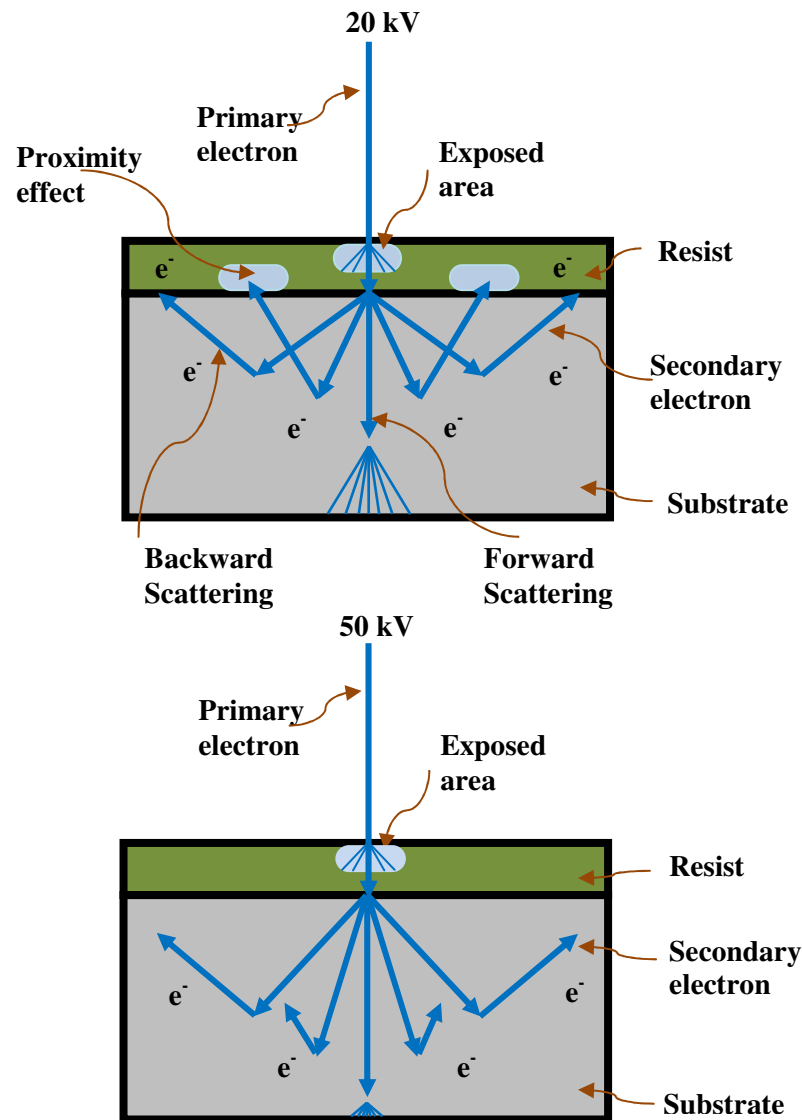


Figure 1.19: Schematic representations of forward and backward scattering in 20 keV and 50 keV ebeam

Forward scattering is more likely than back scattering. However, the presence of heavy atoms (known as high z), such as metals, will increase the probability of back scattering.

In forward scattering the electrons collide with resist or substrate electrons changing their direction and potentially transferring some energy into the resist (or substrate) in the case of inelastic scattering. The deposited energy causes the resist (or substrate) molecule or atom to be excited or ionized. When ionisation occurs an

electron is knocked out of the outer shell of an atom in the resist – this is known as a secondary electron, this secondary electron generation leads to a small angle scattering of the primary electron. If this secondary electron comes from a resist atom, it will typically also cause scission of the molecular chain during ionisation.

In back scattering the electron collides with the nucleus of an atom, and undergoes a large angle scattering event. When this electron is scattered in the substrate it returns back through the resist where it can break molecular chains at a significant distance from where the pattern should be created, causing additional area exposure. These back scattered electrons are the cause of the proximity effect.[57, 58]

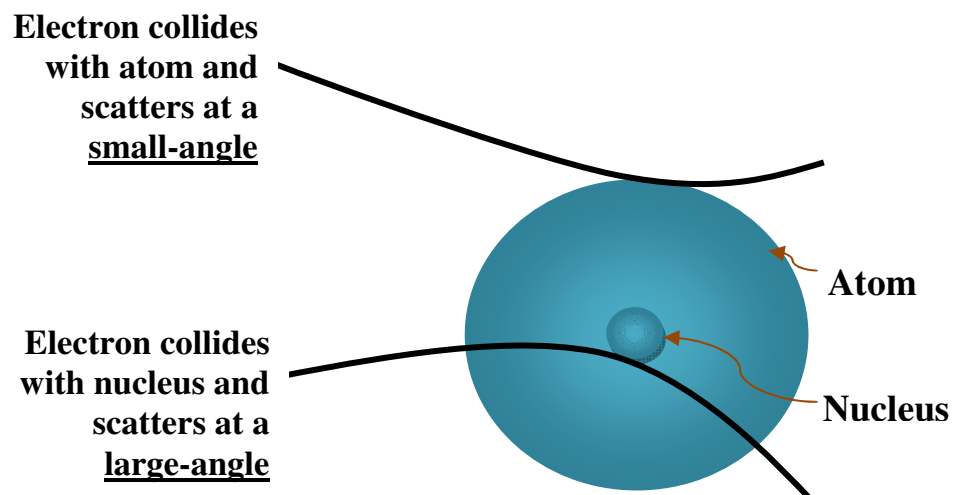


Figure 1.20: Electron scattering angle with atom and nucleus.

During the exposure, the primary electron in the beam, which have high energy, travel a long distance. At the same time they also dissipate energy into the resist by creating secondary electrons. This energy dissipation process continues until the primary electron loses all its energy. Using a beam with relatively low energy primary electrons (e.g. 2 – 50 keV) the travel distance can be minimized to a few tens of nanometers in the film before reacting with the resist molecules, which tends to

increase sensitivity decrease resolution due to scattering. By increasing the primary beam energy (e.g. > 50 keV) the electrons travel deeper into the substrate and generate back scattered electrons too far from the resist to return into it. This method reduces the proximity effect.

As they dissipate their energy via secondary electrons, the primary electrons start to slow down. Most of the patterned areas of the resist get exposed by these secondary electrons. The distance of an electron depends on its energy and the material (i.e. resist and the substrate) that it travels through. Back scattered electrons are dependent to the beam energy and the substrate material. It has been observed that, the substrates with lower atomic number give less backscattering. This backscattering effect is one of the main limiting factors of ebeam lithography.

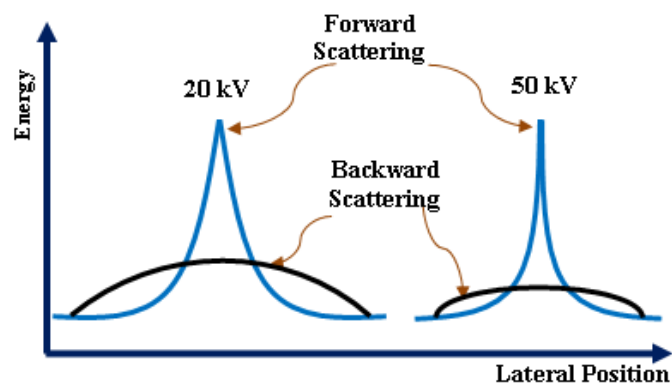


Figure 1.21: Schematic representation of electron–solid interactions within resist/substrate specimen.

As an example, the electron scattering trajectories in resist and in the silicon substrate combined are shown figure 1.21 for ebeam energies of 20 keV and 50 keV. By increasing the ebeam energy, the forward scattering is reduced and the back scattering distribution occurs deeper in the substrate which cause the subsequent secondary electrons to be in the substrate rather than the resist polymer, and thus the proximity effect is reduced or eliminated.

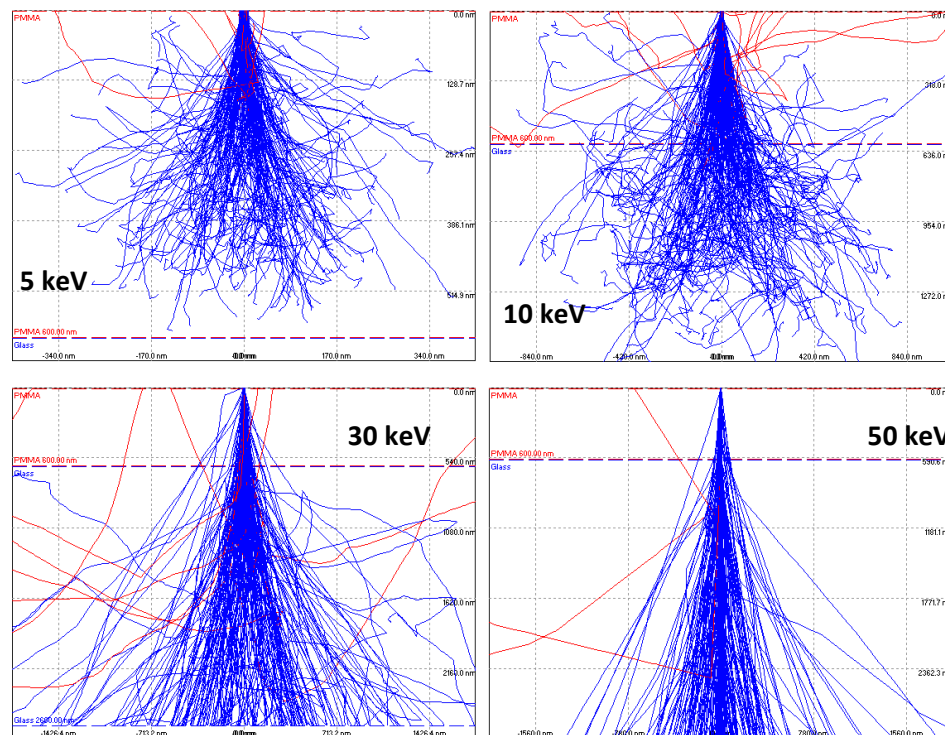


Figure 1.22: Scattering effects at lower to higher energy. The dashed line indicates the resist/substrate interface. Resist film thickness is the same in all cases. (Simulation carried out using Casino software package)

In case of positive tone resist, after exposure, the electron breaks the resist's molecular chain and reduces its molecular weight, which ultimately increases the solubility [59] of the area where the exposure happened. For negative tone solubility is decreased for instance by inducing crosslinking.

1.5 Photoresist

Photoresists are typically polymer compounds, and used to record the pattern on the substrate. They are photosensitive and protect selected areas of the substrate from subsequent etching, diffusion, deposition, or implantation in the device manufacturing processes. As well as sensitivity to the required radiation photoresists must be capable of forming a smooth stable film of controllable thickness on a substrate via an industrially compatible process such as spin coating. The solvents used to coat the

film should be non-hazardous, and the resultant film must be sufficiently durable and stable to form a useful mask during subsequent substrate processing.

1.5.1 Resist Characteristics

A photoresist is characterized by a number of performance characteristics, the most important of which are -sensitivity, contrast, resolution, line edge roughness (LER) or line width roughness (LWR) and etch resistance.

1.5.1.2 Sensitivity and Contrast

The sensitivity of a resist is the minimum exposure dose (i.e. the amount of energy deposited onto a resist per unit area) of radiation required to form a usable pattern. [60]Sensitivity for a positive tone resist is defined as the dose at which the full thickness of the exposed resist areas are removed upon development, D_2 on figure 1.23(a); and for negative tone resist it is defined at which 50% of the thickness is retained, D_3 on figure 1.23(b).[60]

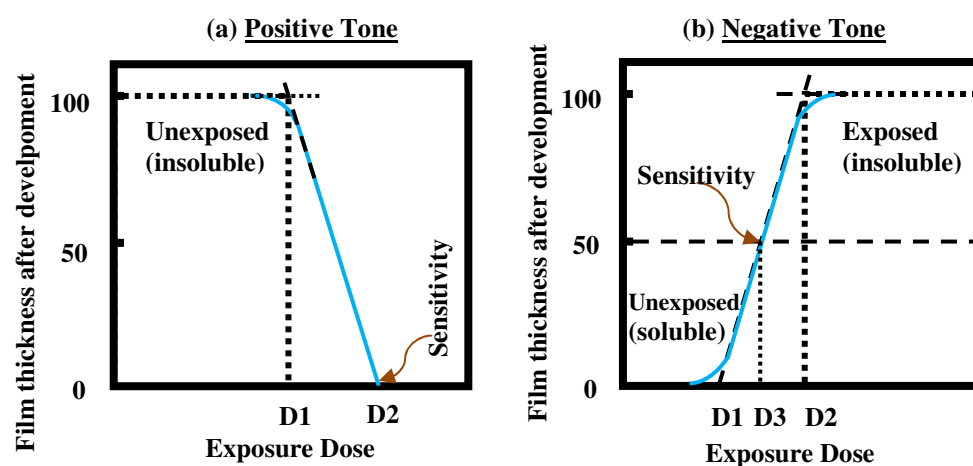


Figure 1.23: Response curve (a) positive and (b) negative tone resist

The unit of EBL dose is $\mu\text{C}/\text{cm}^2$. The contrast is the rate change of a resist's solubility transformation with respect to an increment of dose, at the point at which the dose is sufficient to cause a transformation (i.e. the falling portion of the positive tone response or the rising portion of a negative tone response, respectively).

A high sensitivity resist requires a very low dose and allows fast patterning, which is cost effective for the manufacturer. On the other hand a high contrast resist has capability to provide very good vertical sidewall profiles and generally has better resolution. So an ideal photoresist should have high sensitivity and contrast. The dose (i.e. D) calculation equation is

$$D = \frac{It}{A} \quad (3.1)$$

where, I is the radiation intensity (i.e. ebeam current), t is the exposure time and A is the exposing area.

The sensitivity and contrast of the resist are determined from response curve, which is the graph of remaining resist film thickness (often normalized) versus exposure dose, on a semi-log plot. Figures 1.23 (a) and (b) show positive tone and negative tone response curves, respectively.

It is clear from the graph that as the dose increases in the case of a positive tone resist, after a certain dose less exposed film is retained after development, and at some dose there will be no film left. For the resist to form an effective mask, the patterned areas must be fully cleared, and thus the sensitivity for the positive tone resist is defined as the dose at which all resist is removed, D_2 . [60]

For the negative tone resist, the solubility switch is opposite, so as the dose

increases, the film becomes less soluble, and more of the film in the patterned areas retained, and the thick is the pattern. The sensitivity for the negative tone resist is defined as the dose at which 50% of the thickness is retained, D_3 . [60]

Contrast, γ , is defined as the slope of a linear portion of the curve expressed by [61]

$$\gamma = \left[\log_{10} \left(\frac{D_2}{D_1} \right) \right]^{-1} \quad (3.2)$$

1.5.1.2 Resolution

Resolution determines the minimum feature size one can print in a resist. The feature size depends on the material itself, but also the exposure dose, development process and the material properties of the resist, [61] as well as the required pattern (densely features are harder to resolve).

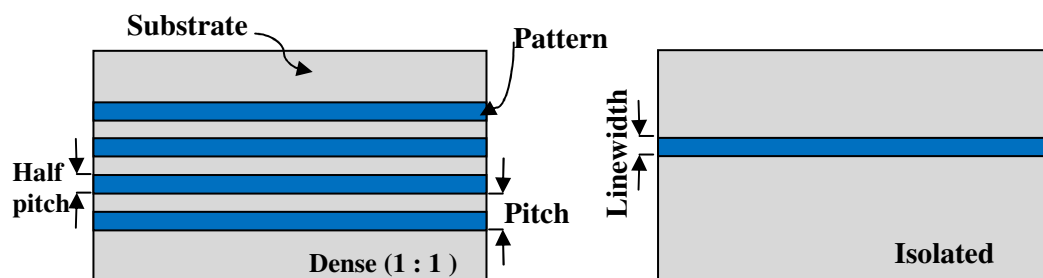


Figure 1.24: Resolution determined by (top) half of the achievable pitch in dense patterns, or (bottom) the linewidth in isolated patterns.

To define the dense and the sparse line resolutions pitch and LW are used, figure 1.24. Pitch is the distance covering a line and a space in a dense (1:1) periodic pattern and linewidth is the width of an isolated line in a sparse pattern.

1.5.1.3 Line-Edge and Line-Width Roughness

In order to function correctly an electronic device requires accurate pattern placement. Fluctuations in the patterned lines can affect the performance of a device. As feature size have shrunk to the nano scale deformities in the trenches become more problematic. To characterize resist performance we define line edge roughness (LER) as the average deviation of the physically patterned feature sidewall from the planned sidewall.

The line width roughness (LWR) describes the deviation of both sides of the feature edge that changes from the target dimension. For uncorrelated roughness LER and LWR are related as shown by [62]

$$LER = \frac{LWR}{\sqrt{2}} \quad (3.3)$$

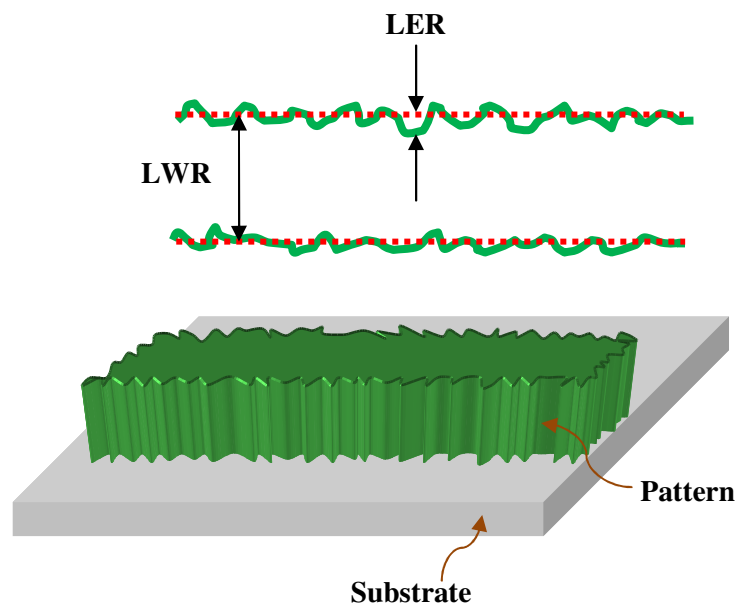


Figure 1.25: Random fluctuations on a pattern's edge

During the exposure, any statistical fluctuation or noise can cause rough edges. When patterning a logic gate the LWR must remain within 10% variance of the nominal dimension to prevent undesirable levels of variation in the electrical

characteristics of the device.[63 – 65] Thus it is very important to control the LER. There are some material factors that one should control to reduce LER. These factors are – the molecular weight of resist components,[66–69] molecular weight distribution,[70] molecular structure,[71, 72] and the distribution of resist components.[73, 74] If the resist has low molecular weight the LER will be lower.

The LER increases due to mask defects,[75] poor aerial image contrast, [76,77] short noise effects due to random fluctuations in exposure dose, and unsuitable development processes.[78 –80] In chemically amplified resists (CAR) acid diffusion can contribute to LER.[67,68, 81].

1.5.1.4 Etch resistance

A resist should have a very good etch resistance for transferring patterns to the substrate using a plasma etching process. The etch rate of a resist depends on etching gases and process conditions, as well as the molecular structure of the resist itself.

The etch rate of a resist will depend on the etch conditions. In general plasma etcher is used, and the conditions that can influence the etch rate include - etchant gas composition, pressure, temperature, and power of the plasma etcher.

A very good etch selectivity of resist is required to allow further substrate etch and less resist loss. However, the molecular structure and composition of a polymer based resist is very complex and to predict the relationship between the chemical structure of the resist and etch rate Ohnishi parameter [82] and the Ring parameter [83] are widely used by researchers.

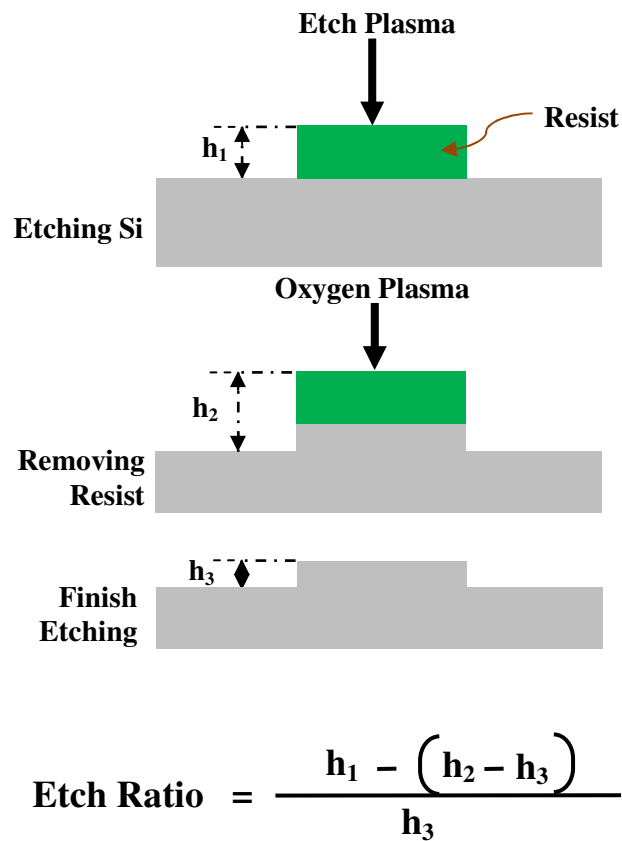


Figure 1.26: Si etching

The Ohnishi parameter states that the etch rate is proportional to the effective carbon content in the polymer, as a function of

$$\frac{N}{N_C - N_O}$$

where, N , N_C and N_O are the total number of atoms, number of carbon atoms, and number of oxygen atoms, respectively, per molecule.[82]The Ohnishi parameter describes the basic etching trend of organic molecules and most polymers follow this trend very well. This parameter is useful when the etching process is done with very high energy (300 – 500 eV) ion bombardment; however it showed a poor relationship to chemical structure for etch rates in a downstream glow discharge.[84]

To find a better predictor for etch rate in a high ion-density and low-ion-energy plasma, Kunz [83] has introduced an additional parameter called the Ring parameter, which is the function of

$$\frac{M_{CR}}{M_{TOT}}$$

where, M_{CR} and M_{TOT} are the mass of the resist existing as carbon atoms contained in a ring structure and the total resist mass, respectively.[83] This parameter is a rough model and only works with the polymers which have atomic rings.

More carbon atoms in aromatic ring leads an improved etch durability resist. Thus if a resist's Ohnishi parameter is small and the ring parameter is high thus suggests that resist will have high etch durability.

1.5.2 Resist mechanism

Resist can be categorized as either non-chemically amplified (non-CA) or chemically amplified (CA). The main different between a non-CA and a CA resist is that the non-CA has lower sensitivity because each incident photon (or electron) causes at most one reaction, and for the CA resist a catalytic chain reaction is initialized by each photon (or electron), given high sensitivity.

1.5.2.1 Non-chemically amplified resist

The mechanism of non-CA resists function is through a molecular weight solubility switch; in case of positive tone non-CA resists (such as PMMA) when the resist is irradiated with light/ebeam the polymer undergoes chain scission of the backbone, resulting in low molecule weight polymer fragments in the exposed area, which are

more soluble. In the case of a negative tone non-CA resist (such as HSQ), irradiation leads to a cross-linking reaction between monomers increasing molecule weight and thus decreasing solubility in the developer.

1.5.2.2 Chemically Amplified Resists

In 1980, the IBM research lab at Almaden developed a new concept for a resist, which had significantly higher sensitivity. This class of resist is known as a chemically amplified resist (CAR). Chemically amplification (CA) relies on a photo generated species to catalyze a cascade of chemical reactions to alter the solubility of resist.[89] It therefore increases the photosensitivity; by allowing a single incident photon to expose many resist molecules.

CA typically involves the release of acid from a photoacid generator (PAG), which catalytically removes an acid labile protecting group from the polymer, leading to a solubility switch. Alternatively the acid may catalytically induce crosslinking for negative tone, e.g. via an epoxy group.

According to Ito,[85] a CAR should ideally – be soluble in commercial by acceptable solvents, form a very uniform and defect free film; have very high sensitivity, contrast resolution and etch resistance; and low LER. It should also be very easy to synthesize, stable enough to store at room temperature (i.e. high thermal stability), have almost no hazards for the environment and health, and be very low cost. The photoactive compound in the CAR system is (typically) a photoacid generator, which decomposes by irradiation, and releases a strong acid (also referred to as a proton). This acid, for instance by causing the removal of a labile group, and importantly is regenerated in the process, see figure 1.27. The regenerated proton then

goes onto reacts with further resist group, leading to the increase in sensitivity.

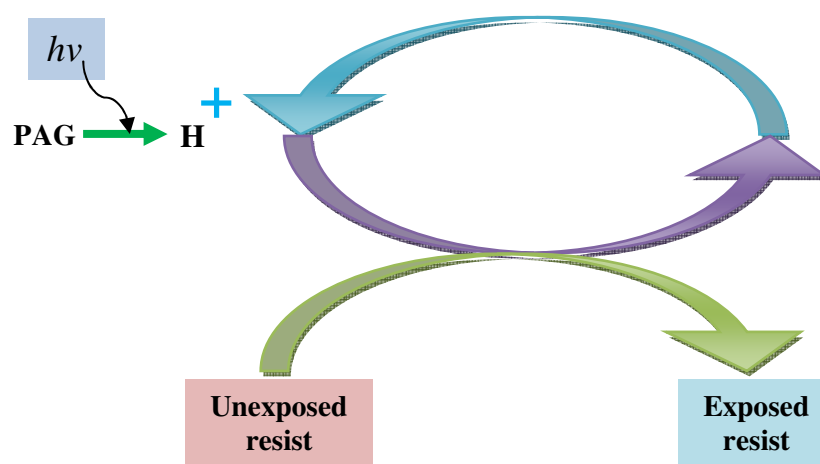


Figure 1.27: Chemical Amplification [48]

As the acid is regenerated the reaction proceeds in a catalytic manner, i.e. one acid can catalyze many de-protection reactions (see figure 1.28). The acid labile group is typically non-polar. When it is removed, it reveals a polar functional group, which changes the solubility of the polymer in appropriate solvents. To activate this catalytic de-protection reaction thermal energy is essential after exposure, and thus a post exposure bake (PEB) is used to promote the acid catalysis.

To form a negative tone resist we can use a solubility switch, but it is also possible to use polymerization.[87] For polymerization, a resist typically consists of a crosslinker, such as an epoxide and photo-initiator. During the curing stage, crosslinking of the epoxy is induced by the photo-initiator (which is often also a PAG, e.g. onium salt [88, 89]). The activated PAG reacts and opens an epoxy ring, which enables crosslinking with other molecules. Eventually this will form a 3D crosslinked network in the exposed area, which becomes insoluble in an organic developer.

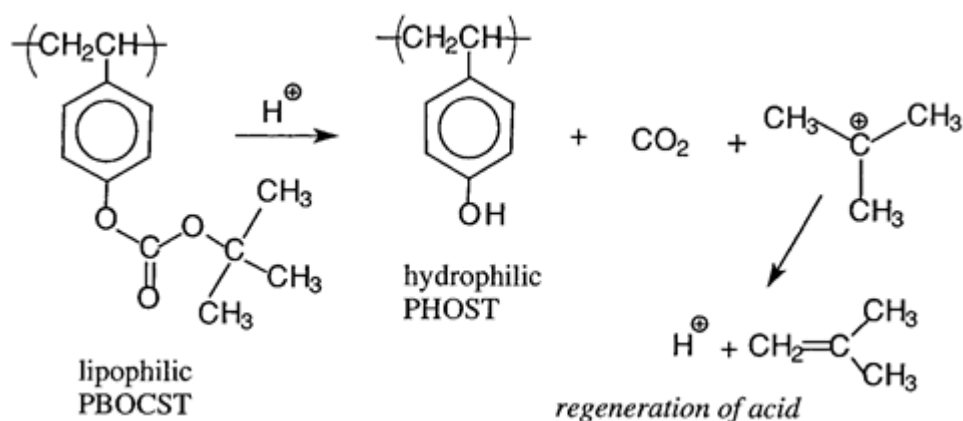


Figure 1.28: De-protection reaction, which leads to the conversion of a non-polar polymer to a polar polymer via an acid catalyzed reaction. Using a polar solvent such as alcohol or aqueous base as a developer, this will form positive image (removed in exposed areas) and using organic solvents such as chloroform or dichloromethane will form negative image. [90]

Figure 1.29 shows an example of a commercially available PAG, triphenylsulfonium hexafluoroantimonate (TPS-SbF₆) generating fluoroantimonic acid (H⁺SbF₆⁻) upon radiation and then initiating crosslinking of 9,9-bis(4-hydroxyphenyl)fluorene diglycidyl ether (EP-2) epoxide.

The primary drawback of crosslinking negative tone resist is the swelling of features that has been observed after development of high resolution patterns. This occurs because the organic solvent penetrates into the crosslinked network during development cause a volume increase which distorts the patterns. This feature swelling problem has been solved by blending polyhydroxystyrene (PHOST) with PAG and an appropriate amount of epoxy novolac resin.[92, 93]

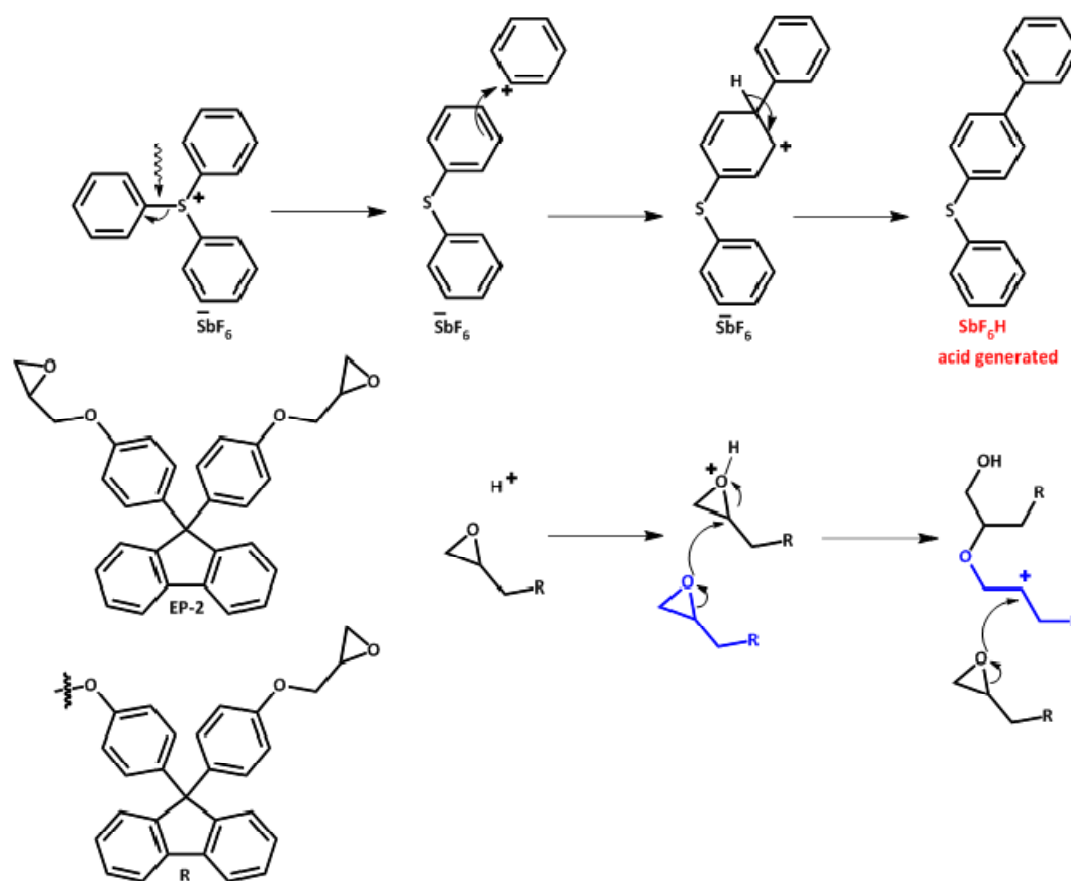


Figure 1.29: Process of acid generation and epoxy crosslinking. [91]

1.5.3 Electron beam resists

There are two main classes of EBL resist – polymer and molecular [94–97] based resist, which can both be either positive or negative tone. When an ebeam irradiates a suitable polymer resist it either crosslinks the polymer architecture by forming insoluble material (i.e. negative tone), or breaks the polymer backbone reducing the polymer molecular weight and forming soluble material (i.e. positive tone). By using suitable developer the unexposed areas of negative tone resist or the exposed areas of positive tone resist will be removed.

Most current resists are polymer based. However, these materials have performance limitations such as line width roughness (LWR) and low resolution.

Small molecule based resists such as – oligomers [94– 98], discotic liquid crystals [8] and inorganic materials are alternatives to polymer resists, which promise improved LWR and higher resolution. Fullerene (C_{60}) derivative based molecular resists have shown promising results [99–105] in negative tone behavior by patterning about 10nm features. For example, the LWR required in current industrial lithography [106] is the same size as the radius of gyration of a polymer molecule in a typical polymer based resist. As resolution continues to increase and future nodes require smaller features, the LWR will become smaller than the polymer molecules. However, the sensitivity of molecular resist is typically very poor, which increases patterning time.

Besides fullerene [100 – 102] another molecular resist that has shown promising results for ebeam lithography is poly-substituted triphenylene.[107 – 109] Both of their molecular diameters are ~1 nm and they are sensitive to ebeam radiation. Because they are carbon rich, they are very etch durable. The low sensitivity of these resists can be overcome by chemical amplification.

1.5.3.1 Positive electron beam resists

According to the definition of a positive tone resist, the areas exposed to ebeam should be completely removed by the developer during the development process. Usually positive tone resists are made with high molecular weight polymers and during the ebeam exposure electrons cause bond breakage (chain scission) in the exposed areas. As a result in the exposed areas the average sizes of the polymer molecules are directly reduced and the remaining fragments are significantly more soluble than unexposed polymer molecules in an appropriate developing solvent. Several examples are given below.

Poly methyl methacrylate (PMMA) is one of the earliest resists developed for electron beam lithography.[110] It is still the most commonly used low cost positive tone ebeam resist. The molecular weight of PMMA resists vary between 50,000 - 2.2 million (according to MiroChem Corp.), it is typically spin coated from anisole or chloroform and developed in MIBK (methyl isobutyl ketone):IPA (isopropyl alcohol) solvents. Depending on the radiation source, equipment, developer, development time and pattern density the sensitivity of PMMA is between 50 – 500 $\mu\text{C}/\text{cm}^2$ at 30 keV electron acceleration voltage. PMMA already has demonstrated resolution below 10 nm,[111] but it has poor sensitivity, poor dry etch resistance and moderate only thermal stability.[112]Although PMMA is suitable for high resolution patterning, patterns with high density and high aspect ratio features tend to collapse or become progressively worse due to swelling.

ZEP is another polymer based resist, which was developed by Nippon Zeon Co. It is based on poly-methyl- α -chloro-acrylate-co- α -methyl-styrene. It is typically spin coated from anisole and developed in n-amyl acetate. ZEP520 has higher sensitivity and etch resistance than PMMA, but the exposed pattern shows elevated LER,[113] at 10 keV the sensitivity of ZEP is 8 $\mu\text{C}/\text{cm}^2$. [111]

Poly(1-butene sulfone) (PBS) is a chain-scission resists and common for mask making for its high sensitivity, which is around 3 $\mu\text{C}/\text{cm}^2$ at 10 keV.[114]Its common developer is MIAK (5-methyl-2-hexanone):2-pentanone (3:1) [115]. However, it has poor etch resistance and needs to be processed at a very well controlled temperature and humidity. [116]

Poly -2,2,2 tri-fluoro-ethyl- α -chloro-acrylate, also known as EBR-9 [117] is used for mask making for its long shelf life, high sensitivity, which is around ~10

$\mu\text{C}/\text{cm}^2$ at 20 keV[118] and has large process latitude, however it swells during the development process.[118] It is typically spin coated from anisole or chloroform and developed in MIBK :IPA solvents.

1.5.3.2 Negative electron beam resists

The pattern formation in a negative tone resist is the reverse of the pattern formation in a positive resist. During exposure, crosslinks form between the polymer chains on these resists, and thus only the unexposed areas dissolve after exposure while the exposed resist areas remain. Several examples are given below.

Microposit SAL601 developed by Shipley is a widely used CA negative tone ebeam resist. It has high sensitivity, which is 7 - 9 $\mu\text{C}/\text{cm}^2$ at either 20 or 40 keV,[119] high contrast; reasonable resolution (less than 0.1 μm in 0.4 μm thick films, exposed with 40 keV ebeam at 8.4 $\mu\text{C}/\text{cm}^2$ [119]) and high dry etch selectivity.[120]The typical developer for SAL601 is Shipley MF-322:water (1:1). However, SAL601 has problem with scum and bridging between dense features, poor adhesion, a very short shelf life and post exposure delay due to acid diffusion.[121]

NEB31 was developed by Sumitomo Chemical, is a negative tone ebeam resist with sensitivity 50 $\mu\text{C}/\text{cm}^2$ at 100 keV,[121] which has shown high resolution (e.g. 28 nm structures), high contrast, good thermal stability; good dry etch resistance, and long shelf-life.[122] However, it has post-exposure instability that limits resolution.[123]The typical developer is Shipley MF-321 or TMAH (tetramethylammonium hydroxide).

Hydrogen silsesquioxane (HSQ) is a negative tone ebeam resist that is also used for nano-imprint and extreme ultra violet (EUV) Lithography.[124 – 127] Although HSQ has shown high resolution (sub ~10 nm),[128] high contrast, minimal line width roughness (~7 nm), good etch resistance, and a high degree of mechanical stability,[129, 130] it has problems with sensitivity (i.e. 800 $\mu\text{C}/\text{cm}^2$ at 100 keV) [131] and contrast stability. It has been observed that by delaying between coating and exposure or between exposure and development its sensitivity decreases and contrast increases. This effect is exacerbated if the baking temperature increases.[132] The typical developer for HSQ is TMAH.

COP is an epoxy based copolymer of glycidyl meth-acrylate and ethyl acrylate. It has very high sensitivity (~0.3 $\mu\text{C}/\text{cm}^2$ at 10 keV).[133] Although it demonstrates good thermal stability, its resolution is very poor (around 1 μm [133]), because of a swelling issue in the crosslinked region it also has poor etch resistance.[133] Typical developer for COP is MEK (methyl ethyl ketone) : ethanol (7:3).[133]

PMMA, ZEP and HSQ are by far the mostly widely used of the electron beam resist.

1.6 Charge dissipation in ebeam lithography

Although electron beam lithography has the capability of producing a high resolution pattern none of the commercial ebeam resists are capable of patterning below 100 nm on an insulating substrate due to resist charging issues.[49–51, 107] The most common problems are pattern displacement, distortion, and difficulties with

alignment metrology. During the exposure, charges will become trapped in the resist and the substrate, if the substrate is made with insulating materials (e.g. glass, quartz, etc.) or coated with (thick) insulating layers (e.g. silicon dioxide). The electron beam is deflected by the charged surface, which can cause pattern displacement.[50, 51, 134, 135] Both the surface charges and the trapped charges are responsible for pattern distortion, and in addition alignment errors in lithographic level-to-level registrations are likely.[136]

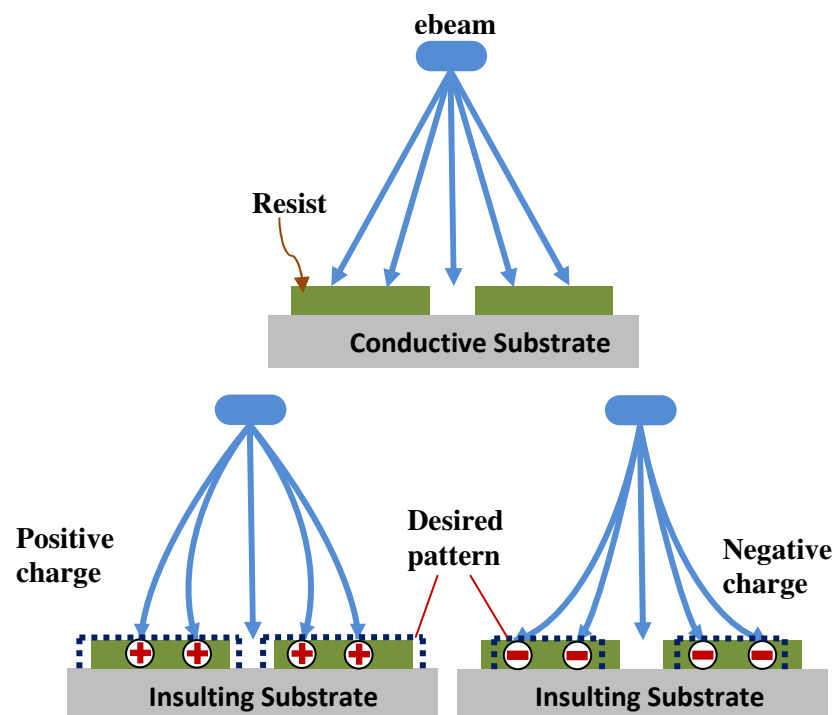


Figure 1.30: Surface charging deflects the incoming ebeam (after N. Okai) [137]

Figure 1.30 shows that when the substrate is a conductive material, e.g. silicon, the electron trajectories are straight, however when the substrate is an insulator, e.g. glass, the electrons will be deflected due charge building up in the insulator, which causes significant pattern displacement. Due to the more static nature of the charging effect it is not possible to correct the distortion via preprocessing.

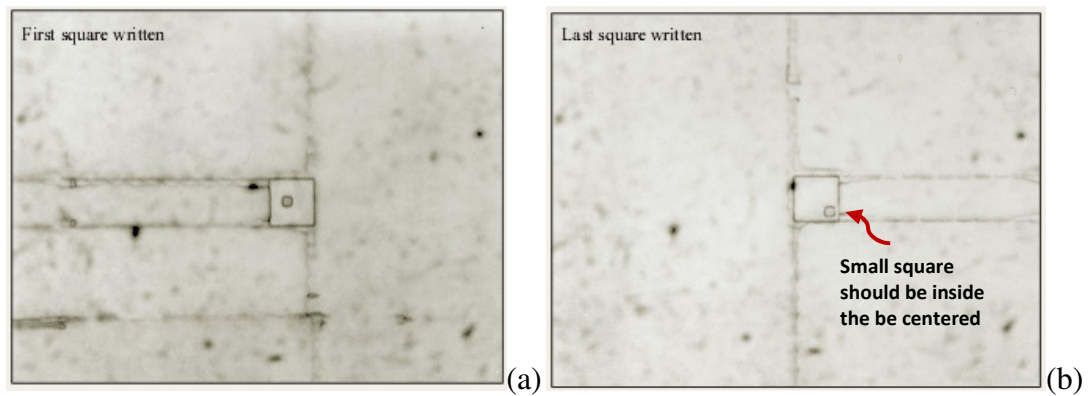


Figure 1.31: Example of pattern displacement due to increasing charging (low (a) to high dose (b)) of the substrate over the course of an exposure run [18]

Figure 1.31 shows an example of pattern displacement between first and the last square written on a sample without applying a conducting layer underneath or top of the ebeam resist, a displacement greater than $5\mu\text{m}$ is measured across a 5mmchip.[18]



Figure 1.32: Pattern distortion due to substrate charging [138]

Figure 1.32 shows an example of pattern distortion on an insulating substrate without any discharge layer. Here the feature should be 90° angles, however there is significant a variable distortion.

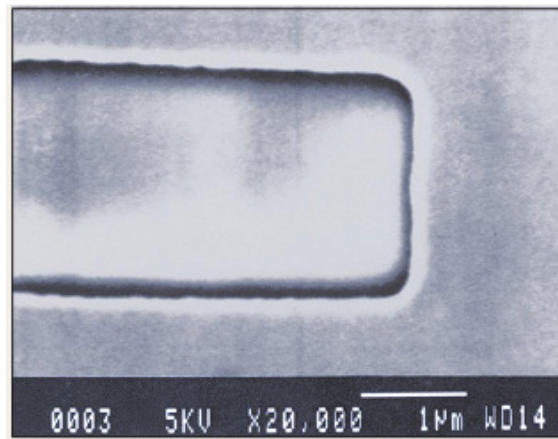


Figure 1.33: Image charging at 5keV [139]

Figure 1.33 shows an example of too much charging at 5 keV under SEM with no conducting layer on top of the pattern before taking the image.[139]The brighter areas around and on top of the feature shows significant trapped charges inside the resist.

It has been reported that conductivity greater than or equal to 10^{-2} S/m will prevent pattern displacement.[140] Thus to overcome pattern distortion conducting materials can be integrated with the resist system by coating them above or below the resist, to work as a discharge layer.

For example - indium tin oxide (ITO) [140] or carbon films (coated by chemical vapor deposition (CVD) [141]) or any thin metal coating [142, 143] can be applied as an electron discharge layer. However, these solutions are not ideal. These materials require special deposition methods and techniques, which can introduce issues. For example, during the CVD method the process generates heat and radiation, which ultimately decomposes or degrades the resist and decreases lithographic performance. At the same time post lithography removal of these coated materials is quite difficult, which makes the fabrication process more complicated.

Some conductive polymers [144, 145] also been proposed as charge dissipation layers, such as polyphenylene,[146] polypyrrole,[147] polythiophene,[148] polyaniline,[149] or poly(3,4-ethylenedioxythiophene) poly(styrenesulfonate) (PEDOT:PSS).[136] These materials can potentially be spin coated below or above the ebeam resist. However, the discharge layer underneath the resist enhances the EBL process.[150] Although these processes may solve pattern distortion or displacement issues, they add complexity and cost for industries that require patterning on insulating substrates.

Water-soluble ammonium poly(p-styrenesulfonate) [151, 152] can be used as an ionically conducting charge dissipator. Although it features easy process steps, such as, preparation by spin coating, its conductivity is very low and the efficiency of charge dissipation is very small,[153] hence it is not very useful to use as a charge eliminating layer for insulating substrates.

In order to avoid all these complexities it would be ideal to develop a resist that is conductive enough to dissipate electrons through the resist itself, and that will therefore overcome the substrate charging issues and pattern distortion. At the same time this resist should be capable of recording very high resolution patterns with high etch resistance and high sensitivity for fast patterning.

Thus, it is necessary to engineer a new conductive resist to avoid the limitations of current systems. The concept of this new resist is to achieve high resolution with low LER by utilizing a small molecule material instead of polymer.

1.7 Why Triphenylene derivatives

In this project a triphenylene derivative based resist (2,3,6,7,10,11-hexapentyloxy triphenylene (C5C5) [107]) and its derivatives are studied. These materials were developed in collaboration with the School of Chemistry at the University of Birmingham, to show sufficient conductivity to eliminate the need for any sort of separate charge dissipation layers.

Triphenylene ($C_{18}H_{12}$) is a poly aromatic hydrocarbon molecule with four benzene rings fused together. Many of its derivatives are well known discotic liquid crystal materials. Derivatives have demonstrated performance as negative tone ebeam resists. The sensitivity range of pure C5C5 was found to be between 1.5 – 6.5 mC/cm² at 20 keV.[107 – 109]

The conductivity of a triphenylene derivative has been found to be $\sim 10^{-9}$ S/m [154] and it has also been observed that by adding 50 – 66% of trinitrofluorenone (TNF) it is possible to increase its conductivity up to 10^{-8} S/m [155], see figure 1.34.

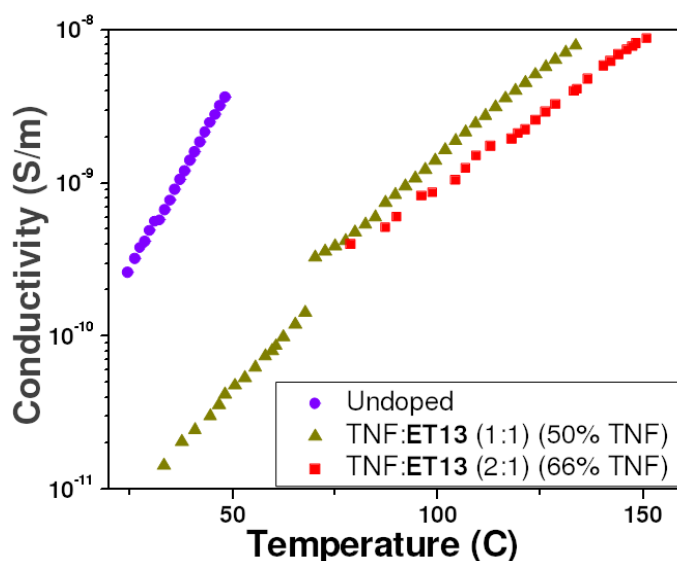


Figure 1.34: Conductivity vs. temperature for a pure and doped film of a Triphenylene derivative [155].

Triphenylenes are excellent photoconductors.[156] These molecules are very well ordered into columns, as shown in figure 1.35,[108] (as has been demonstrated by small-angle x-ray scattering (SAXS)). Due to their hexagonal columnar discotic liquid crystal structure [157] they showed fast hole mobility (e.g. $10^{-3} \text{ cm}^2\text{V}^{-1}\text{s}^{-1}$) along the columns.[158]

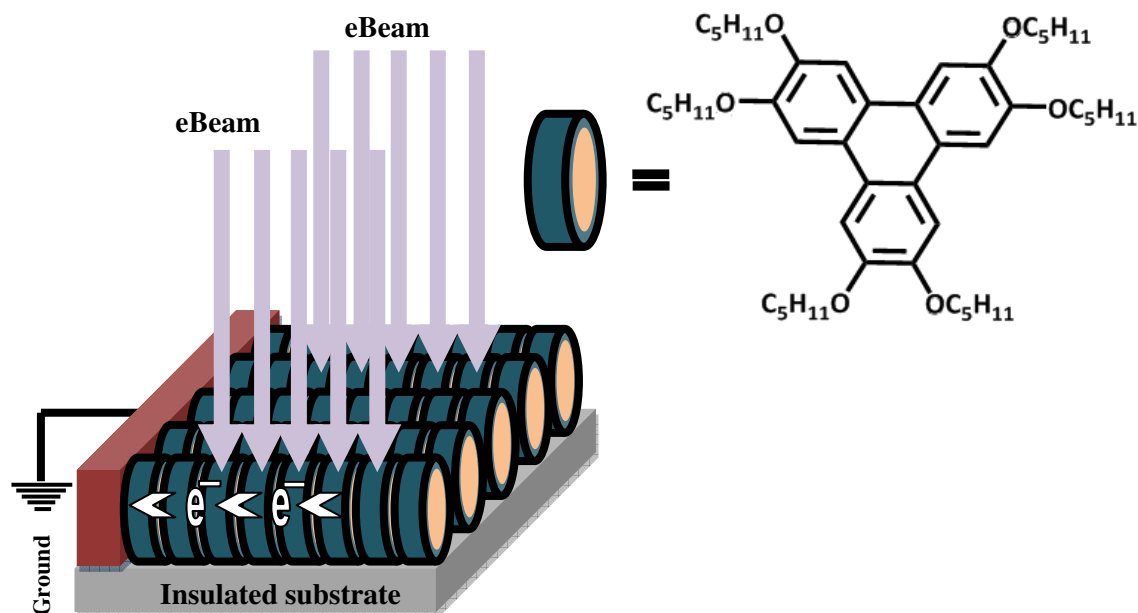


Figure 1.35: Triphenylenes' columnar structure demonstrating the proposed discharge mechanism (after J.A. Preece) [108].

Triphenylene based resists demonstrate both positive and negative tone behavior [103, 159, 160] when irradiated with an ebeam.[113] They have very high resolution; low LER and high etch durability compared to polymer resists.[160] Each triphenylene has three-fold rotational symmetry in a planar aromatic structure, figure 1.36(a), and can easily be functionalized at multiple sites, as shown in figure 1.36(b).

These molecules are easily dissolved in chloroform, propylene glycol monomethyl ether, propylene glycol monomethyl ether acetate, ethyl lactate, cyclohexanone and other solvents. For spin coating and as a negative tone resist the

same solvents may serve as developer, together with others such as chlorobenzene and n-butyl acetate. In the positive tone mode a polar developer such as an alcohol is preferred.

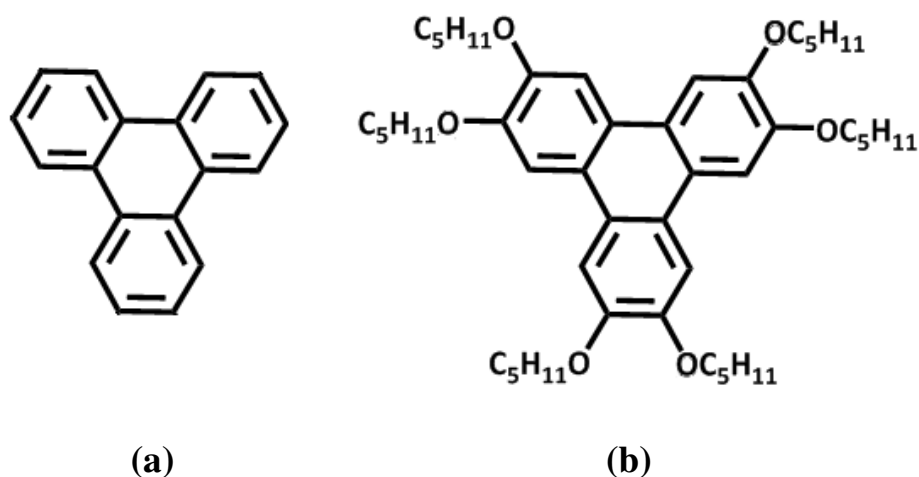


Figure 1.36: (a) Pure triphenylene (b) Triphenylene derivative with functional groups

To make a CA resist, three types of compound will be mixed in appropriate ratios. These are – C5EPX, C5OH and a PAG. The C5EPX has a triphenylene core with epoxide arms, which allows crosslinking during exposure to give the patterning mechanism. A PAG (e.g. TPS SbF_6 , TAS SbF_6 etc.) that will open the epoxide and cause polymerization is incorporated to enhance sensitivity. The function of the C5OH in the CA resist is to terminate the polymerization reaction of a given epoxy chain; otherwise the reaction will continue which will cause larger line width roughness and poor resolution.

Chapter 2

Experimental Techniques

2.1 Thin film processing

It is first necessary to formulate the resist. A suitable solvent should be used to dissolve the resist compound perfectly in order to make a smooth homogenous film on the substrate. The C5C5, C5EP, C5OH and the PAGs all dissolve well in chloroform. However, due to health hazards chloroform is not accepted by the semiconductor industries. Therefore other solvents such as – propylene glycol monomethyl ether acetate (PGMEA), cyclohexanone, ethyl lactate (EL) and anisole were also used to prepare the resist. As well the performance compared to the chloroform performance cast film results for both lithography and conductivity measurements. More details of resist preparation with different solvents and tests is given in chapter 3, section 3.1.

For lithography experiments both silicon and insulating substrates, such as – glass, quartz, fused silica, borosilicate and atomically smooth glass were used. For the conductivity measurements only the glass substrate was considered. For different experiments different sizes of substrates were sliced using a Disco DAD321 dicing saw.

For preparing the resist film, the very first step is to clean the substrate. This process starts by soaking the substrates in acetone with ultrasonic agitation for 5 – 10 minutes, and then dipping it into isopropyl alcohol (IPA) with ultrasonic agitation for 5 – 10 minutes. This step is to remove soluble contaminants and dust from the substrates. After cleaning, all substrates were rinsed in de-ionized (DI) water for 2 – 5 minutes. Then they were dried with dry nitrogen.

In some cases where difficulties may arise with film formation due to poor resist wetting to the substrate it can help to prepare a hydrogen-terminated substrate. This can also help when poor resist adhesion is observed upon development. This step should start right after the acetone/IPA cleaning and DI water rinsing. The substrates are immersed in a solution of sulfuric acid (H_2SO_4) and hydrogen peroxide (H_2O_2) in a 1:1 ratio for 10 minutes, then rinsed in DI water, immersed into a weak aqueous solution of hydrofluoric acid (HF) for 1 minute, and then finally rinsed in DI water and dried with nitrogen. To achieve the best result it is recommended to spin coat immediately after the HF cleaning step.

To coat a thin film, a spin coater was used. The substrate is placed on a vacuum chuck that can be rotated at a controllable angular velocity for a given time. A quantity of resist is deposited onto the substrate and the chuck rotated while the resist dries to ensure the solution spreads evenly on the substrate as it dries. To produce different thickness of films it is necessary to control the resist concentration and/or the spin speed. Spin coating starts with setting a spinning recipe into the spinner's system. This spinning recipe controls the spin chuck's rotation angular velocity (i.e. revolution per minute or RPM), spinning duration, and ramp speed (i.e. how quickly the tool reaches the required spin speed). The full spinning process can require multiple stages as shown in figure 2.1. In some cases, where the resist's casting solvent evaporated very fast, e.g. chloroform, it is necessary to skip the

spreading step. When the recipe settings are complete, the substrate should be placed on the vacuum chuck of the spin coater, and then a pre-measured amount of resist (e.g. 100 μL) should dispense onto the substrate with a pipette. If the resist's casting solvent is chloroform, to achieve the best film formation, it is necessary to start the spinner immediately without any delay. Because chloroform evaporates very quickly, the resist solution may already have partially dried in the event of a delay, which will lead to non-uniformity in the film thickness.

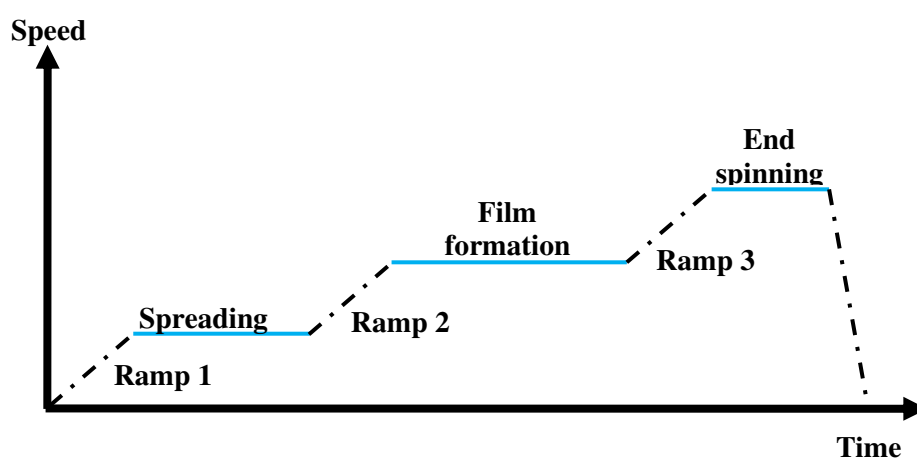


Figure 2.1: Film formation stages by spin coater

Although most of the solvent evaporates during spin coating, a bake may be applied to remove any residual solvent. This may be referred to as a soft bake, or a post application bake (PAB). For these materials the soft bake was typically 50 $^{\circ}\text{C}$ for 2 minutes (a more typical temperature for PAB is around 100 $^{\circ}\text{C}$ but the liquid crystal nature and the triphenylenes limit the maximum used here). The PAB process can also give adhesion improvement, and slightly reduce film thickness by removing residual solvent and compactifying the film. For some resists, higher temperatures may decompose the photoactive compound and can also cause undesirable crosslinking or oxidization, and thus it is necessary to optimize the PAB conditions for different resists.

After the spinning step the sample is ready for lithography or conductivity measurements. For lithography the exposure process was performed by a scanning electron microscope (SEM), modified to include a pattern generator for electron beam lithography. More detail of this process will be discussed in section 2.3.1.

After the exposure, a post exposure bake (PEB) may be required depending on the resist. PEB is typically an essential step for chemically amplified resists, which drives the catalytic reaction; the PEB causes some chemical reaction, which creates a solubility difference between the exposed and unexposed parts of the resist. It is very important to optimize the PEB for such types of resists.

The development process should start either right after the exposure (e.g. many non-CA resists) or after the PEB process (e.g. for CA resists). Development process starts with immersing the exposed sample into a developer, such as - monochlorobenzene (MCB), ethyl lactate (EL), propylene glycol monomethyl ether acetate (PGMEA), etc. for certain amount of time. For example, for CA triphenylene resist one might immerse it into MCB for 10 seconds, and then rinse in DI water.

In some cases, to make the resist more durable another baking step, known as the hard bake, applied after development, often at higher temperature (e.g. ≥ 120 °C). This baking step can further remove residual solvents and gasses that may be trapped within the resist pattern, and will make the resist durable in subsequent harsh environments for instance more stable for etching.

2.2 Measuring Conductivity

Electrical conductivity varies widely with different materials' electrical transport nature and electronic structure. Materials are generally classed as – metals, semiconductors or insulators as shown in figure 2.2.

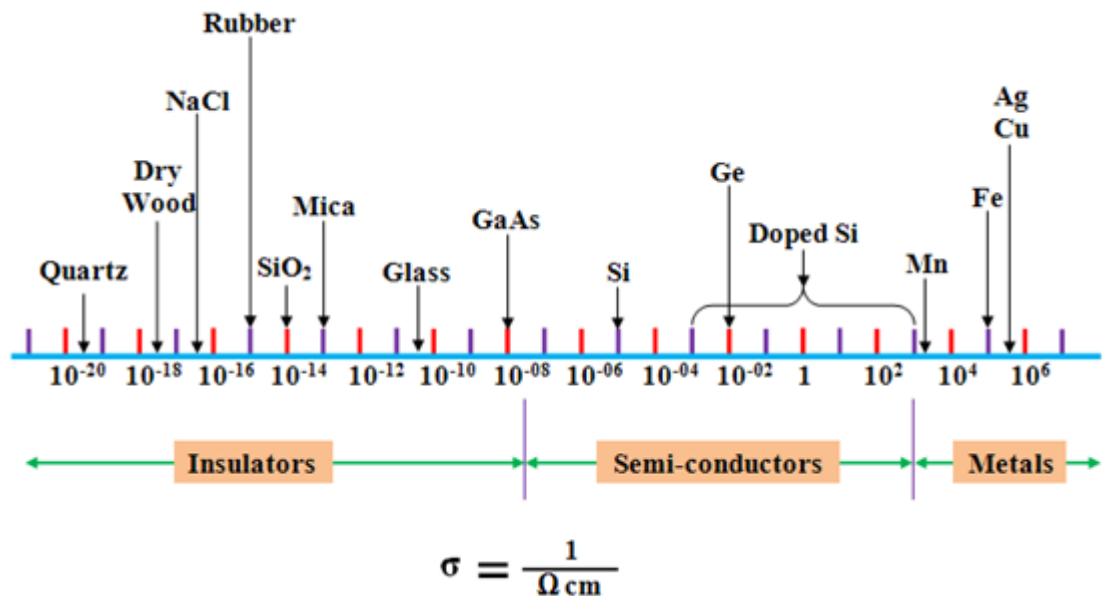


Figure 2.2: Conductivity scale for various materials at room temperature.

Scaling effects are one of the big problems for measuring conductivity for thin films, as they then influence the electrical properties of materials. Thin film conductivity depends on – (i) the film thickness, (ii) dimensions, (iii) material purity, (iv) surface roughness and (v) stability of the electrical transport. The conductivity for any material defined as,

$$\sigma = \frac{1}{\rho} \quad (2.1)$$

where, ρ is the resistivity, and the unit of σ is - Siemens/cm or S/cm.

2.2.1 Two and Four Point probe techniques

Two-point (see figure 2.3a) and four-point (see figure 2.3b) probe techniques are two common methods to measure resistivity. Both two-point and four-point methods are widely used in the semiconductor industry for test purposes, but generally the four-point method is used for precision and two-point for comparative purposes.

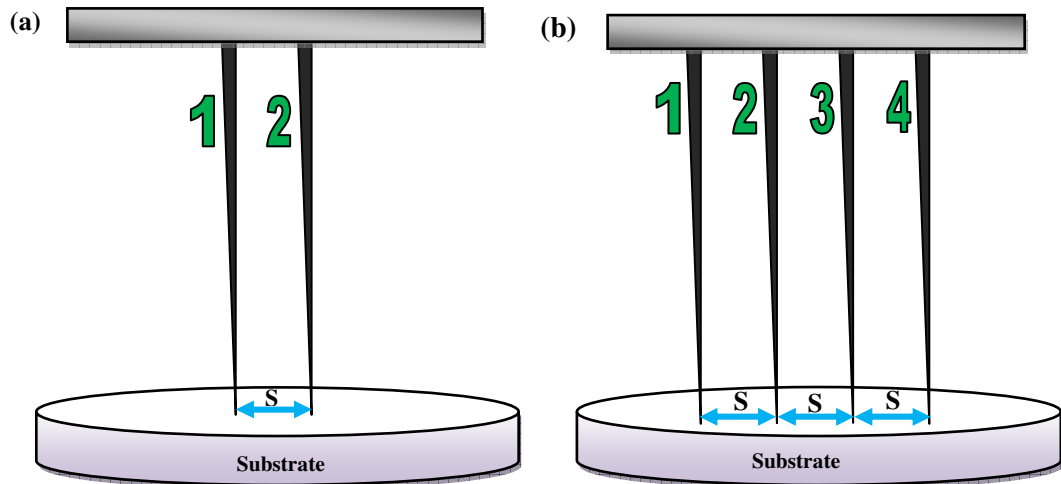


Figure 2.3: (a) Two point and (b) Four point probe test setup.

In the two-point probe technique, two probes are placed at a fixed spacing on the material surface, [161] Current is supplied through the probes, [162] and the voltage between the probes is measured using a voltmeter.[162] Thus the total surface resistance (R) between two probes can be measured as

$$R = 2R_C + 2R_{SP} + R_S \quad (2.2)$$

where, R_C is the parasitic contact resistance between the material surface and the probe touching the surface.[162, 163] R_{SP} is the spreading resistance, or the parasitic resistance caused by current flowing into the sample surface in direction other than between the probes and R_S is the surface resistance of the material.[162, 163]

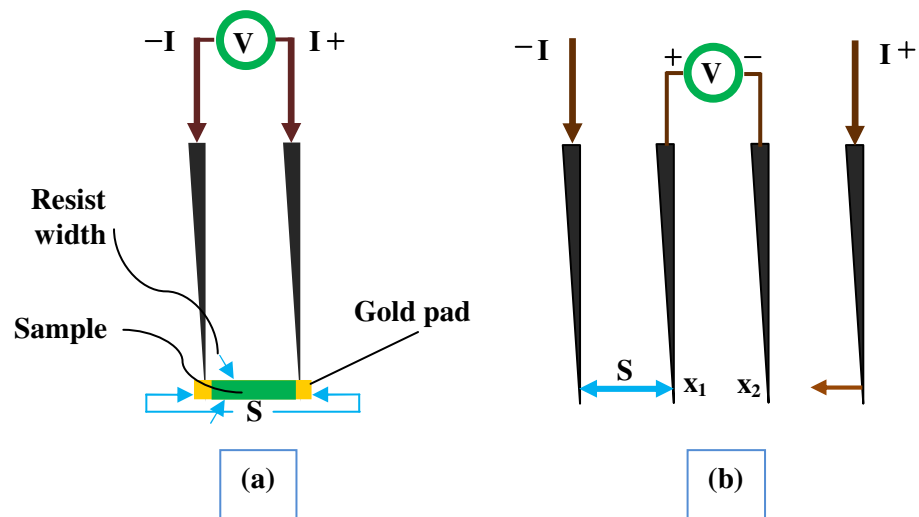


Figure 2.4: Schematic of (a) two-point probe and (b) four-point probe configuration

Figure 2.4(a) shows the two-point probe method where current is supplied and voltage measured by using two probes. The typical probe spacing (s) is around 1mm. In the two-point probe setup, both probes (e.g. 1 and 2) are carrying current (I), and measuring voltage (V).

Figure 2.4(b) shows the four point probe measurement technique, where a probe with 4 equally spaced metal tips with finite radius is placed in a contact with the sample to be measured, current flows between two outer probes (e.g. 1 and 4) and voltage is measured between two inner probes (e.g. 2 and 3). [163]

The four-point probe technique was first described by Wenner in 1916. [161,162] By having two additional probes the four-point probe technique measures the voltage potential of the material surface, which helps to eliminate the parasitic resistances R_c and R_{SP} , measured in the two-point probe method. [161 - 163] Thus the resistivity (ρ) may be calculated as

$$\rho = \left(\frac{V}{I} \times \frac{w}{S} \times t \right) \quad (2.3)$$

where, I is the applied current, V is the measured voltage, w is the sample's width, S is the separation of probes and t is the thickness of the sample.

With both two and four-point probe techniques it is possible to measure resistivity of any bulk or thin samples.

For measuring a bulk samples resistivity in the four-point probe technique few assumptions were made i.e. a spherical projection of current spreading out from an outer probe tip, an infinitesimal tip and that the sample is semi-infinite in the lateral dimension. Thus the differential resistance is given by

$$\Delta R = \rho \left(\frac{dx}{A} \right) \quad (2.4)$$

Integrating ΔR , between the x_1 and x_2 points of the inner probes, we get

$$R = \int_{x_1}^{x_2} \rho \left(\frac{dx}{A} \right) \quad (2.5)$$

where, A is the measured area and $A = 2\pi x^2$, thus eq. (2.4) becomes

$$R = \int_{x_1}^{x_2} \rho \left(\frac{dx}{2\pi x^2} \right) \quad (2.6)$$

$$R = \frac{\rho}{2\pi} \frac{1}{2s} \quad (2.7)$$

where, s is the uniform probe spacing. Because of the superposition of current at the two outer tips, the resistance will become

$$2R = \frac{V}{I} \quad (2.8)$$

Substituting eq. (2.8) into (2.7), we get the resistivity,

$$\rho = 2\pi s \left(\frac{V}{I} \right) \quad (2.9)$$

When measuring the resistivity of a thin sample or thin film the thickness t is much smaller than a probe spacing s , i.e. $t \ll s$, and the area $A = 2\pi xt$, and thus eq. (2.5) becomes

$$R = \int_{x_1}^{x_2} \rho \left(\frac{dx}{2\pi xt} \right) \quad (2.10)$$

$$R = \frac{\rho}{2\pi t} \ln 2 \quad (2.11)$$

Substituting eq. (2.8) into (2.11), we get the resistivity,

$$\rho = \frac{\pi t}{\ln 2} \left(\frac{V}{I} \right) \quad (2.12)$$

$$\frac{\rho}{t} = \frac{\pi}{\ln 2} \left(\frac{V}{I} \right) \quad (2.13)$$

$$R_s = \frac{\pi}{\ln 2} \left(\frac{V}{I} \right) \quad (2.14)$$

$$R_s = 4.53 \left(\frac{V}{I} \right) \quad (2.15)$$

where, $R_s = \rho/t$, is the sheet resistance of the measured sample. Low sheet resistance indicates better conductivity. The resistivity is sometimes also called specific resistance because it derives material properties that give electrical resistance. In the case of a thin material sheet or thin film, the sheet resistance has to calculate first, and by multiplying it with the sample's thickness the resistivity can be obtained.

2.1.2 Van der Pauw Technique

It is difficult to measure the resistivity if the sample has a complex geometry. In this case the Van der Pauw (VdP) technique is more appropriate. The VdP technique is widely used in the semiconductor industry to determine the resistivity of hydrogen

samples.[165, 166] This technique has high accuracy for any arbitrary shaped sample as long as the sample is approximately two dimensional. A minimum two measurements should be performed, however to reduce the effects of thermo electromagnetic forces (EMF) in the contacts, a total eight measurements is recommended.[164] The sample should be flat, homogeneous, isotropic and have uniform thickness with no isolated holes.[165, 166] The probes must be placed at the edge of the sample and the contact area must be smaller than the sample's area.[165, 166] For measuring a sample with the VdP method, it is best to fabricate samples with a suitable geometry,[166] as illustrated in figure 2.5.

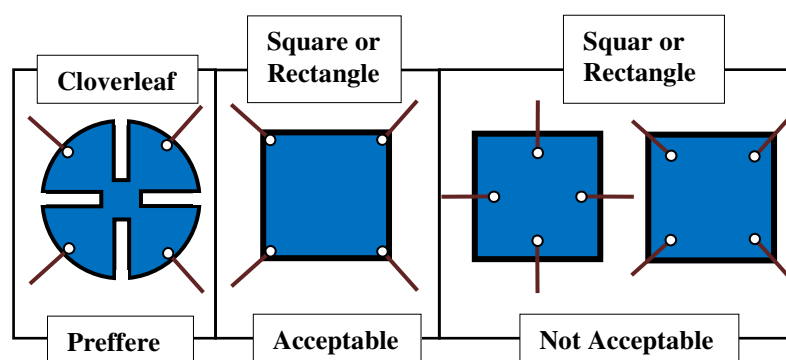


Figure 2.5: Sample geometries for Van der Pauw resistivity measurement.

The cloverleaf design will have the lowest error due to its smaller effective contact size, [166] however, as it is difficult to fabricate, generally the square or rectangle shape is acceptable.

According to VdP technique the sample's resistivity can be obtained by

$$e^{\left(-\pi\frac{R_A}{R_S}\right)} + e^{\left(-\pi\frac{R_B}{R_S}\right)} = \mathbf{1} \quad (2.16)$$

Here R_S is related to R_A and R_B , which are the two characteristic resistances of the sample.

To determine the values of R_A , R_B and R_S of a thin sample or thin film the geometry shown in figure 2.6 is used. For a perfectly symmetric sample where $R_A = R_B$, then the R_S will be

$$R_S = \frac{\pi}{\ln 2} R_A \quad (2.17)$$

For non-symmetric contacts with sample $R_A \approx R_B$, then the average of R_A and R_B is used to calculate R_S .

$$R_S = \frac{\pi}{\ln 2} \left(\frac{R_A + R_B}{2} \right) \quad (2.18)$$

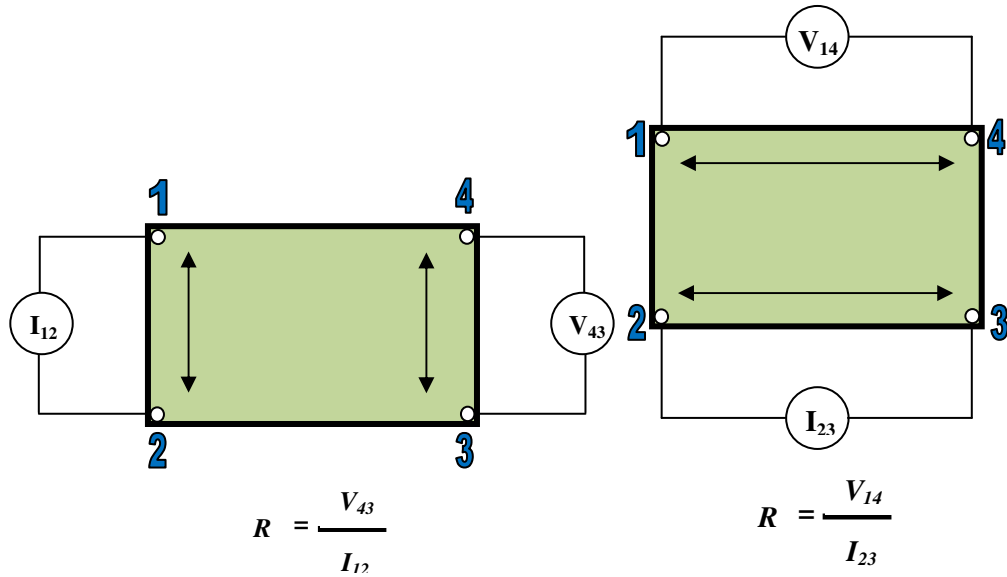


Figure 2.6: The VdP configuration to determine the two characteristic resistances R_A and R_B .

From figure 2.6, when current I_{12} is applied, voltage is measured across V_{43} whilst for $I_{23}V_{14}$ is measured. Thus by changing the contact positions one can set eight configuration measurements of I and V . Using ohm's law R_A and R_B can be calculated as:

$$R_A = \frac{1}{4} \left(\frac{V_{43}}{I_{12}} + \frac{V_{34}}{I_{21}} + \frac{V_{12}}{I_{43}} + \frac{V_{21}}{I_{34}} \right) \quad (2.19)$$

$$R_B = \frac{1}{4} \left(\frac{V_{14}}{I_{23}} + \frac{V_{41}}{I_{32}} + \frac{V_{23}}{I_{14}} + \frac{V_{32}}{I_{41}} \right) \quad (2.10)$$

Now by substituting eq. 2.19 and 2.20 in eq. 2.18, R_S can be calculated. Thus the sample's resistivity (ρ) would be

$$\rho = R_S \times t \quad (2.21)$$

2.3 Equipment

2.3.1 Scanning Electron Microscope

To study resists lithographic characteristics an XL30 SFEG (figure 2.7) scanning electron probe microscope (SEM), modified for electron beam lithography was used. The primary modification was the addition of a pattern generator to control how the ebeams is scanned over the substrate. The SEM works by focusing a beam of electrons, emitted from an electron gun, to a fine spot on the surface. For imaging the spot is rastered across the sample (i.e. swept from side to side whilst progressing mainly downwards) using deflection coils. The scattered electrons are detected to form an image. For the lithography the pattern generator (Raith Elphy Plus) assumes control of the deflection coils, allowing the beam to be moved to arbitrary locations for controlled durations to expose the resist.

Such a modified SEM can pattern nano-scale features. This patterning process is the interaction of the electrons with a resist when electrons are scattered by atom in the resist energy can be deposited and reactions occur. This has been described in chapter 1.

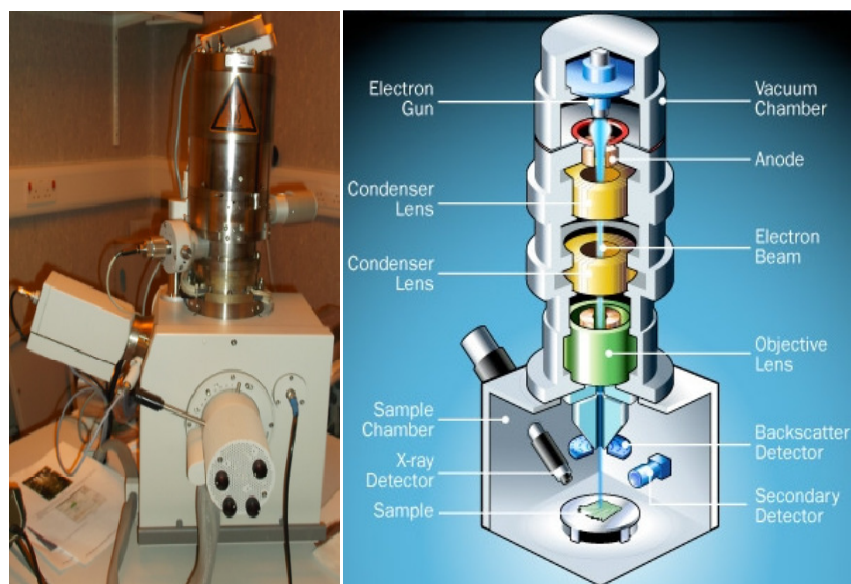


Figure 2.7: Left – the SEM used in this study. Right – schematic of an SEM with important components labeled [167].

In an SEM up to six types of signals are typically monitored. These are – secondary electrons (SE), back scattered electrons (BSE), characteristic X-rays, cathode luminescence (CL) light, specimen current and transmitted electrons. These signals are mainly generated from the interaction of ebeams with atoms on the sample's surface or near to it. It is rare to find a SEM which has detectors for all of these signals. SEs and BSEs are most common signals that most SEMs can detect, as is the case for the XL30 SFEG used in this work.

SE detectors are most common and standard in SEMs. The microscopes can image conductive substrates with very high resolution – less than 10 nm. The ebeam is highly focused and very narrow and has a very large depth of field. The SE's signal is most strongly affected by the topography of the sample.

BSEs are generated by high angle reflection of the primary beam electrons from the sample. BSEs generally give the information on the element distribution of the sample, as back scattering is strongly affected by the atomic number of the sample.

2.3.1.1 Electron Beam Lithography

The addition of a pattern generator to the SEM allows for EBL to be undertaken. As previously discussed the pattern generator takes control of the SEM's deflection coils (and also the beam blanker) in order to arbitrarily position the beam on the sample for a given duration. To pattern a sample the pattern generator is programmed using a computer.

The write field is the size of area within which the pattern will be exposed. The write field area can be from a few microns to one millimeter on a side, and is the size that can be patterned without moving the stage. Depending on the pattern resolution, the write field size needs to be set up correctly in order to achieve the desired pattern. Every write field is divided into fixed a number of addressable exposure elements, which is set by a digital analog converter (DAC) in the pattern generator. To achieve the maximum resolution the overall write field size should be set so that the exposure element size is the same as the minimum beam spot size of the tool. In practice using a write field size of 50×50 microns a minimum element size of 10 nm is achievable. Some patterns can be bigger than the available write field size; in that case the stage will need to be moved during the exposure. Where multiple write fields must be joined the process is known as stitching. Stitching accuracy depends on the type of stage that the ebeam tool. Interferometric controlled stages show significantly better results than mechanical stages. Temperature, humidity and acoustic noise can also cause some drift during the patterning process. The tool used here did not have good stitching control available.

The beam current is the number of electrons that hit the sample per second. Generally as the current increases exposure is faster, but due to space charge effects it is harder to focus the beam to a fine spot. To have a very high resolution pattern with

this tool the ideal beam current range is 0.01 to 0.1 pA. This current can be determined by setting acceleration voltage and spot-size or by varying the size of the mechanical aperture on the tool.

The exposure dose is the amount of energy that is deposited per unit area (e.g. $\mu\text{C}/\text{cm}^2$). The required doses are depends on the resist's sensitivity and the pattern density and dimensions being written on the resist. During exposure the acceleration voltage and the beam current are fixed but the dose, which was set by the software, is varied by modulating the time that the beam exposes any given point (the dwell time).

When the electrons hit the sample, then go through several elastic and inelastic scattering events, and may expose resist microns away from the desired area, which causes the proximity effect [168]. These unwanted features are only revealed after development. The effect can be reduced by using higher acceleration voltage. It is possible to predict highly proximity effects using stochastic modeling, and this can be used to modify the actual exposure pattern to get the required pattern after patterning. This process is called proximity effect correction.

2.3.1.2 Pattern Design

For fabricating any device it is necessary to draw a pattern that can be read by the ebeam tool. This pattern should define precisely every single dimension and the geometry of the device. Depending on the type of resist (e.g. the tone) and subsequent processing requirements (e.g. etching, etc.) one may need to expose the desire geometry or this design can be generated in any suitable CAD software. However, it is also necessary to incorporate the dose information, and the lithography file format GDSII [169] is used to combine the design a dose info into a file the ebeam tool can accept.

During the exposure, the GDSII files are then translated into a machine file, which gives all the required information to the pattern generator to direct and scan the beam as per the design.

2.3.1.3 Steps before the Exposure

Before exposure the ebeam tool needs to be calibrated. First the electron gun and the electron optics (column) alignment have to be checked. The write field size is calibrated against a physical standard to ensure accurate pattern dimensions. Once the beam accelerating voltage and current have been selected, the beam is carefully adjusted and the stigmatism of the beam adjusted to ensure the beam spot is circular, by using electromagnetic stigmator coils in quadruple, sextuple or octagonal orientations inside the column.

2.3.1.4 Exposure

When all calibration and adjustments have been done the exposure is run by the software. The software takes care of everything including stage movement, if necessary. Once the exposure is complete the sample can be removed for subsequent processing (e.g. post exposure bake and development), as described earlier.

2.3.2 Etcher

For etching a PlasmaPro 80 Inductively Coupled Plasma (ICP) from Oxford Instrument was used. Plasma is one of the four fundamental states of matter. Etching plasma is created by ionizing a suitable etching gas such as sulfur hexafluoride. The plasma contains ions, free radicals and other byproducts. The ions and free radicals

react with the substrate material creating volatile products which are removed by a vacuum system. Additionally the ions may be accelerated towards the surface and ablate it by sputtering.

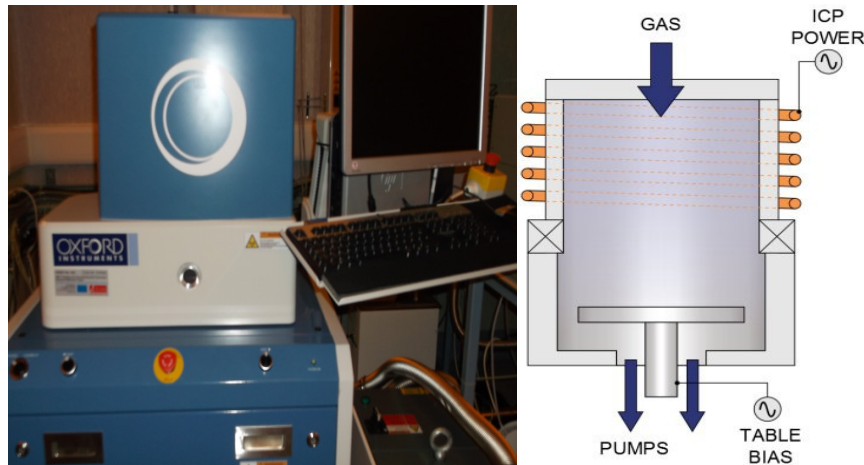


Figure 2.8: Left - Oxford Instruments PlasmaPro 80 ICP in Physics Cleanroom, University of Birmingham. Right – Schematic of ICP tool (source: Oxford Instruments)

In Inductively Coupled Plasma (ICP) a high frequency alternating electric current is passed through a coil surrounding the gas chamber inducing a varying magnetic field in the gas chamber. By inductively coupling of radio frequency (RF) the plasma is generated in the ICP source, and at the same time the ion energy can be independently controlled by bombarding on the substrate by applying a bias power to the substrate. By varying ICP power, bias, chamber, pressure, temperature, and the etchant gas a range of material (e.g. silicon or chromium) can be etched, as can the anisotropy of the process. Etching occurs either through a chemical process where chemically active species in the plasma react with the substrate to create volatile products; via a physical process where the ions bombard the substrate causing sputtering; or via a combination of both.

In order to etch a wafer, first it is loaded into the vacuum chamber of the ICP etcher and clamped to the etcher chuck. Helium is pumped behind the wafer to ensure

good thermal contact with the chuck. In case of smaller samples thermally conductive glue is used to attach the sample to a sacrificial wafer. The etching process starts by generating plasma by applying 13.56 MHz RF to the ICP coil. To generate pure inductively coupled plasma an electrostatic shield is used around the ICP tube. This process stops sputtering of the tube material onto the sample and at the same time it minimizes high energy ions that damage the sample.

2.3.3 Sputter Coater

The sputter coater allows deposition of material onto a suitable substrate by using a technique known as physical vapor deposition (PVD). In This process material is ejected from a target source by sputtering and deposits onto the substrate (figure 2.10). Generally in PVD deposition the source material is first vaporized by physical means, then the vapor is transported across a region of low pressure from its source to the substrate,[Edwards FL400 system manual] and at the end the vapor condenses on the substrate to a the thin film.



Figure 2.9: Edwards FL 400 in the Physics Cleanroom, University of Birmingham.

Sputtering is the mechanism by which atoms or molecules are ejected from the target material in this case. Argon ions are accelerated to and impact on the target, knocking atoms off the target. These ejected atoms then travel through the vacuum until they can condense on a surface, such as the substrate, and form a thin film (figure 2.10 and 2.11).

Figure 2.10 shows the process. Typically argon (Ar) gas is introduced into the chamber and then ionized. When a negative voltage is applied to the target, positive ions (i.e. Ar^+) in the discharge region are drawn to the target plate, and neutral atoms are ejected from the target. These atoms pass through the discharge region to be deposited on a substrate.

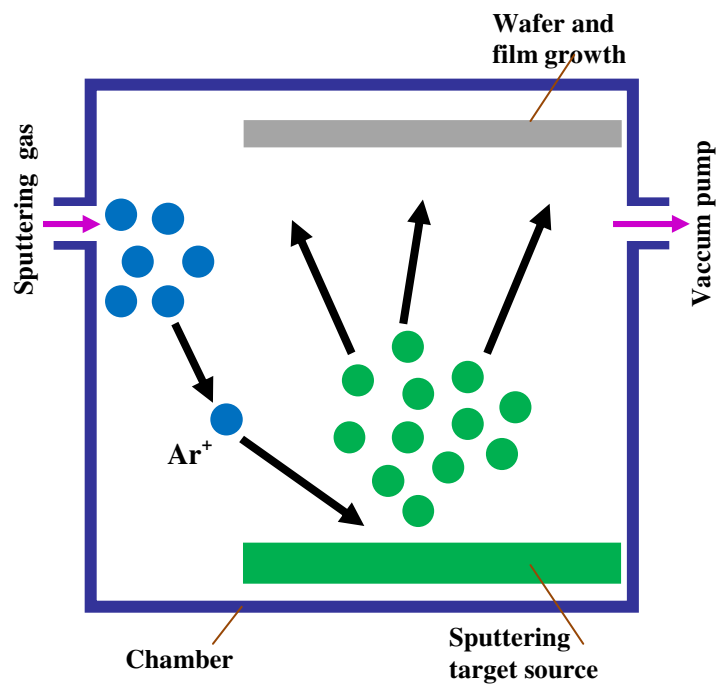


Figure 2.10: Sputtering Chamber

During sputtering to achieve greater plasma density and stability, a magnetic field can be applied across the target. This approach is known as magnetron sputtering. In magnetron sputtering, DC or RF voltage can be applied.

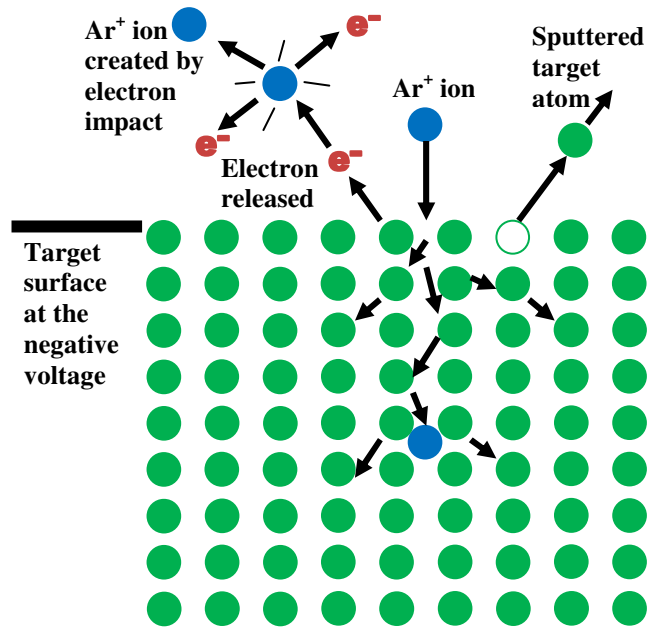


Figure 2.11: Deposition process by atom bombardment [170]

In this work DC magnetron sputtering is used. DC magnetron sputtering is characterized by high sputtering rates, which are proportional to the power consumed, and to the square of the current density, and inversely dependent on electrode spacing.

2.3.4 Plasma Asher

The Plasma Asher is a special tool that is used for removing unwanted organic material from a substrate without harming the sample.



Figure 2.12: TePla 100-E in Physics Cleanroom, University of Birmingham.

In this process TePla 100-E (see figure 2.12 and 2.13) was used several times to remove any contamination from the substrate either before or after the resist was on the substrate or before/after the sputter coating. This equipment is microwave plasma system, which is intended for strip and de-scums of resist. The minimum pressure of the system is 8×10^{-5} Torr and the plasma process are done by O₂ only. Depends on the contamination on the substrate the plasma ashing process takes 1–15 minutes.

2.3.5 Surface Profiler

For measuring film thickness a Dektak³ ST surface profiler was used (figures 2.13 – 2.14). A diamond-tipped stylus is placed in contact with the sample with a controllable force. The sample is then moved laterally and the vertical of the tip is measured.

The vertical motion of the stylus is measured electrically and then plotted against the lateral position of the sample to give a one dimensional line profile of the topography of the sample. Any sufficiently hard surface such as hard baked photoresists can be measured with a vertical range of up to 65.5 μm . The maximum sample thickness is 20 mm, and the smallest vertical resolution is 5–10 nm.



Figure 2.13: Dektak³ ST Surface Profiler in Physics Cleanroom, University of Birmingham.

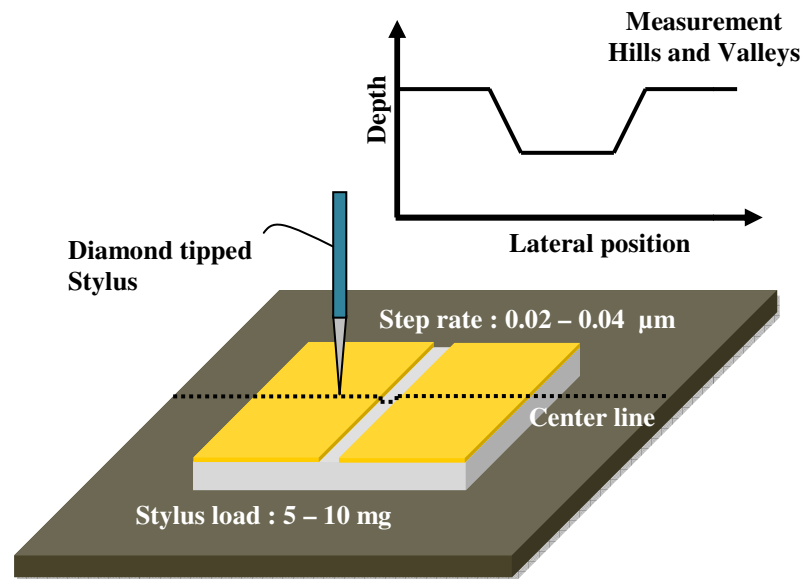


Figure 2.14: Schematic of working mechanism of Dektak³ ST

2.3.6 Keithley source measure unit

For the conductivity testing Keithley 236 & 237 source measure units (SMU) were used, (see figure 2.15). The 236 (or 237) SMU is a combination of three different instruments in one [171] – a sensitive electrometer for measuring current and voltage at the same time, independent voltage and current source.



Figure 2.15: Keithley 236 SMU

The main difference between 236 and 237 is the later is a high voltage (up to 1000V) source unit. However, both can source and measure current and voltage at the same time. For example, if the source is selected current (I) it will measure the voltage (V) and display the measured value on the screen.

Both have remote sensing, meaning that when sourcing voltage, in remote sensing mode, it will allow the voltage to be sensed (i.e. measured) at the load for better regulation. When the remotely sensed-V of the device under test (DUT) is lower than the programmed-V, then the actual V-output will be increased till the sensed-V is equal to programmed-V. This gives assurance of exact programmed voltage at the DUT. When either measuring or sourcing 1 mA or more, it is ideal to use the remote sensing option [171, 172].

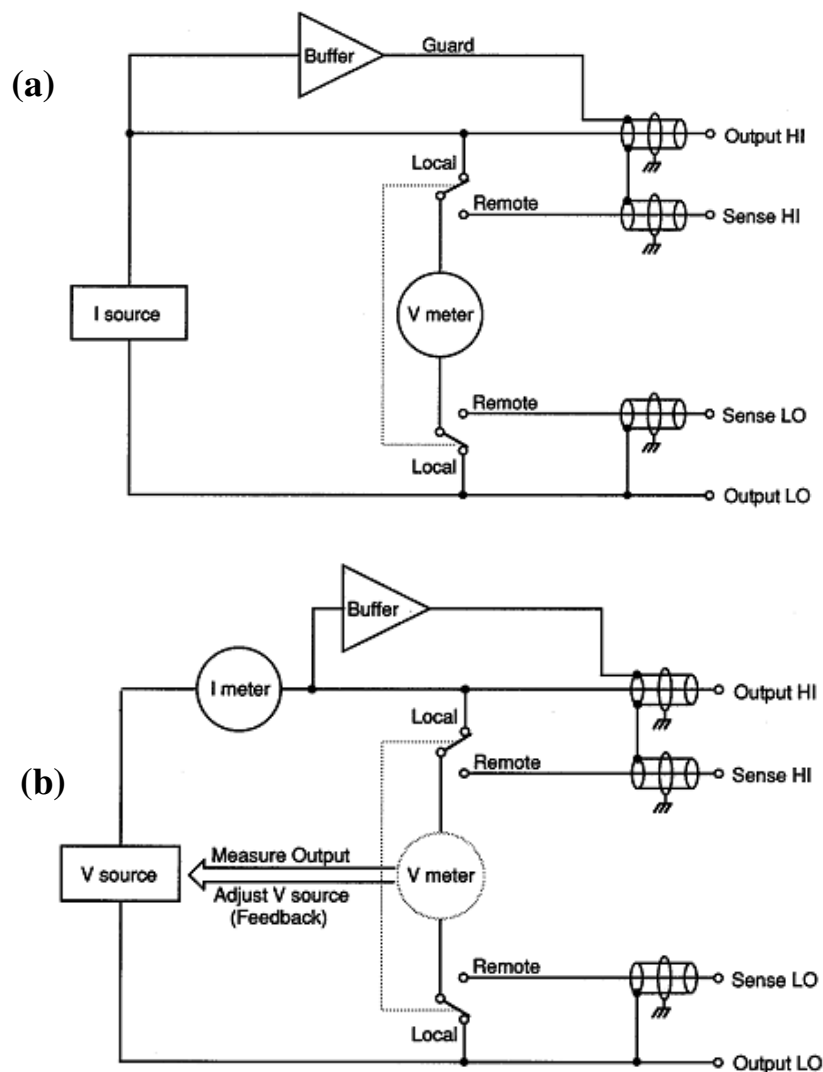


Figure 2.16: (a) Source I, Measure V. (b) Source V, Measure I [171, 172].

In the case of measuring very high resistance materials, leakage current causes inaccurate measurements. In both Keithley SMUs, a very effective guarding system has been introduced, which eliminate the effects of any leakage current and of parasitic series resistances. A driven guard has been placed surrounding output high (figure 2.16). In order to generate accurate low-level measurements and results fully guarded tri-axial cables are used throughout the measurement system. During measurements at low current, this guarding will help to reduce the influence of charging currents and electromagnetic interference. Without a properly driven guard, the leakage current could affect the performance of the SMU. It is recommended to always use the guard whilst sourcing or measuring current below 1 micro amps, and also very high speed measurements [171, 172]. By using a coaxial cable this guarding can be extended all the way to the DUT [171, 172].

The measurement data are stored inside the internal memory system of the SMU. To retrieve data the SMU has been connected with a computer. LabView based software was written to control the SMU and record the data. Data collection software was developed in LabView by customizing a four-point probe program from Keithley Instruments.

Figure 2.17 shows the front panel (top) and the block diagram (bottom) on the software, which was used for conductivity tests in University of Birmingham. This program can measure either current or voltage following linear stair increment steps. The remote sensing option has been implemented in the software to source or measure more than 1 mA current. Suppression was applied to subtract offset values from measured data. By filtering 32 readings for each sweep the measurement noise was stabilized. A delay time is also introduced in the software in order to allow the ammeter or the voltmeter to settle down between measurements.

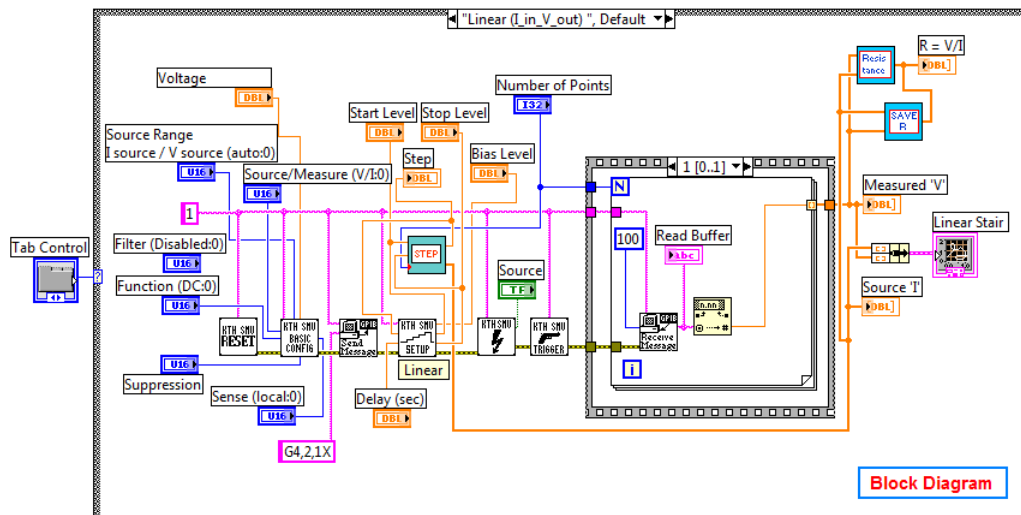
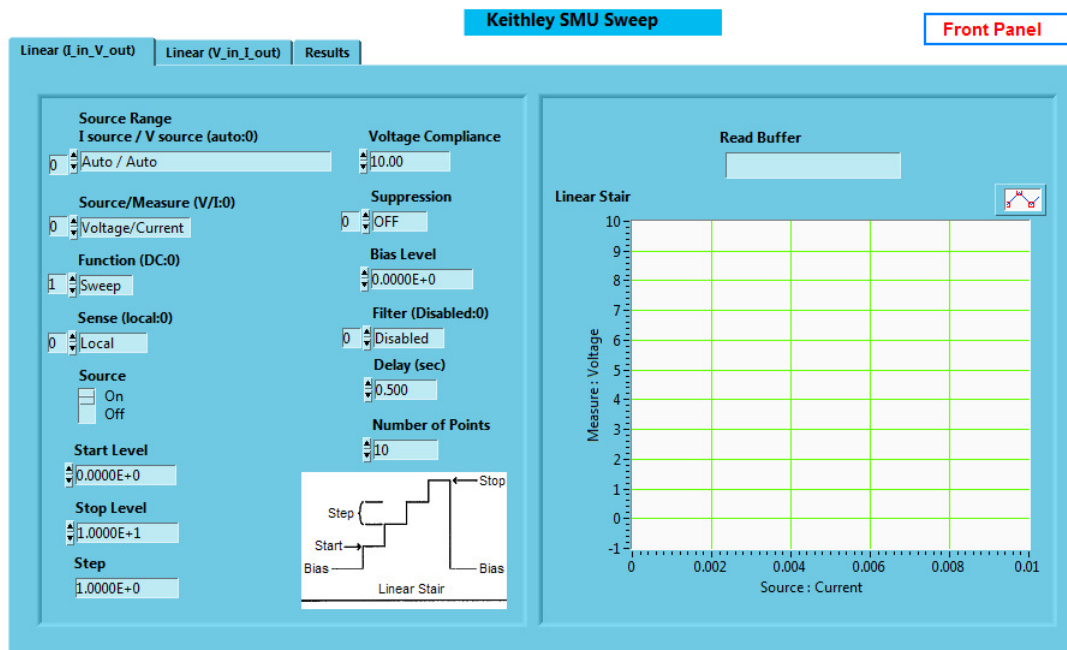


Figure 2.17: Linear Stair program LS v8.3 developed in LabView

To ensure accuracy of the experiments repeated measurements were performed in order to quantify the errors.

2.4 Conductivity Approaches

For conductivity measurement three different experiment setups have been designed. The first experimental setup was for four-point probe measurements, with four gold coated spring probes placed inside a grounded metal box (I-V box).

The sample was a spin coated C5C5 onto a 1.5 cm^2 glass substrate. Both current and voltage were swept with the Keithley 236. To find the conductivity the VdP method was used. Figures 2.18 and 2.19 show the I-V box and the schematic of the experimental setup. Various thicknesses of C5C5 were measured, however with this setup hysteresis was observed due to insufficient shielding, and poor contact between the probes and the sample.



Figure 2.18: I-V Box (left), chip holder (right)

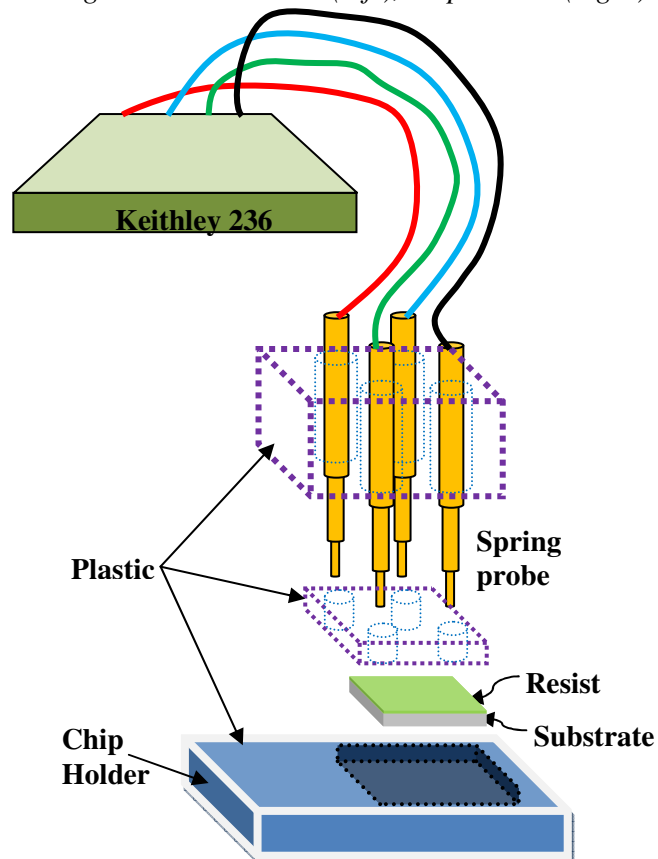


Figure 2.19: Schematic of the 4-point I-V box and the connection to the Keithley 236

In the second experimental setup, to improve the contact between the probes and the sample at first crocodile clips were used, later copper probes and silver paint was used, see figure 2.20. The copper probes were made by the coaxial cable's center copper wire, which was sharpened and modified to a needle point, see figure 2.21.



Figure 2.20: Four point probe station with Copper probes.

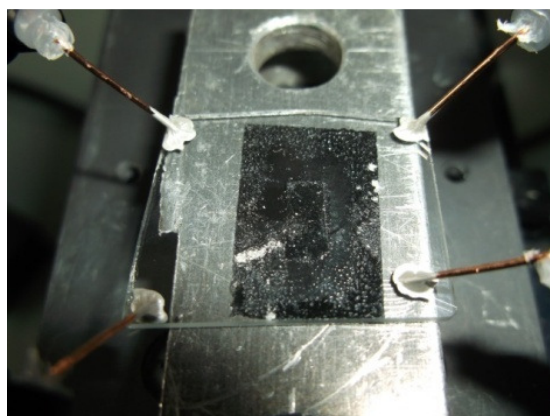


Figure 2.21: Copper probes with silver paint on a glass substrate

Various thicknesses of C5C5 were spin coated on glass and the conductivity was calculated with the VdP method. The whole probe station, the sample and the wires were covered with a grounded aluminum cage. By having very good contact between the sample and the probes, the problem of hysteresis was eliminated. Finally fully insulated cables and tungsten needle probes were used (figure 2.22) and

conductivity tests using the VdP method with or without silver paint, were undertaken (figure 2.23).

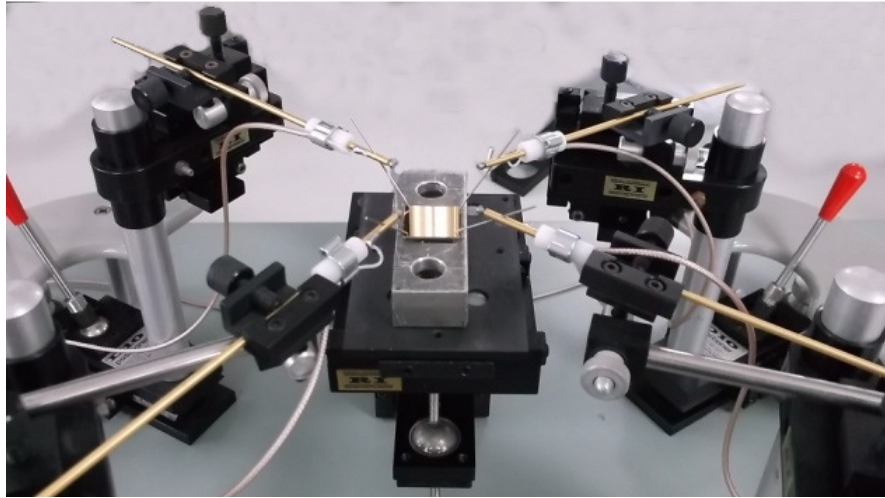


Figure 2.22: Four point probe station with Tungsten probes

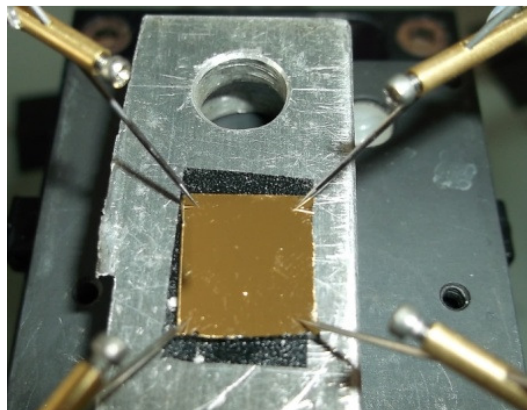


Figure 2.23: Tungsten probes without silver paint on ~100 nm gold sample

Although a significant improvement was seen using tungsten probes and silver paint, the samples resistances were high. In order to reduce it, it was decided to fabricate four probe gold (~100 nm) taken on glass to reduce the conductive path length. After spin coating the resist (pure C5C5 or CAR), most of the resist area were wiped off, except the center area of few millimeter (figure 2.24). The detailed fabrication steps will be given in chapter 3, section 3.4.2.

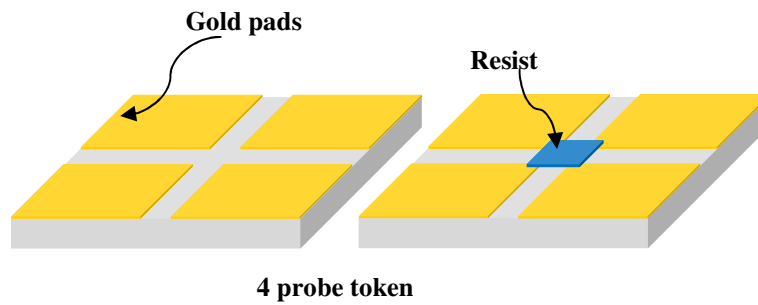


Figure 2.24: Four probe token with Au-pads and Resist

Separately conductivity was also investigated using a two probe method. This provided conductive data with the four probe method and allowed investigation of the effect of resist temperature during the voltage or current sweep. For this test several two-probe Au-pad tokens were fabricated with varied probe distance, see figure 2.25. The detail fabrication steps will be given in chapter 3, section 3.4.2.

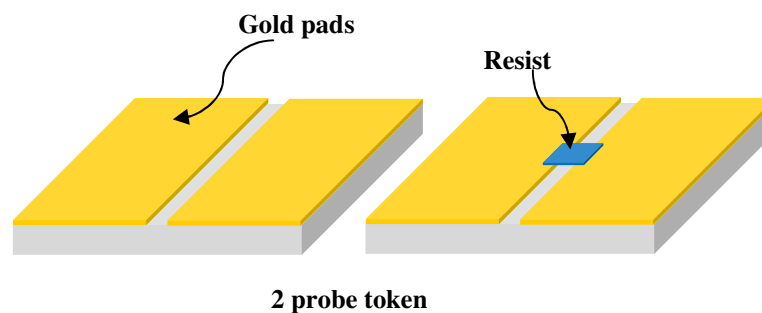


Figure 2.25: Two probe token with Au-pads and Resist

After spin coating resist onto the two-probe token and baking, most of the resist was wiped off except for a few millimeters in the center. This sample was mounted on a heater using thermal glue (figure 2.26) and the Au-pads connected with copper wires and silver paint. The heater and sample were placed inside a Faraday cage (figure 2.27) and connected to Keithley 236 (or 237). After sourcing either voltage or current, the corresponding data was recorded with respect to both heating and cooling. To record the sample's surface temperature a thermocouple was mounted to it, see figure 2.27.

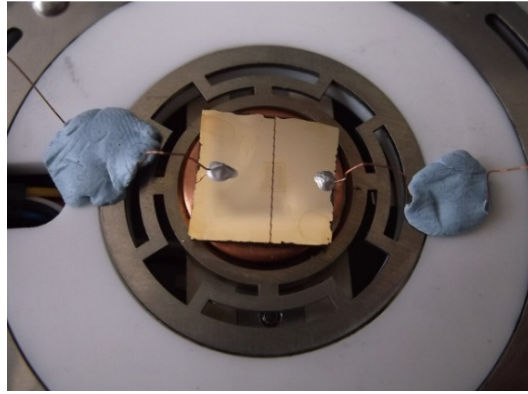


Figure 2.26: A two-probe token is mounted on a heater with silver paint

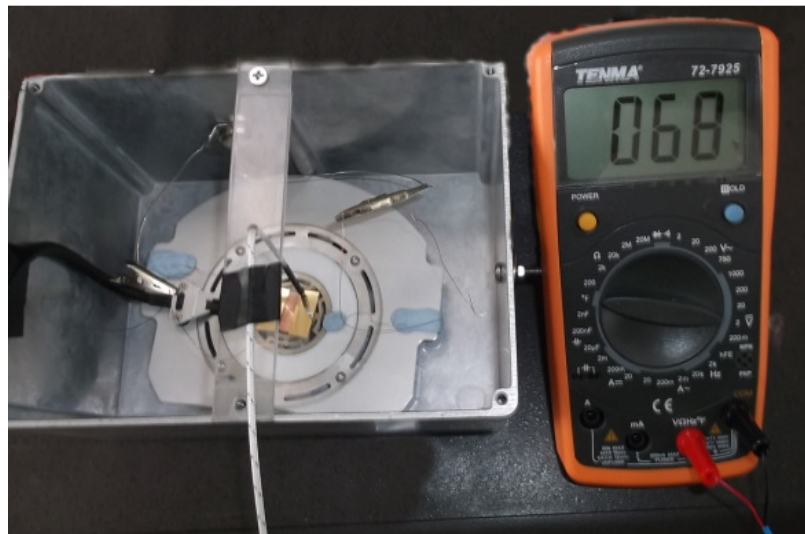


Figure 2.27: The heater with token inside a Faraday cage and a thermocouple on top of the token's surface.

2.5 Measurement error handling

At the very beginning of the conductivity tests hysteresis in the I-V curves was found. Some electronic systems do demonstrate a memory effect, i.e. a resistance change depending on the previous state of the system. However, for high resistance measurements it is more likely to be an error of the measurement system, for instance a capacitance effect. The results of hysteresis will be in chapter 3, figures 3.7 and 3.8.

The shunting effect can be another concern if the wires are not properly

shielded, because this effect diverts most of current where the obstruction occurring in. The first few experiments the wires within the probe station had no shielding, which caused shunting effect inside the probe station.

Johnson or thermal noise also affects any electrical measurement. Every voltage source has Johnson noise due to having resistance itself, which creates a thermal energy spread of electrons at finite temperatures. This noise can be reduced by lowering the temperature of the source resistance and decreasing the measurement's bandwidth.

Most of these errors were reduced by placing the probe station and the sample inside a Faraday cage.

Chapter 3

Conductivity tests

Electron beam resists for use with insulating substrates are liable to charge, as discussed in the introductory chapter section 1.6, which can lead to pattern distortion. From the literature it was found that the incorporation of a conductive charge dissipation layer is the typical solution. In this work the charge dissipation functionality is a property of the resist film itself. It has been reported that such a resist film would need conductivity in the region of 10^{-2} S/m [140] to dissipate charge effectively. Triphenylenes and their derivative are known to demonstrate reasonably good organic material conductivity as seen from the work of S.K. Gutpa [155] described in chapter 1 section 1.7. However, previous work has focused primarily on the measurement of thick triphenylene films in sandwich cell configurations. For resist material conductivity evaluation it is more appropriate to look at thin films and planar conductivity measurements. This chapter presents such measurements for both pure triphenylene derivative films and chemically amplified resist formulations.

3.1 Sample preparation

For conductivity tests, glass substrates (1.5 cm × 1.5 cm) were prepared. A simplified substrate cleaning procedure was used, involving sonication in IPA (15 minutes), then

acetone (15 minutes) then a rinse in DI water. This was used for both C5C5 and CAR to produce smooth films on these substrates with chloroform as casting solvent. For some tests in Chalmers, MC2 (see section 3.12) quartz, borosilicate, fused silica and atomic smooth glass substrates were used.

For producing thinner films (50 – 150 nm) 10 g/L C5C5 was used, whilst 50 g/L C5C5 was used for thicker films (424 – 785 nm) by spin coating. To produce films in excess of one micron drop casting was used – 50 μ l of 50 g/L C5C5 was dispensed on the glass and allowed to dry without spinning. All these samples were then baked at 70°C for 5 minutes. For CAR, only 10 g/L CAR was used to produce ~100 nm films on glass by spin coating (1000 rpm, 60s) and baking for 2 minutes at 50 °C.

A range of different experimental techniques have been undertaken for conductivity measurements with C5C5, CAR and PMMA, as described in chapter 2. The results are presented here. Measurement of these high resistances, low thickness organic materials provide to be exceptionally challenging. Significant variability in the measured values for conductance of a given organic material were seen, but are not presented here, unless found to be relatively consistent with known values from the literature.

3.2 C5C5 - thickness vs. conductivity

For conductivity tests, C5C5 coated on glass samples were measured with a Keithley 236 SMU. Various thicknesses (100 nm – 5 μ m) of C5C5 film were prepared on glass.

A fixed range of sweep current (-5.0×10^{-12} to 5.0×10^{-12} amps), and sweep

voltage (−3.0 to 3.0 volts), were applied for measuring voltage, and current respectively. Fifty readings were taken for each polarity with linear-stair step measurements. The voltage or current was scanned from the lower limit to the upper limit. A sweep delay time (e.g. 0.5 seconds) was set in between each reading. The test was carried out at a temperature 15–16 °C and the humidity was recorded at 44.8 – 55.7%. Figure 3.1 and table 3.1 show that conductivity decreases with increasing film thickness.

Table 3.1: C5C5 conductivity measurements as a function of film thickness

Film Thickness (nm)	Conductivity (I-input) S/m	Conductivity (V-input) S/m
100	5.51×10^{-6}	7.44×10^{-7}
120	2.89×10^{-6}	3.30×10^{-7}
150	2.71×10^{-6}	3.27×10^{-7}
424	1.57×10^{-6}	1.90×10^{-7}
785	7.00×10^{-7}	5.83×10^{-8}
2000	4.52×10^{-7}	1.81×10^{-8}
5000	1.09×10^{-7}	7.32×10^{-9}

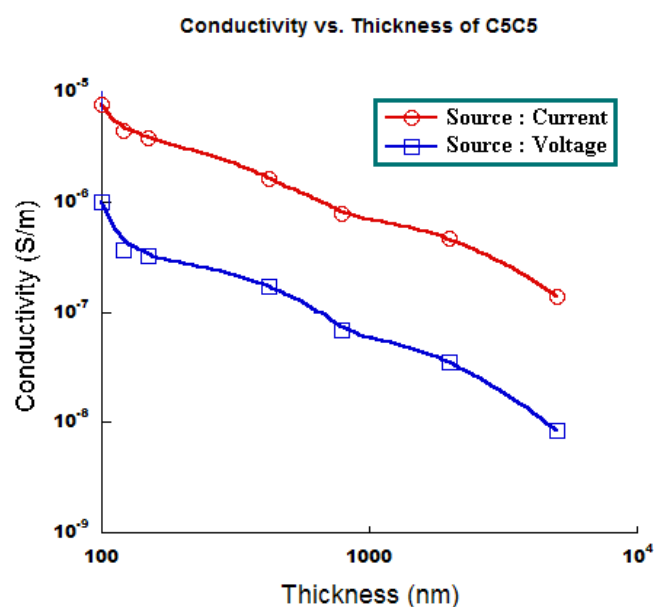


Figure 3.1: Thickness vs. Conductivity C5C5, Sourcing current and voltage

Electrical conductivity is proportional to the drift mobility and the charge

carrier concentration, and depends on the number of electrons available to participate in the conduction process. Figure 3.1 shows that when source is current the conductivity is higher, which means, the number of free electrons that were excited by electric field was higher than when the source is voltage. A thickness dependent conductivity between 10^{-6} to 10^{-9} S/m was found.

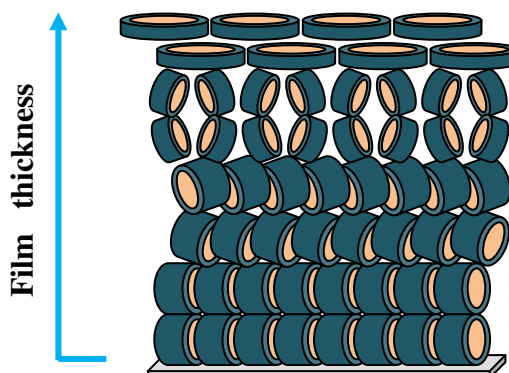


Figure 3.2: Speculated molecular layers of Triphenylene depend on thickness

It has been observed by small-angle X-ray scattering (SAXS) [108] that the triphenylene molecules are well arranged in columnar order horizontally on the substrate when the film thickness is around 100 nm. In thicker films the columns are known to be oriented vertically [108]. It is also known that the charge transfer is faster in the column parallel direction [108]. It is speculated (figure 3.2) that the change in conductivity with film thickness maybe related to this, but this would need to be confirmed with additional SAXS measurements.

Further tests have been carried out to identify the molecular orientation of C5C5 after spin coating in University of Cambridge. Figure 3.3 shows the disoriented structure of C5C5 film (~200nm) on silicon. The picture was taken under polarizing microscope after spin coating and baking 70 °C for 5 min. The darker areas suggest that the molecules are stacking on top of each other and lighter areas are when the

molecules are in disordered relative to each other. They are not all in the columnar packing on the horizontal surface – some areas are columnar but others are disordered. This suggests having lower conductivity for C5C5 when the thickness increases.

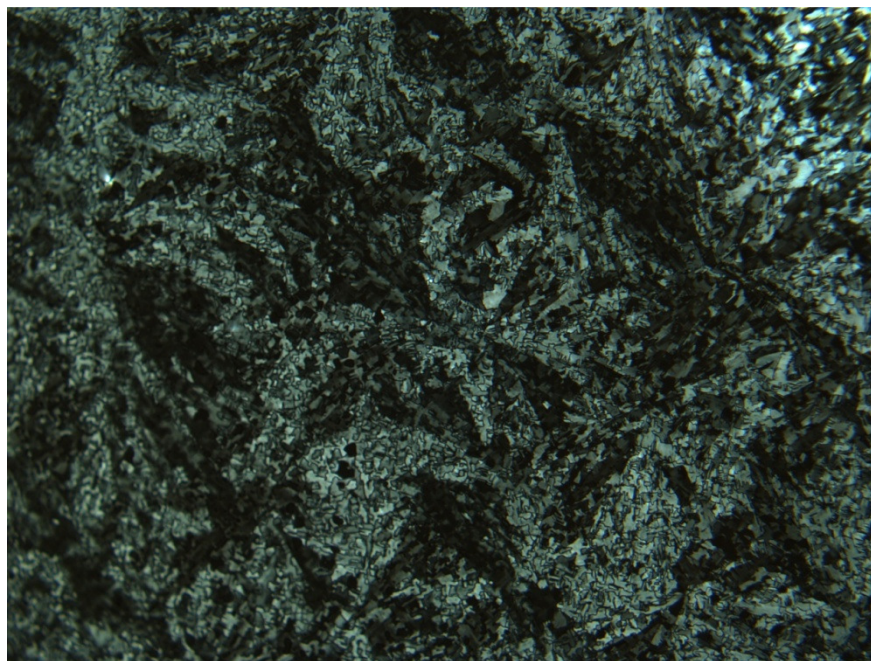


Figure 3.3: Film thickness of ~200 nm of C5C5 on silicon under a polarizing microscope.

In order to identify any potential hysteresis with the Keithley 236 SMU with this (C5C5) high resistance film -1 to +1 volt was supplied and two sets of slow and fast measurements were taken. Figure 3.4 shows the results of the slow scans, whilst the fast scans are shown in figure 3.5. Both show classical hysteresis feature. As C5C5's resistivity is very high, it might be overwhelmed by the capacitance of the whole system. The hysteresis measurements indicate that this is a valid concern, and measures to mitigate the issue were taken as described in chapter 2.

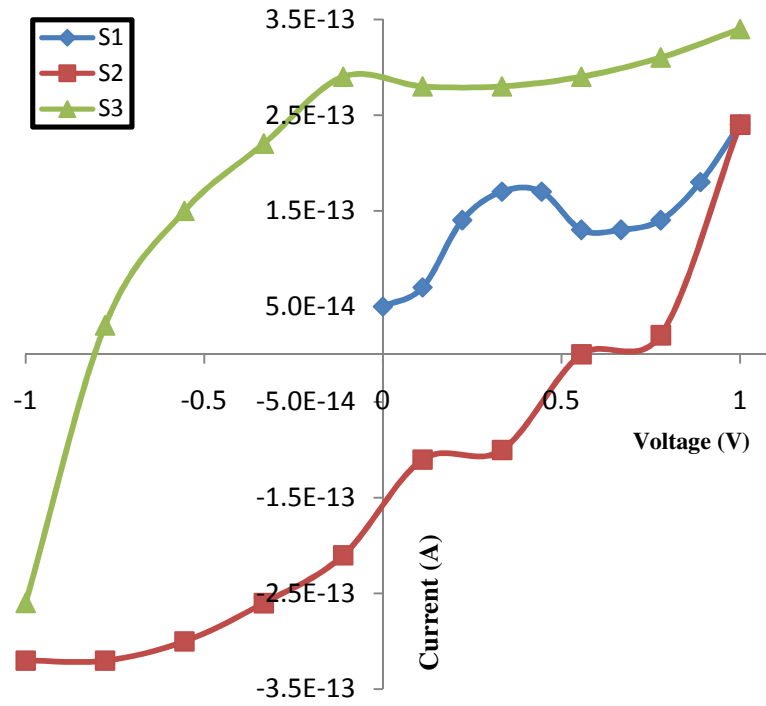


Figure 3.4: Slow measurement loop

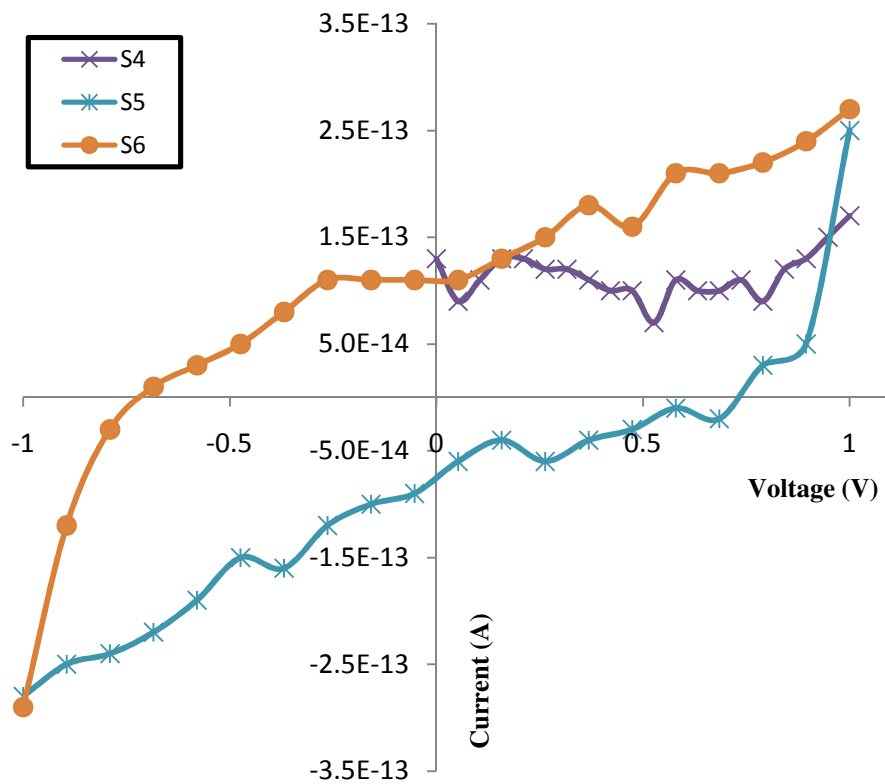


Figure 3.5: Fast measurement loop

3.3 Conductivity tokens

Two and four probe tokens were fabricated on glass by sputtering ~30 nm of chromium followed by ~90 nm of gold on top of chromium to form pads as shown in figure 3.6.

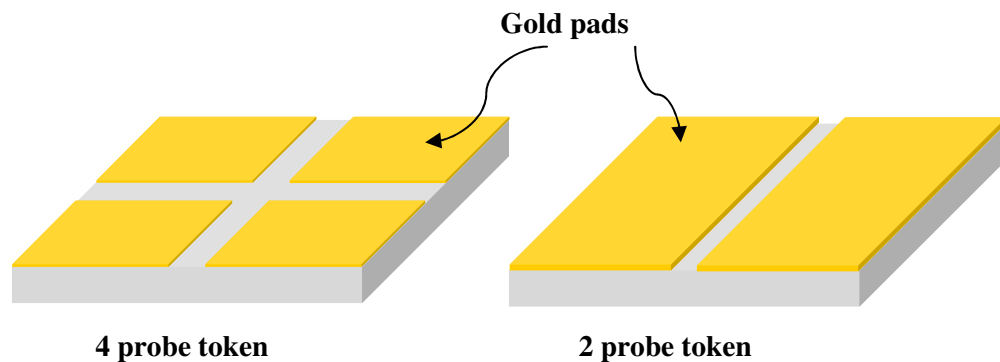


Figure 3.6: Around 110nm gold plus chromium on glass substrates

The sheet resistance on a 100 nm gold film sputtered on glass, was using Keithley 236 and found to be $14.8 \Omega/\square$.

The two-probe token was fabricated by sputtering chromium and gold on a $2 \text{ cm} \times 2 \text{ cm}$ glass slide. A ~3 micron PMMA 950 C7 resist film was spin coated onto the gold coated sample. A 2 cm long and 100 micron wide line was patterned using an ebeam, then baked at $120 \text{ }^\circ\text{C}$ for 5 minutes and developed in MIBK:IPA (1:3) for 1 minute. After 3 minutes plasma ashing to clear scum, the sample was etched with the ICP etcher using an argon sputter etch for 3 minutes to etch the gold. The trench was cleared and no bridges was found between the pads, see figure 3.7 (left).

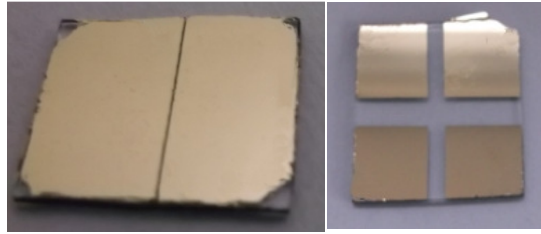


Figure 3.7: Conductivity tokens for two-probe (left) and four-probe (right) measurements

For fabrication the four-probe token, a 2 cm \times 2 cm substrate was masked with tape prior to sputter coating. The gaps were 3 and 5 mm. After sputtering chromium and gold onto the glass substrate, the tape was removed and the token cleaned with acetone, IPA and a plasma ashing process; see figure 3.7 (right).

Several four-probe tokens were fabricated with various gap widths using the same process. Both of these tokens' hysteresis was checked. By using improved shielding around the samples, no hysteresis was found, see figures 3.8 and 3.9.

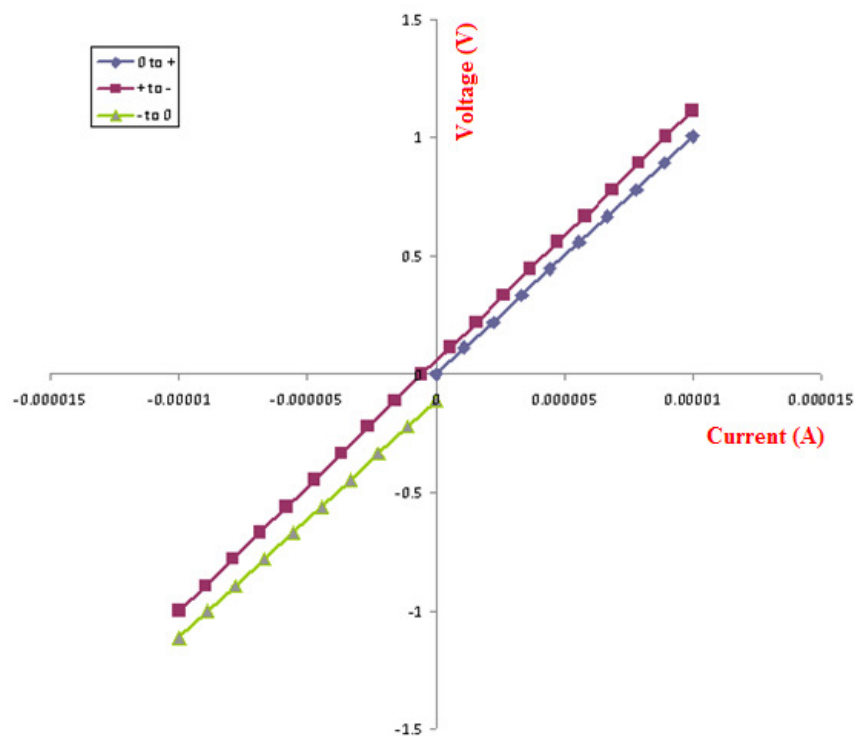


Figure 3.8: Hysteresis test on the 4-probe system, applying current and measuring voltage

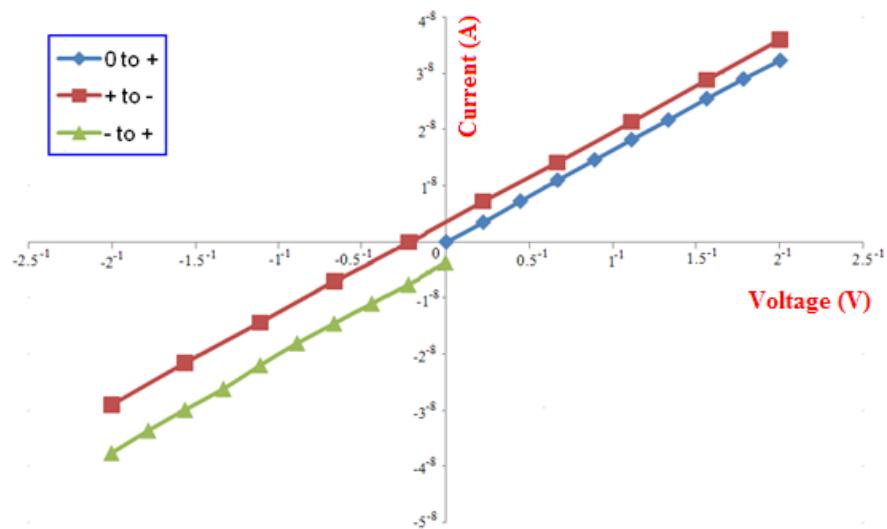


Figure 3.9: Hysteresis test on the 4-probe system, applying voltage and measuring current

3.4 Resistivity of glass

The bulk resistivity of the glass substrate (~ 1.1 mm thick) was measured at $\sim 10^8 \Omega\text{m}$ at 15°C . On the other hand, the electrical resistivity of glass at 250°C is around $\sim 10^9 \Omega\text{m}$. [177] Different glass contains various dopants in addition to silica and it is thus necessary to characterize the specific glass used.

3.5 PMMA, C5C5 and doped C5C5

For this experiment, a four-probe Van der Pauw (VdP) measurement process was undertaken using a probe station where all the four probes were made with copper wires and silver paint was used to connect to the four corners of the sample, see figure 3.10. Three samples prepared with PMMA 950 A2 (~ 170 nm), pure C5C5 (~ 70 nm) and 1% doped Pyrometallic dianhydride in C5C5 (~ 70 nm). The C5C5 resist was in 10 g/L PGMEA. Because of dewetting issues both doped and pure C5C5 had very bad film formation on the substrate.



Figure 3.10: Experimental setup with copper probes with silver paint

The table 3.2 shows the results with or without shielding around the sample. The shielding was a large grounded aluminum box, which covered the whole probe station with all its cables.

Table 3.2: VdP measurements of PMMA, C5C5 and Doped C5C5 with and without EMF shield

Resist	Thickness (nm)	Sheet Resistance (Ω/sq)		Conductivity (S/m)	
		Shield OFF	Shield ON	Shield OFF	Shield ON
PMMA 950 A2	170	3.60×10^{11}	4.46×10^{11}	2.40×10^{-5}	1.31×10^{-5}
Pure C5C5	70	1.13×10^{12}	2.33×10^{11}	1.28×10^{-5}	7.67×10^{-5}
1% Pyrometallic dianhydride in C5C5	70	9.11×10^{11}	4.20×10^{11}	2.68×10^{-5}	6.23×10^{-5}

From the literature it was found that the $5\mu\text{m}$ thick PMMA [178] cell gives around $10^{15}\Omega/\square$ sheet resistance, in this case it was about $10^{11}\Omega/\square$ for the 170nm spin-coated film, which makes the conductivity $\sim 10^{-5}$ S/m, potentially indicate measurement errors.

3.6 PMMA

The conductivity of PMMA 950 A2 was measured with the same experimental setup as shown in figure 3.9, however five different conditions were applied – (i) after spin coating the film was baked at 120 °C for 5 minutes, (ii) no baking after spin coating, (iii) after spin coating the sample was baked at 120 °C for 5 minutes and then kept in a desiccator for 1 day, (vi) no baking after spin coating and then kept in the desiccator for 1 day. All these tests were done both with the 4 probes directly on the gold-pad or attached to the gold-pads using conductive silver paint. The results are in table 3.3, which shows the average of 100 tests per sample.

Table 3.3: Conductivity of PMMA 950 A2

Resist	Thickness	Condition		Sheet Resistance (Ω/\square)	Conductivity (S/m)
PMMA (Spin Coated on Glass)	2.2 μm	Baked	Probe on Au-Pad	2.64×10^{11}	3.50×10^{-6}
			Probe in Ag-Paint	2.88×10^{11}	2.07×10^{-6}
		Not Baked	Probe on Au-Pad	2.85×10^{11}	2.20×10^{-6}
			Probe in Ag-Paint	2.74×10^{11}	3.15×10^{-6}
		Baked (Desiccator)	Probe on Au-Pad	2.91×10^{11}	2.44×10^{-6}
			Probe in Ag-Paint	2.91×10^{11}	2.10×10^{-6}
		Not Baked (Desiccator)	Probe on Au-Pad	2.87×10^{11}	1.90×10^{-6}
			Probe in Ag-Paint	2.80×10^{11}	2.62×10^{-6}

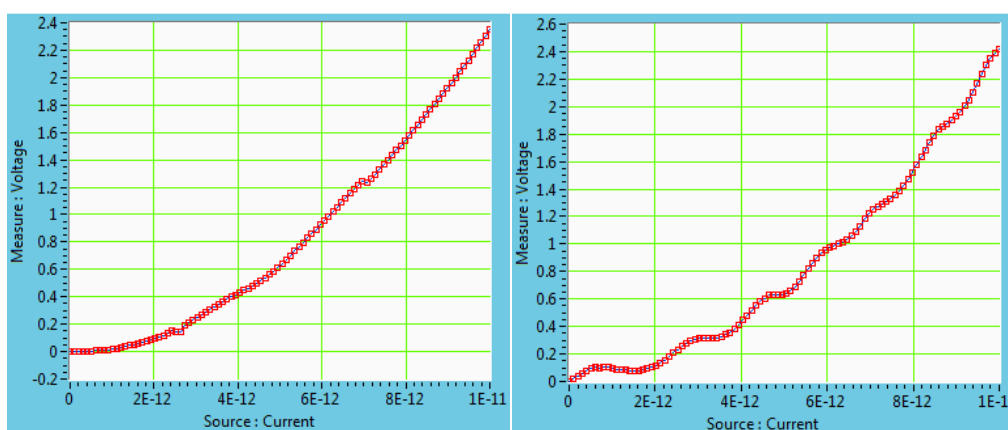


Figure 3.11: Current input – baked (left) and not baked (right) PMMA. Probes are on gold pads and with conductive silver paint.

The sheet resistance did not vary, but was found to be $\sim 10^{11} \Omega/\square$ in all cases. These tests were done with the aluminum shield on, and with input current 0 to + 10 pA. Figure 3.11 shows that the I-V curves for both baked and non-baked samples, where both achieved around ~ 2.4 volts.

3.7 CAR – Conductivity vs. Temperature

Two glass tokens were made with ~ 110 nm gold sputtered on top. The pad separation was $10 \mu\text{m}$ in one case, and 3 mm in the other. Both tokens were spin coated with ~ 100 nm thick CAR (10 g/L chloroform).

For measurement of the conductivity the Keithley 237 was used. Voltage was supplied and the current was measured. At the same time the temperature was increased from room temperature $16.7 \text{ }^\circ\text{C}$ to $105 \text{ }^\circ\text{C}$. Figure 3.12 shows the experimental setup of the 2-probe token mounted on a heater with copper wire and silver paint, which was placed inside a Faraday cage and connected to the Keithley 237. The hysteresis test has been performed by supplying 0 – 100 volt and no hysteresis was found.

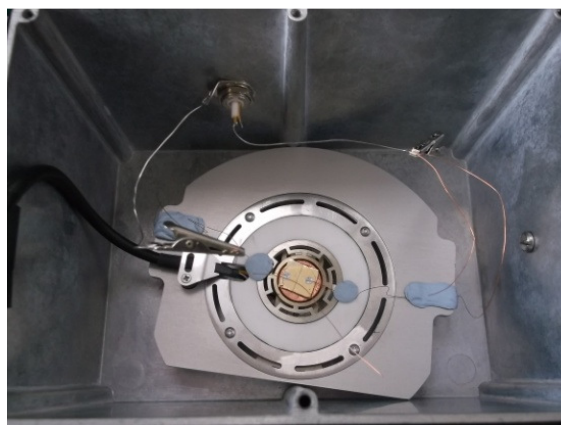


Figure 3.12: Sample on a heater, placed inside a Faraday cage

At 16.7 °C, 1 - 3 mV was supplied and the current measured was in the pico amp range. After this measurement cycle the heater was turned on and the temperature increased to 25 °C. After the temperature had stabilized 1-3 mV was supplied and again the current measured. This was repeated at various temperature steps up to 105°C, results are shown in figure3.13.

The conductivity was measured between $\sim 10^{-5}$ to 10^{-7} S/m. The higher conductivity has been observed at 100 °C, when the triphenylene is in its iso-phase [155]. It can be assumed that there might some effects of PAG, which might generate extra proton into the system that may cause higher conductivity for CAR.

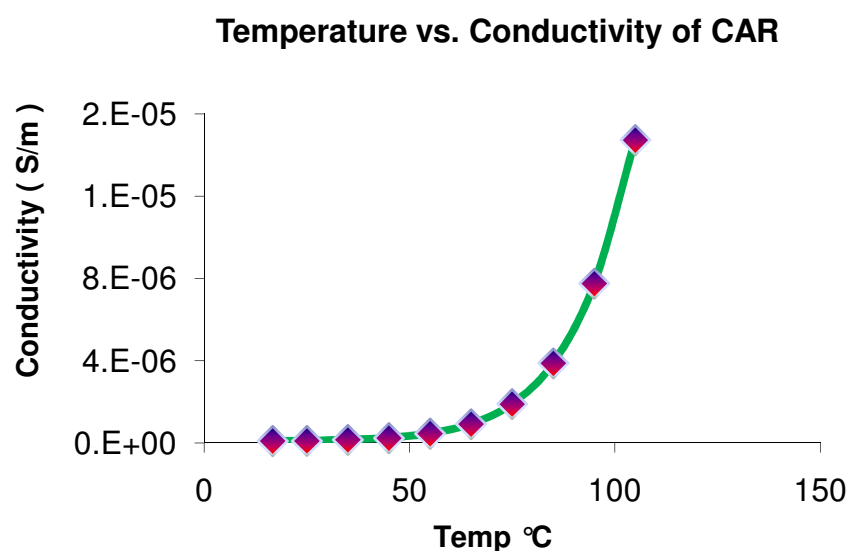


Figure 3.13: Temperature vs. Conductivity (S/m) of CA resist

3.8 C5C5, C5OH and C5EPX

To find out the effect of the PAG on the conductivity effect in the CAR, three samples were prepared (C5C5, C5OH and C5EPX) on three 2-probe tokens with 5 mm pad distance. Each of these samples had around ~100 nm thick film. To get the accurate temperature a thermocouple was placed on the sample's top surface, see figures 3.14 and 3.15.



Figure 3.14: When the heater read 20 °C, the thermocouple read 68 °F = 20 °C

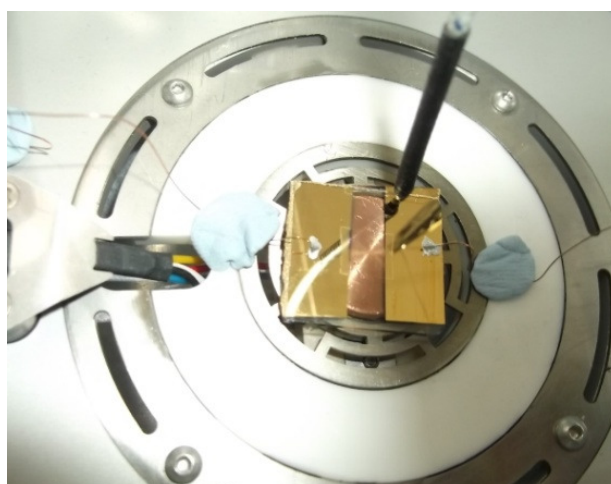


Figure 3.15: Thermocouple in contact with the gold-pad

Before measuring the conductivity of the organic films, control measurements of the conductivities of glass substrate and the gold pads were undertaken. A voltage was applied, and current measured, with respect to temperature in the range 18 – 105 °C, both when heating up and cooling down.

The conductivity of the glass was found to be $\sim 10^{-12}$ S/m at 18 °C and 10^{-10} S/m at 105 °C. The results are shown in figure 3.16.

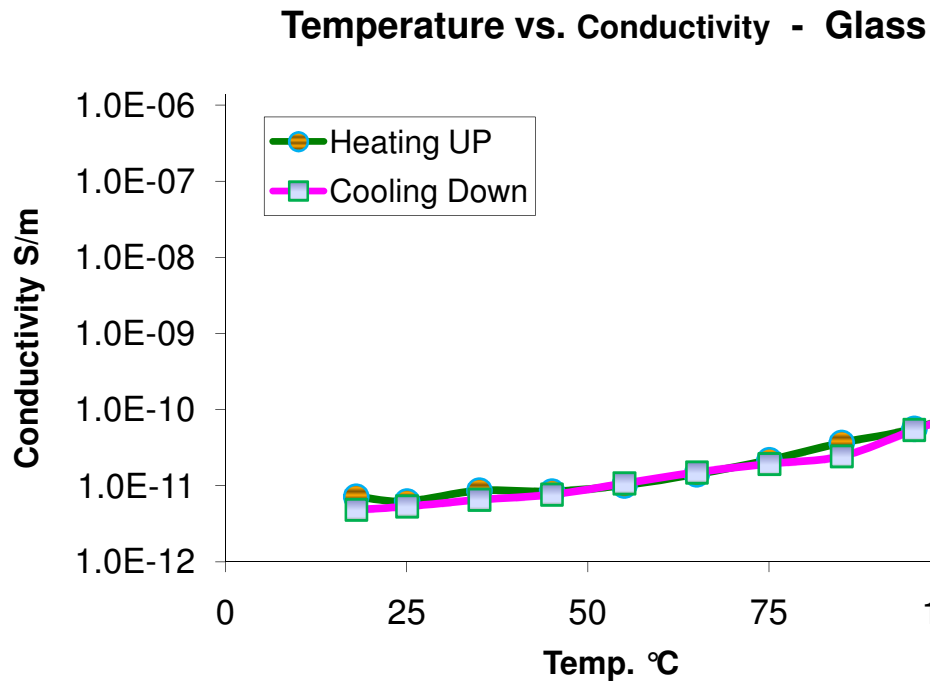


Figure 3.16: Temperature vs. Conductivity tests of glass

The conductivity of the ~ 100 nm thick gold pads was found to be a 10^6 S/m. Figure 3.17 shows that the temperature change does have a small effect on the conductivity of the gold (plus chromium) film.

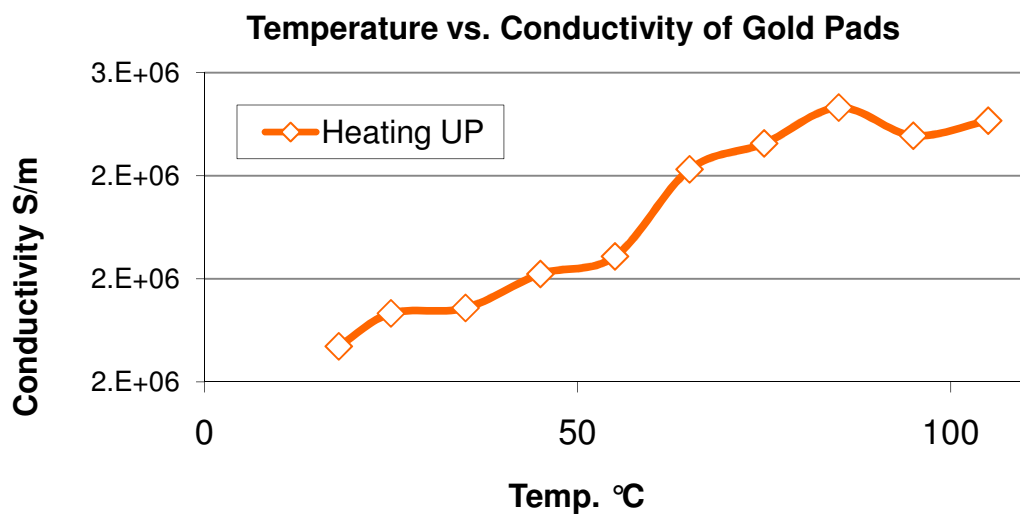


Figure 3.17: Temperature vs. conductivity tests of gold pads

In this experiment, measurements were taken in two different ways – firstly, a thermocouple was placed in contact with the top of the gold-pad, and secondly, a thermal compound was placed around the thermocouple end point on the gold-pad. In both cases, for each sample 0 – 50 mV was applied, and the sample heated up from 18 to 105 °C and then cooled down whilst the output current was measured.

For C5C5 it was not possible to collect useful data. Conductivities were measured to be several orders of magnitude too high (up to 10^7 S/m), indication of a short circuit on the system.

For C5OH (~100 nm film) a voltage range of 0 – 105 V was used, and the temperature range was 19 – 105 °C. The conductivity was found to be $\sim 10^{-6}$ S/m at 19 °C and 10^{-5} S/m from 40 °C to 105 °C. Figure 3.18 shows the conductivity of C5OH as a function of temperature.

For C5EPX and the CAR film similar results to C5C5 were observed, with conductivities as high as 10^4 S/m seen – again indicative of a measurement failure.

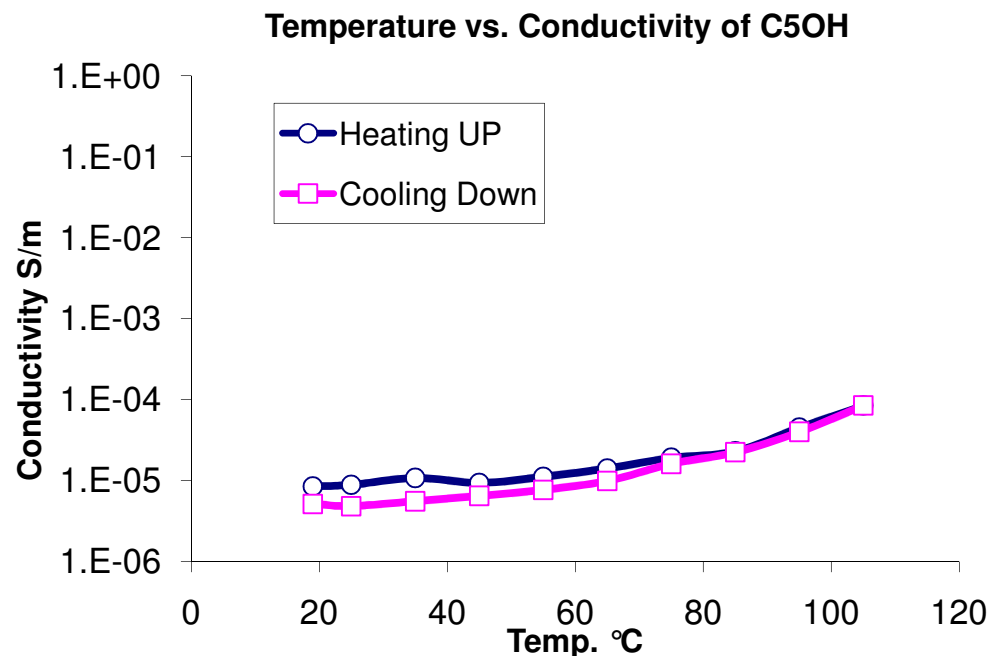


Figure 3.18: Temperature vs. Conductivity tests of C5OH on Glass

3.9 CAR in toluene

The effects of using toluene instead of chloroform for the casting solvent of the CAR were investigated. A ~50 nm thick CAR film (10 g/L in toluene) was prepared on a 10 μm gap Au-token. The sample was kept in a desiccator for 4 days, after which it was baked to 80°C for 5 min, see figure 3.19.



Figure 3.19: CAR in Toluene on two-probe token

Applied voltage ranges were 0 – 0.1, 10, 100V and temperature was 18, 25, 35, 45 and 105 °C. In the 0.1V applied voltage range a very noisy I-V characteristic was measured at all ranges, as shown in figure 3.20. Similar results were seen at larger applied voltage ranges as shown in figure 3.21.

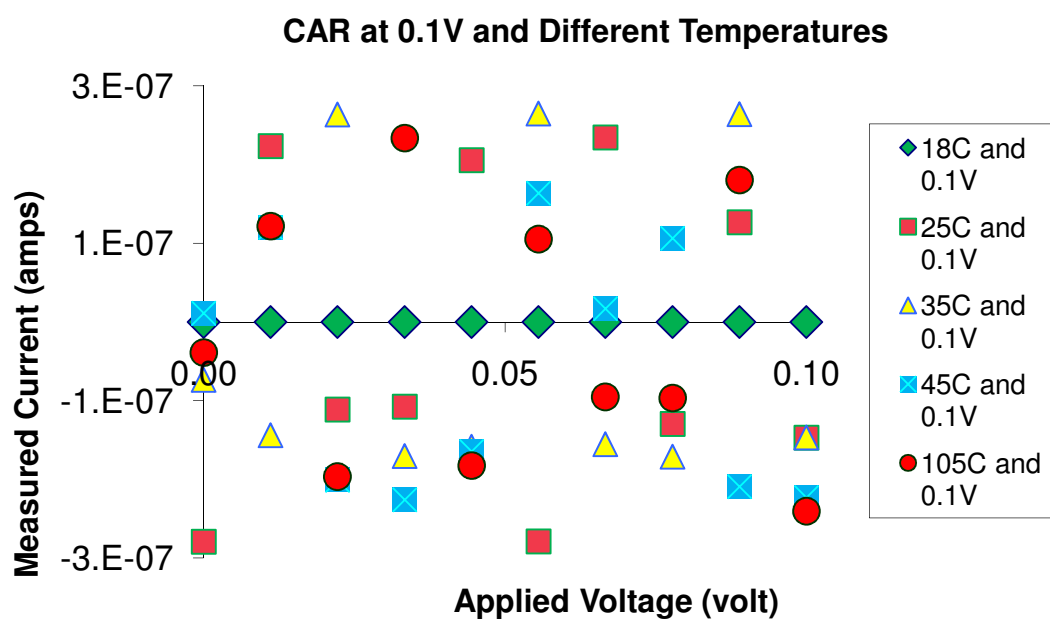


Figure 3.20: I-V curve of CAR. Applied voltage 0 – 0.1V at 18 – 105 °C

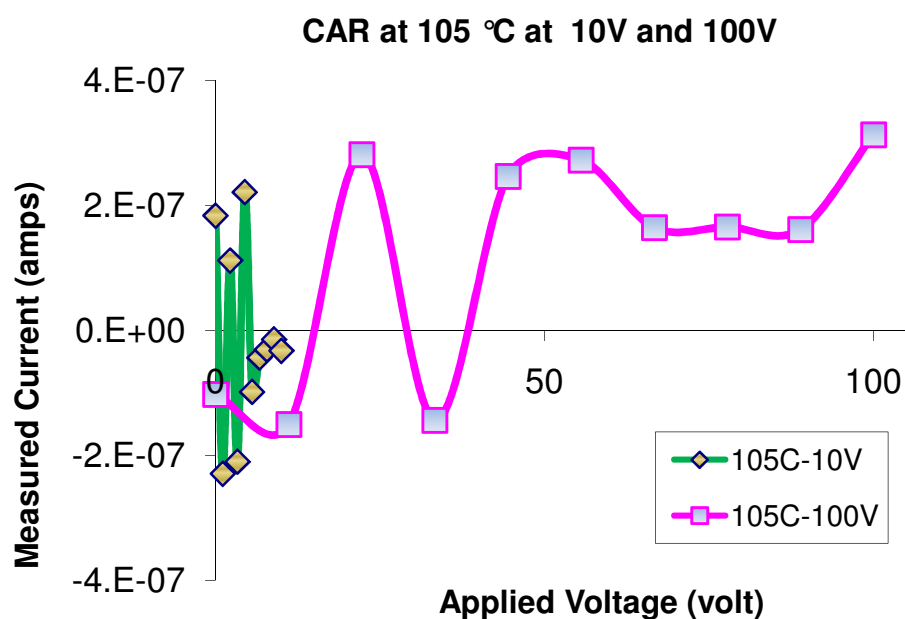


Figure 3.21: I-V curve of CAR. Applied voltage 0 – 10V and 0 – 100V at 105 °C

From figure 3.22, the I-V curve shows that at 0 – 10V there is some improvement when the sample was cooled down to 18 °C, indicate that the heater may be interfering with the measurements whether tests were conducted with the heater off after the sample had reached the required temperature. Using the same sample with the heater off, and voltage range to 100V, several repeatable measurements were taken as shown in figure 3.23. Table 3.4 shows the conductivity results.

Table 3.4: Conductivity of CAR (in toluene) at 18 °C

Temperature (°C)	Voltage (v)	Conductivity (S/m)
18	10	1.4×10^{-6}
	100 (1 st time)	4.2×10^{-6}
	100 (2 nd time)	3.7×10^{-6}
	100 (3 rd time)	3.2×10^{-6}

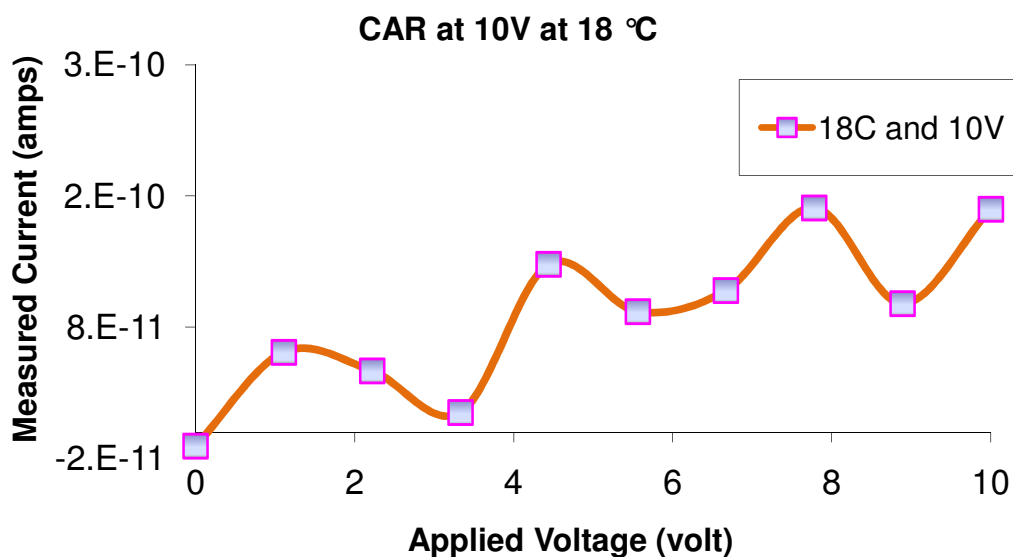


Figure 3.22: I-V curve of CAR. Applied voltage 0-10 Volt at 18 °C

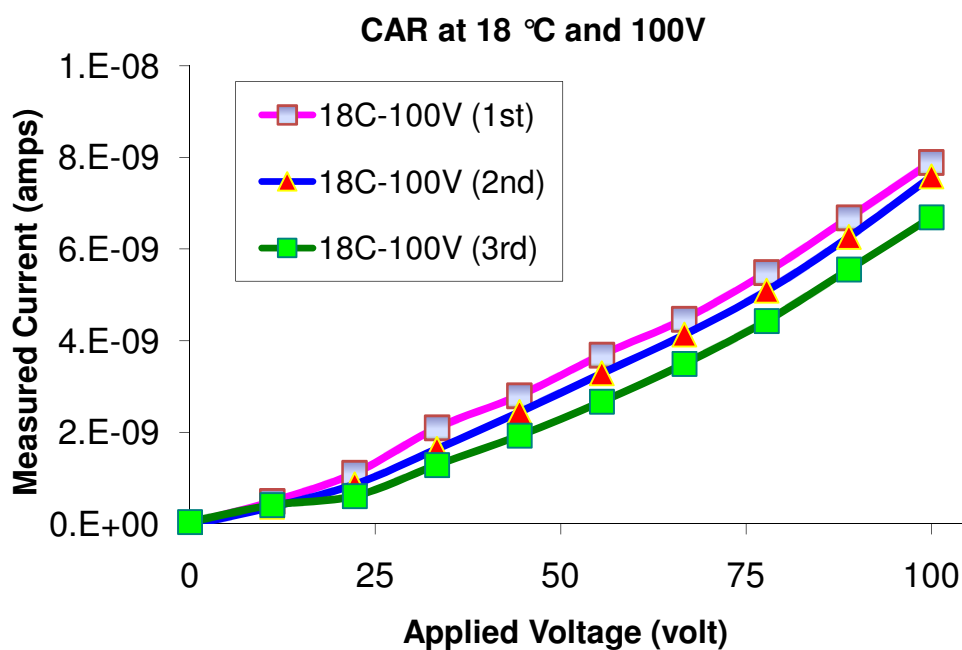


Figure 3.23: I-V curve of CAR. Applied voltage 0-100V at 18 °C

The conductivity of CAR in toluene at 18 °C was 10^{-6} S/m. It is seen that the conductivity is higher for larger voltage ranges which may be due to the triphenylene molecules becoming more aligned by increasing the voltage.

3.10 CAR (in toluene) – age test

The effects of film aging on conductivity were now examined. A ~60 nm thick CAR film (in 10 g/L in toluene [173, 174]) was prepared on the 10 μm gap Au-token. The sample was kept in the desiccator for 4 days to evaporate as much as of the solvent as possible. After 4 days the sample was baked at 80°C for 5 min, then left in the desiccator again for 7 days before measurements.

Two sets of measurements were taken one after 11 days and again after 14 days. In both cases sample temperature was 20 °C. The 14 day measurement is shown in figure 3.24 and the results summarized in table 3.5. No significant change in conductivity was seen.

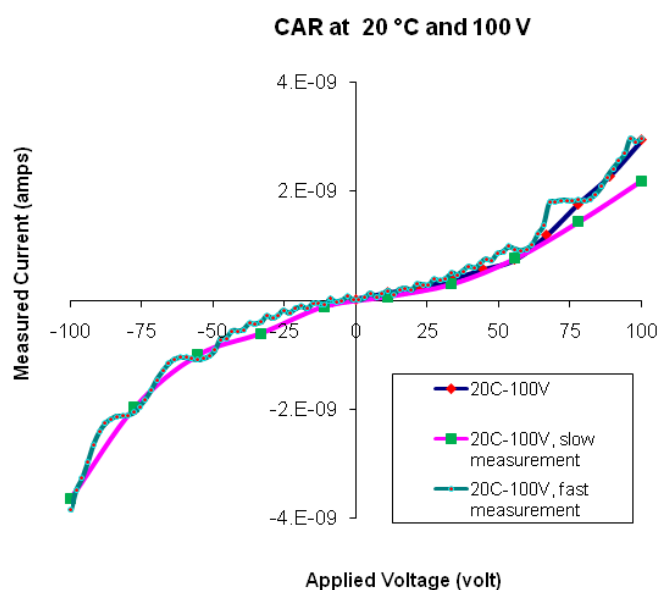


Figure 3.24: I-V curve of CAR. Applied voltage -100V to +100V at 20 °C

Table 3.5: Conductivity of CAR (in toluene) at 20 °C

Temperature (°C)	Measurement	Conductivity (S/m)
20	Day 11	1.16×10^{-6}
	Day 14 (slow)	1.18×10^{-6}
	Day 14 (fast)	1.19×10^{-6}

3.11 Conductivity tests in Cambridge

Four-probe VdP and two-probe measurements were carried out for both C5C5 and CAR at the University of Cambridge. Keithley 4200 was used for supply current/voltage and to record data. A four-probe station was used, which was placed inside a large Faraday box. For both two and four probe measurements, a 110 nm thick Au-coated glass token was used. Figure 3.25 shows the equipment used for this test.

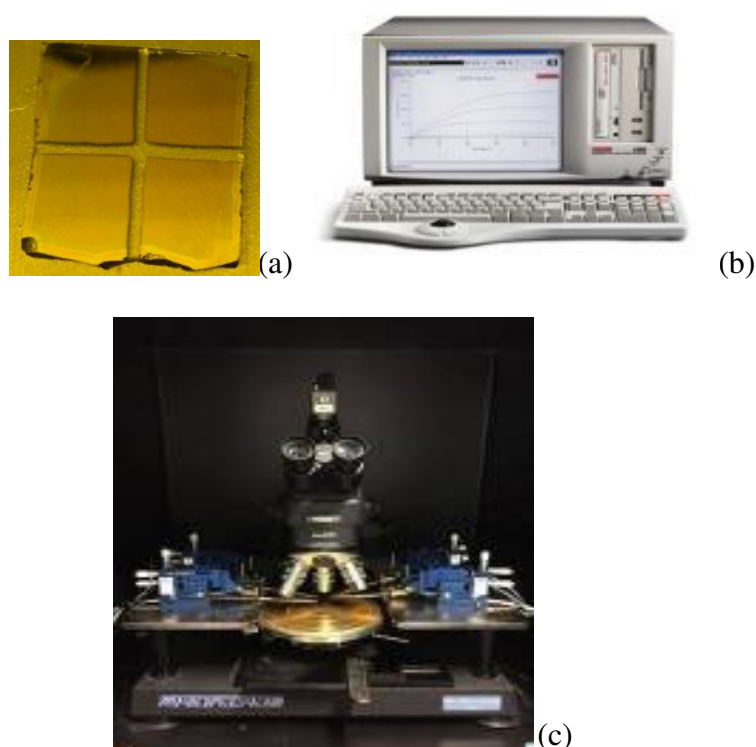


Figure 3.25: (a) Au-token, (b) Keithley 4200 [175] & (c) Probe-station inside a Faraday box

Both C5C5 and CAR film thicknesses were ~ 100 nm. For VdP measurements 1 and 10 pA current was supplied and voltage measured. The conductivity for both resists ranged between 10^{-4} to 10^{-6} S/m. For 2-probe measurements, 0-5V was supplied for both resists and for both cases the conductivity was 10^{-4} S/m. All these tests were performed at room temperature.

3.12 Conductivity tests at Chalmers University

Further confirmation of the results was sought using equipment at MC2 lab of Chalmers University of Technology. I-V measurements were carried out for both C5C5 and CAR with both the four-probe VdP and the two-probe method. Measurements were taken for samples at room temperature, and for samples that had been heated to 100 °C on a separate hot plate and then transferred to the probe station for measurement after cooling. A Keithley 4200 was used and 100V was supplied, however no Faraday box was available. Two Au-tokens were used for both the 2 and 4-probe measurements, and a Dektak 150 was used for measuring film thickness. Figure 3.26 shows the MC2 test equipment.

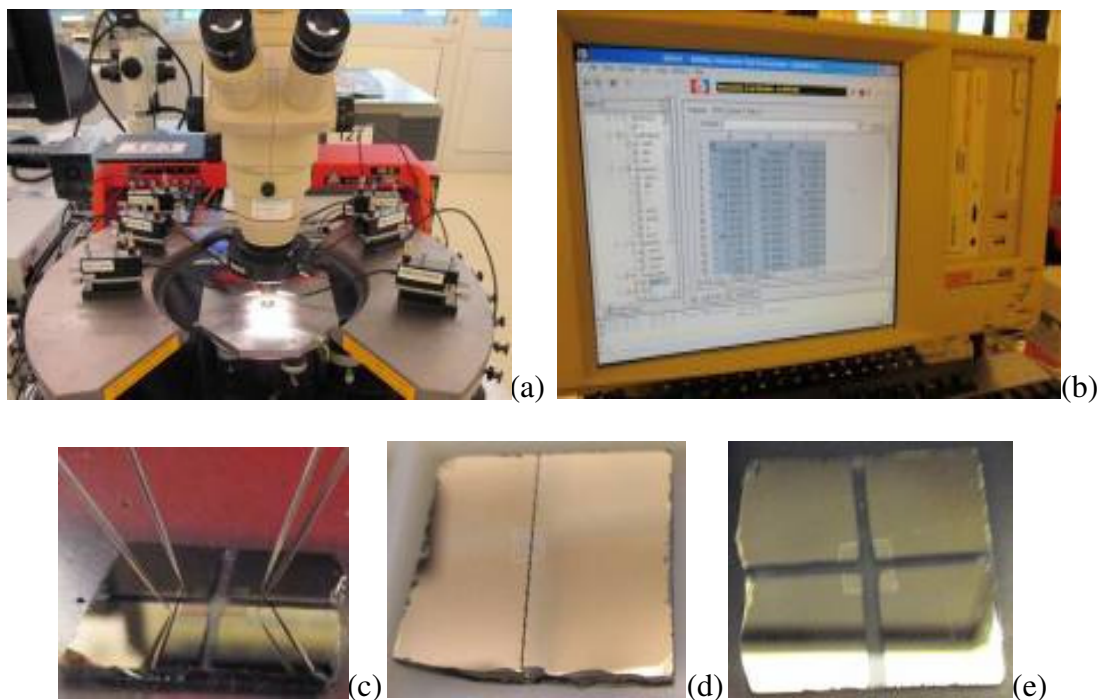


Figure 3.26: (a) MC2's Probe-Station without Faraday box, (b) Keithley 4200 (c) Sample under test (d) & (e) ~100 nm film on 2 and 4 probe-token

Around ~100 nm each of C5C5 and CAR was spin coated onto both tokens and a series of tests were run. Measurements were taken before and after heating each sample to 100 °C. The results are shown in table 3.6. For both C5C5 and CAR's conductivity was found between 10^{-4} to 10^{-5} S/m, somewhat higher than measured using the Birmingham equipment, but aligned with the Cambridge results.

Table 3.6: Conductivity of C5C5 and CAR at MC2, Chalmers

Resists	Probes	Temperature (°C)	Voltage (volt)	Conductivity (S/m)
C5C5	2	18	0 to 100	2.44×10^{-5}
	4		0 to 100	1.44×10^{-4}
CAR	2	18	0 to 100	1.70×10^{-5}
		After 100	0 to 100	1.56×10^{-5}
	4	18	0 to 100	1.22×10^{-4}
		After 100	0 to 100	1.39×10^{-4}

3.13 Conclusion

Various approaches have been performed to try to achieve consistent conductivity results for both C5C5 and CAR. All these results clearly display the high resistivity of triphenylene. Resists such as C5C5, CAR, PMMA, C5EPX, and C5OH have been compared; age test; influence of temperature and voltage have been examined; in all cases their conductivity is found to be between 10^{-4} and 10^{-6} S/m. Conductivity as a function of thickness has been examined. It is shown that when the thickness increases the conductivity decreases, due to a change in the orientation of the molecules within the film; specifically, the triphenylene molecules stack in an aligned manner for films of ~100 nm thickness and below, when spin coated onto the

substrate. However, as the thickness is increased the molecular alignment becomes increasingly disordered, which affects the conductivity measurement.

Further work is clearly required to re-investigate the resist's conductivity performance inside an ideal faraday box and with more controlled tokens, and with varied probe distance.

Chapter 4

Lithography tests

It is not sufficient for a material to simply be conductivity to form a good electron beam resist. The material must demonstrate a change in solubility upon exposure to electrons so that a pattern can be formed. The critical metrics for a resist are the sensitivity to irradiation, the resolution (smallest pattern able features) and the line edge roughness. In electron beam exposure on insulating substrate resolution is the highest challenge, although it is also important to consider that charging can be reduced through the use of a fast (sensitive) resist. In this chapter is presented the lithographic evaluation of the triphenylene based electron beam resists on normal conductive substrates and typical insulating materials such as glass.

4.1 Resist preparation

The very first task was to find the appropriate casting solvent for the resist (i.e. pure C5C5 and the CAR). In previous [176] tests it was found that C5C5 is well dissolved in chloroform.

To investigate casting solvents 10 g/L C5C5 was dissolved in chloroform, propylene glycol monomethyl ether acetate (PGMEA), cyclohexanone, ethyl lactate

(EL) and anisole. The C5C5 was well dissolved in all the solvents; although extra ultrasonic agitation was required for the PGMEA solution. After this, the resist was spin coated to 1.8 cm × 1.8 cm Si-wafer with 2000 rpm for 60 seconds. Bad film formation has been observed with cyclohexanone, ethyl lactate and anisole due to de-wetting. To reduce de-wetting several surface treatments were tested including priming with hexamethyldisilazane (HMDS) and substrate cleaning, as described in the section 3.2, both of which change the substrate hydrophobicity. Additionally conditions and spinning profiles were investigated. In all cases chloroform solutions produced the best (most uniform) films. PGMEA also produced acceptable pure C5C5 films but did not dissolve C5EPX. Whilst chloroform is not a popular solvent choice from an industrial perspective, it was used unless noted in this work

4.2 Substrate cleaning

For testing conductivity of C5C5 and CAR, the glass substrate was used and for sensitivity and high resolution tests both silicon and glass substrates were used.

Where a hydrophobic surface was desired a multistep cleaning process was used as described here. First 1.8 cm × 1.8 cm Si or 1.5 cm × 1.5 cm glass chips were diced to the appropriate size and then immersed in IPA and sonicated for 15 minutes, followed by rinsing with de-ionized (DI) water for 1 minute. Then chips were dipped in the freshly made piranha solution (1:1; H₂SO₄:H₂O₂) for 10 minutes to remove contamination (and, for Si, to oxidize the substrate). Then Si chips were washed in DI water for 1 minute. Finally the Si was immersed in 49:1 of H₂O:HF for 1 minute, followed by rinsing in DI water for 1 minute. Hydrogen fluoride (HF) removes the oxide and leaving hydrophobic hydrogen terminated Si. Results of this extensive cleaning procedure are shown in section 4.4.1.

In other cases, a simplified cleaning procedure was used; involving sonication in IPA (15 minutes), then acetone (15 minutes) then a rinse in DI water for both C5C5 and CAR films with chloroform as casting solvent.

4.3 Film processing

For sensitivity tests 10 g/L C5C5 and CAR in chloroform solution was prepared and filtered with a 0.2 μm filter. Samples were placed on a spin coater with the rotation speed and duration set to 600 rpm for 60 seconds. 100 μl of resist solution was dispensed onto the Si substrates (1.8 cm \times 1.8 cm) and the spin coater was started. This formed a 100 nm thick film, which then received a bake at 70°C for 5 minutes to remove the residual solvent.

For resolution tests, 5 g/L C5C5 in chloroform solution was prepared and filtered. This was spun at 2000 rpm and baked at 70°C for 5 minutes to form a 20 – 40 nm thick film. For CAR, 5 g/L CAR was used to produce 20 – 40 nm thick film with a spin speed of 2000 rpm for 60 seconds and then a bake for 2 minutes in 50 °C.

For PGMEA, the procedure was same as chloroform with both C5C5 and CAR on glass and Si substrates. For producing CAR films, a solution was prepared with C5EPX:C5OH:PAG in 1:0.67:1 ratios with chloroform and PGMEA. Two PAGs triphenylsulfonium hexafluoroantimonate (TPS SbF_6) and triarylsulfonium hexafluoroantimonate (TAS SbF_6) were used with the latter producing better quality of smooth films on both Si and glass substrates.

The C5EPX:C5OH:TPS SbF_6 (1:0.67:1) resist in 10 g/L PGMEA was spin coated with a speed of 500 rpm for 5 seconds in the 1st ramp, then 1200 rpm for 60 seconds in 2nd ramp and in 3rd ramp the speed was set to 2000 rpm for 10 seconds.

After baking for 5 minutes in 70 °C it was possible to produce a 17 nm film, which was later used for high resolution tests.

The C5EPX:C5OH:TAS SbF₆ (1:0.67:1) resist in 10 g/L chloroform was spin coated at 500 rpm for 5 seconds in the 1st ramp and then 1000 rpm for 60 seconds in the 2nd (final) ramp, which produced vary smooth ~25 nm film which was backed for 50 °C for 2 minutes after spin coating.

In addition to the conditions specified above the effect of HF cleaning substrates (or not), and the effect of baking conditions, on the patterning capability was evaluated for the CA resists.

4.4 Lithographic Performance: Sensitivity and Contrast

To measure the resist sensitivity and the contrast, after exposure and development, the residual film thickness was measured using the surface profiler as a function of dose. The thickness measurements were normalized to the unexposed film thickness. The data was fitted with a sigmoidal function to represent the curve. The curve is given in eqn. 3.1.

$$f(x) = \frac{1}{1+Ax^{-B}} \quad (3.1)$$

From this and setting $f(x) = 0.5$, eqn. 3.1 can be rearranged to give the negative tone setting ($E_{50\%}$) as

$$E_{50\%} = A^{\frac{1}{B}} \quad (3.2)$$

whilst the contrast, γ is given by eqn. 3.3

$$\gamma = \left(\frac{\ln 10}{4}\right) B \quad (3.3)$$

where, A and B are fitting parameters.

All sensitivity plots in this project were fitting using the KaliedaGraph v4.0 software.

4.4.1 Pure C5C5

To measure sensitivity, the ebeam energy was set to 20 keV and a large electron beam spot size was chosen (to maximize the current). A film of C5C5, of thickness 100 nm was prepared on a silicon substrate. A pattern of 15 squares (25×25 micron) was designed with a dose range from 400 – 21,676 $\mu\text{C}/\text{cm}^2$. The beam current was ~0.17 nA and the exposure time was 55 minutes. After exposure the samples were developed in pure monochlorobenzene (MCB) for 20 seconds and rinsed in IPA for 3 – 4 seconds and blow dried with nitrogen. The sensitivity was found to be 4.3 mC/cm^2 and the contrast 3.7 (figure 4.1).

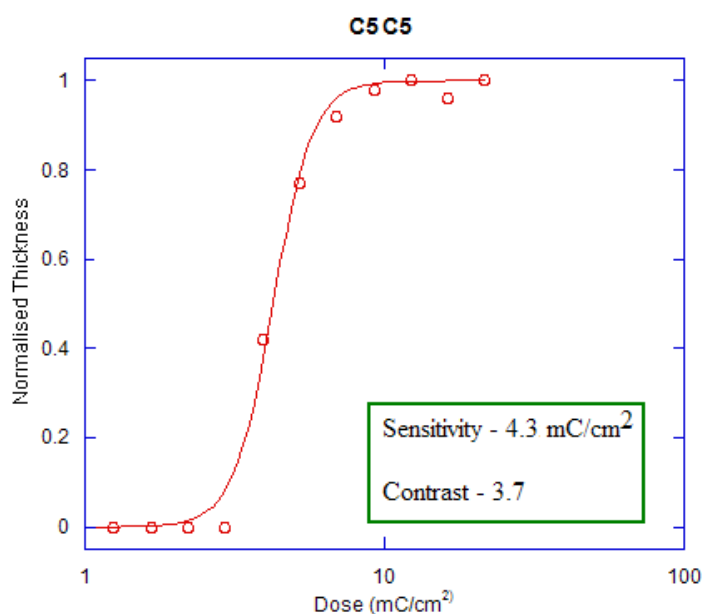


Figure 4.1: Sensitivity of pure C5C5

4.4.2 Chemically amplified resist

For all of the sensitivity tests using the CAR a formulation ratio 1:0.67:1 of C5EPX:C5OH:TAS SbF_6 was used. Solutions of strength 10g/L were prepared in various casting solvents. Films were prepared using PGMEA and chloroform, whilst cyclohexanone and anisole were not suitable for this resist system.

4.4.2.1 CAR in PGMEA

Sensitivity testing was performed on silicon substrates, which were cleaned with acetone and IPA and spin coated with the CAR using a multistep spin profile (500 rpm for 5 seconds; 700 rpm for 60 second; 2000 rpm for 10 seconds) to produce ~40 nm smooth films.

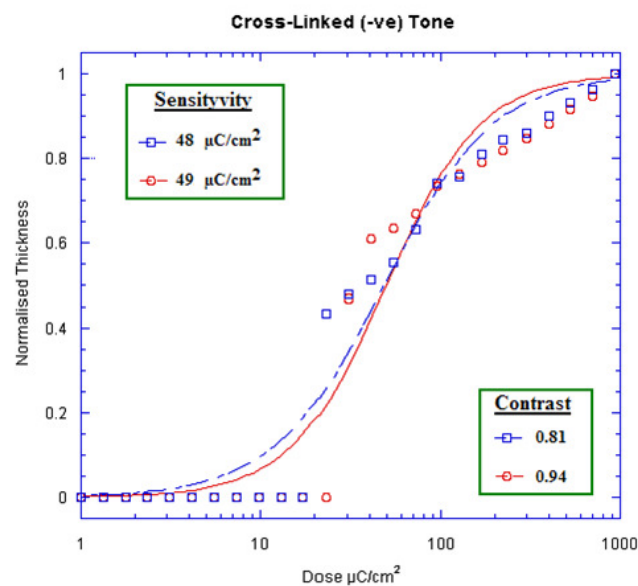


Figure 4.2: Sensitivity of (-) tone CAR

An ebeam current of 0.138 nA was set, with 20 keV and spot size 3. A pattern of 25 squares (25×25 micron) was designed with a dose range from 4 – 937 $\mu\text{C}/\text{cm}^2$. After exposure, each sample was baked with 100°C for 1 min and then developed with

PGMEA for 3 seconds. After development, the residual film thickness was around 16 – 35 nm. The sensitivity was found $48 \mu\text{C}/\text{cm}^2$ (blue line) & $49 \mu\text{C}/\text{cm}^2$ (red line) and the contrast was 0.81 and 0.94 (see figure 4.2).

4.4.2.2 CAR in chloroform

Samples were prepared using CAR in chloroform solution, and with three different Si-substrate treatments – (i) HF cleaned Si substrate (ii) IPA/acetone cleaned Si substrate with no post application bake (PAB) applied after the spin coating, and (iii) IPA/acetone cleaned Si substrate with 70 °C for 2 min PAB procedure.

Development was in MCB for 10 seconds. After spin coating (500 rpm 5 seconds; 700 rpm for 60 seconds; and 2000 rpm for 10 seconds) the film thickness (i) 35 nm, (ii) 40 nm & (iii) 33 nm, for respective cleaning procedures.

The film quality samples (i) and (ii) are similar, but for sample (iii) signs of film crystallization due to the baking step can be seen (figure 4.3). To exposure these samples, the beam energy was set to 20 keV, and spot size 3. The current was found to be 0.137 nA. A pattern of 25 squares (25×25 micron) was designed with a dose range from 4 – 937 $\mu\text{C}/\text{cm}^2$.

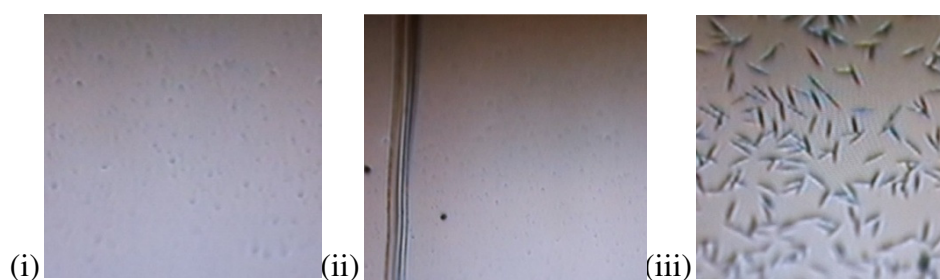


Figure 4.3: Film condition after spin coating

After the exposure and the development, for all three samples the patterns were not well defined. In case of sample (iii) in particular, the top surface of the exposed squares looked very uneven with very high peaks (see figure 4.4).

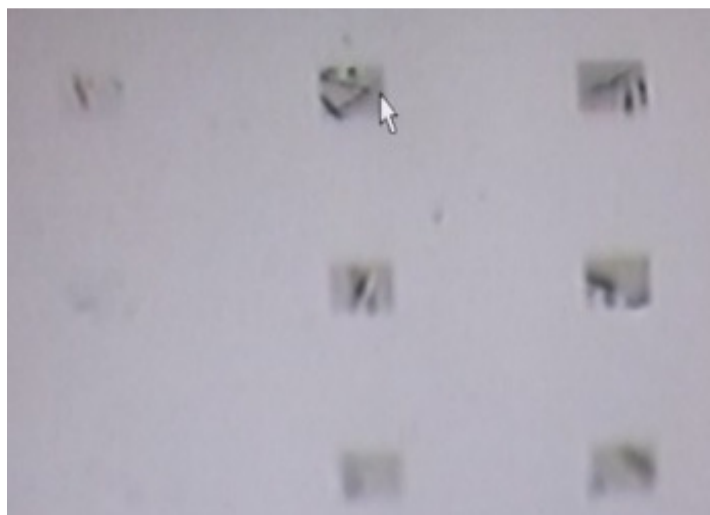


Figure 4.4: Uneven top surface of each square (sample iii)

Although there was significant loss of material in the exposed areas it was possible to measure the sensitivity to be $26 \mu\text{C}/\text{cm}^2$ for sample (i) but higher doses were required for the other two samples, see figure 4.5.

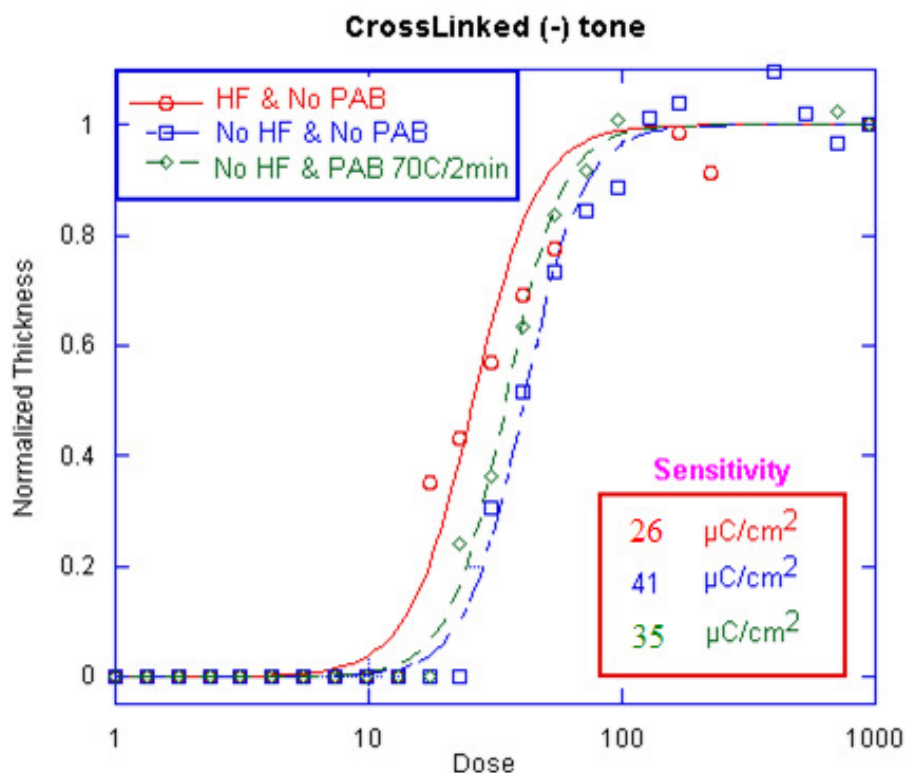


Figure 4.5: Sensitivity of (-) tone CAR, where the sensitivity of the sample (i) $26 \mu\text{C}/\text{cm}^2$, sample (ii) $41 \mu\text{C}/\text{cm}^2$, sample (iii) $35 \mu\text{C}/\text{cm}^2$ and the contrast of the sample (i) 1.96, sample (ii) 2.15, sample (iii) 2.23

4.4.2.3 Optimizing film formation

To optimize film formation, several solvents with various PAB combinations were investigated. Chloroform, MCB and PGMEA spun samples were prepared and various PAB conditions applied. The concentration of the resist solutions were the same in each case, i.e. 10 g/L.

A multistep spin profile (500 rpm for 5 seconds; 1000 rpm for 60 seconds) was used for all samples. Sample 1, which was dissolved in 10 g/L chloroform, with no PAB showed crystallization of the ~84 nm film. Sample 2 (10 g/L chloroform with 2 minutes PAB 70 °C) showed less particles in the film and it produced ~122 nm thickness film. In the third sample as film thickness of ~188 nm was formed using 10 g/L chloroform with a 5 minutes PAB 70 °C. The film was highly crystallized. Using MCB as the casting solvent (10 g/L) with a 5 minutes PAB 70 °C, a very smooth film with no particles and film thickness of ~35 nm was produced. Finally using 10 g/L PGMEA, and additionally filtering with 0.2 µm syringe filter, before spinning and applying a 5 minutes, with 5 minutes 70 °C PAB, showed a very smooth film with no particles and film thickness ~35 nm. Figure 4.6 shows the films achieved for each condition.

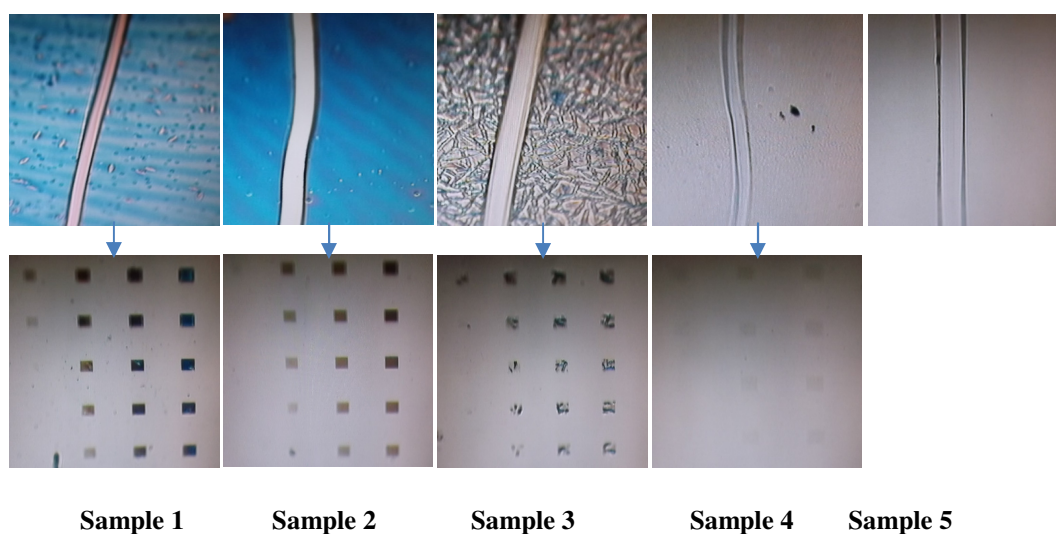


Figure 4.6: Samples after spin coating and after developing

To calculate the sensitivity the ebeam was set to 20 keV with 0.4 nA beam current (spot size 4). A dose range from 4 – 937 $\mu\text{C}/\text{cm}^2$ was used. After exposure, all five samples were baked for 1 min at 100 °C and then developed in MCB for 10 seconds.

Except for the PGMEA film, all of the samples showed some patterning after exposure. Due to broken and non-uniform patterns, the residual film thickness could not be measured for the highly crystallized sample 3. No patterns have been seen with sample 5 (CAR in PGMEA) possibly due to the filtering step. The best sensitivity was found for sample 2 ($80 \mu\text{C}/\text{cm}^2$), see figure 4.7.

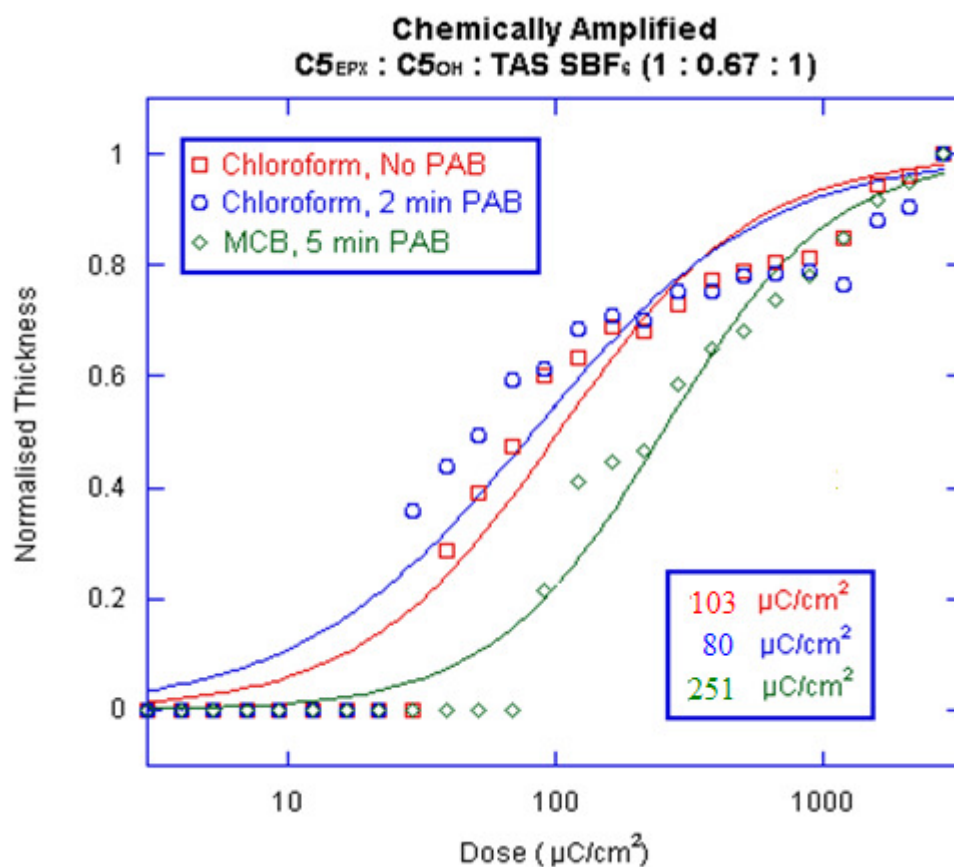


Figure 4.7: The sensitivity of the sample 1 is $103 \mu\text{C}/\text{cm}^2$, sample 2 is $80 \mu\text{C}/\text{cm}^2$, sample 3 is $251 \mu\text{C}/\text{cm}^2$ and the contrast of sample 1 is 0.68, sample 2 is 0.58, sample 3 is 0.78.

4.4.2.4 CAR on glass

Due to the charging issue it is very difficult to see image patterns on glass using the SEM. To undertake lithographic patterning it is necessary to achieve good focus, but due to continuous charging of the glass, or any insulating substrate, this is very difficult to achieve. Therefore for the focusing purpose a very thin layer (~ 10 nm) of gold was sputtered on the corner of the glass substrate, see figure 4.8. The pattern was generated about 100 μm away from the gold coated focusing.

After spin coating (500 rpm for 5 seconds; 1000 rpm for 60 seconds) the CAR in chloroform produced a ~80 nm film on glass. After performing several tests it was found a PAB of 50 $^{\circ}\text{C}$ for 2 minutes gave a very smooth and reliable film for patterning.

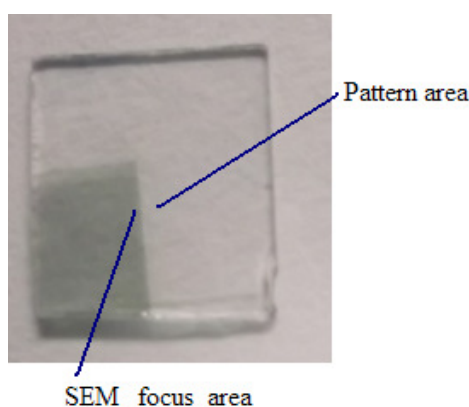


Figure 4.8: Au on glass for focusing under SEM

The ebeam energy was set to 20 keV with 0.38 nA beam current (spot size 4). A dose range from 4 – 937 $\mu\text{C}/\text{cm}^2$ was chosen and a sensitivity matrix patterned. A second sample also was patterned using same dose range. Both samples were baked for 2 minutes at 50 $^{\circ}\text{C}$ and then developed in MCB for 10 seconds. For imaging purposes ~4 nm of gold was sputtered on top of the developed sample.

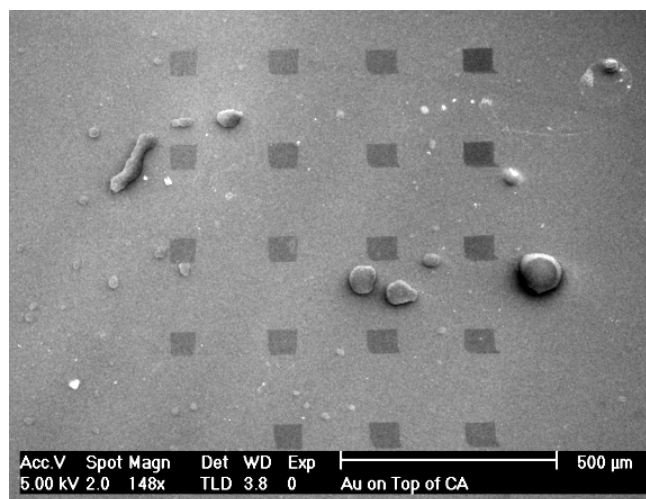


Figure 4.9: After sputtering ~4 nm gold on top (1st sample)

Figure 4.9 shows the dose matrix of the higher dose range sample. The four squares on the left hand side look very sharp, where doses are between 11 – 108 $\mu\text{C}/\text{cm}^2$. As the doses were increased over 108 $\mu\text{C}/\text{cm}^2$ the squares become deformed, indicate of over dosing.

Similar results were seen for the second sample shown in figure 4.28. Clear patterns were seen in the dose range 17 – 92 $\mu\text{C}/\text{cm}^2$. As the doses were increased over 91.5 $\mu\text{C}/\text{cm}^2$ the squares started to deform. From figure 4.9 and 4.10, it can be seen that an area dose of 92 $\mu\text{C}/\text{cm}^2$ or below is required to achieve sharp squares at 20 keV exposure.

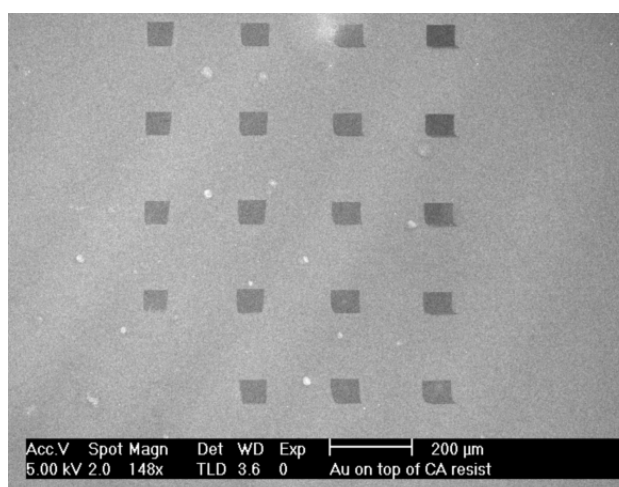


Figure 4.10: After sputtering ~4 nm gold on top (2nd sample)

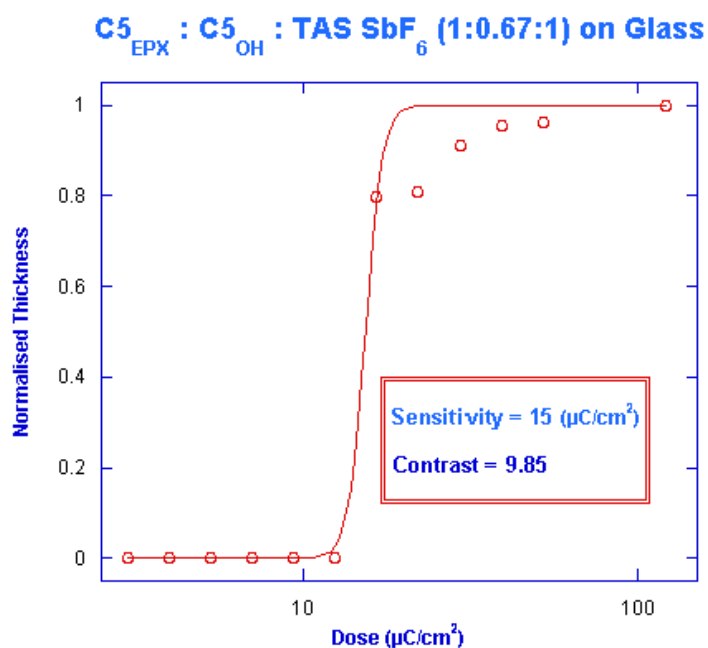


Figure 4.12: After gold sputtered on top.

4.5 Resolution

For high resolution tests on glass chloroform was used as a casting solvent and both pure C5C5 and CAR (C5EPX:C5OH:TAS SbF₆, 1:0.67:1) had concentration of 10 g/L.

4.5.1 Pure C5C5

A 28 nm of C5C5 film was prepared on Si. The ebeam voltage was set to 30 keV with 0.047 nA beam current (spot size 2). A line dose range of 5 – 162.5 nC/cm was chosen. A pattern of dense as isolated features at a range of line widths and pitches was used. After exposure the sample was developed in MCB for 1 minute and then it rinsed in IPA for 5 seconds. No baking step was applied.

To measure resolution, after exposure and development, the patterns were observed with the SEM (5 keV beam energy, ultra-high resolution mode). The feature

size was measured using the microscope's built-in software.

Figure 4.13 shows a 14.1 nm pattern written with a dose of 32 nC/cm. Dense features with 13.8 nm line-width on a 40 nm pitch were patterned with 62 nC/cm line dose, and are shown in figure 4.14.

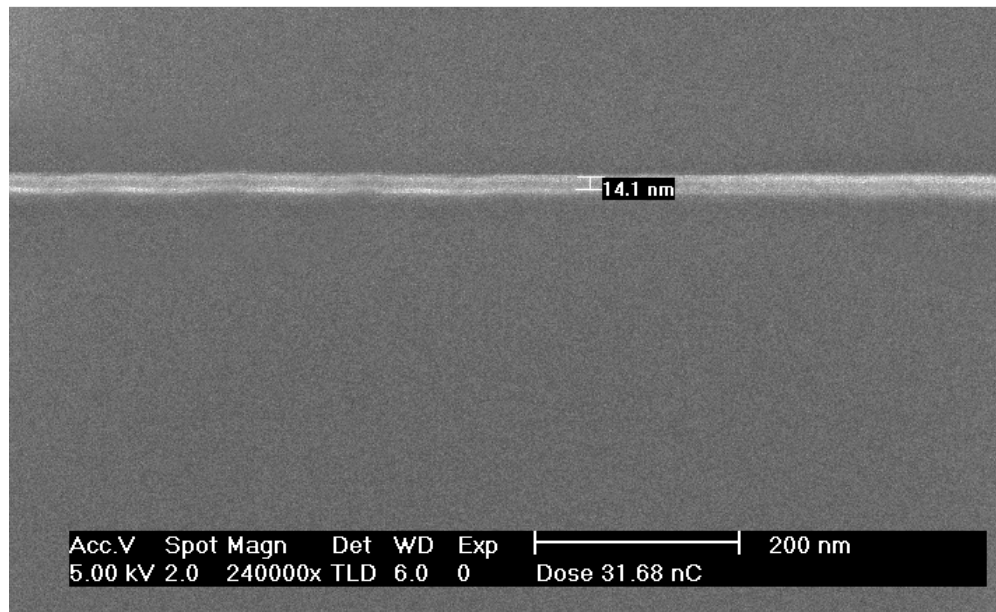


Figure 4.13: 14.1 nm pattern in a 28 nm C5C5 film at 32 nC/cm dose

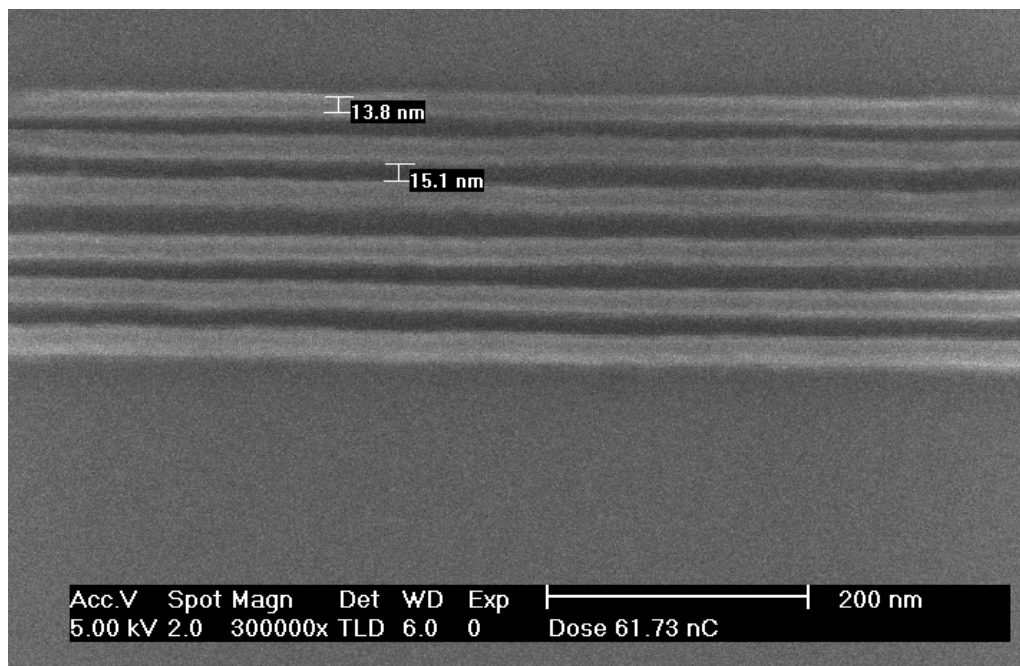


Figure 4.14: 20 nm half pitch lines in a 28 nm C5C5 film at 62 nC/cm dose

4.5.2 CAR

4.5.2.1 CAR in chloroform on silicon

Two samples were prepared for the high resolution test of the CAR. For the first sample an acetone/IPA cleaned Si substrate was used, and for the second sample a HF cleaned Si substrate was used. After spin coating the first sample was baked for 2 minutes at 70 °C and for the second sample no baking step was applied. Both samples had a film thickness of ~25 – 30 nm, with good smoothness.

For patterning the beam energy was set to 30 keV with 0.042 nA beam current (spot size 2), the applied line dose for both samples was 0.05 to 1.62 nC/cm. After exposure the samples were baked for 1 minute at 100 °C, and then developed in MCB for 10 seconds and rinsed in DI water.

After development it was observed that (figure 4.15 – 4.18) the resist showed patterning at resolutions down to 50 nm half pitch on the non-HF cleaned Si at a line dose of 0.34 nC/cm. Feature sizes in excess of 60 nm were well resolved.

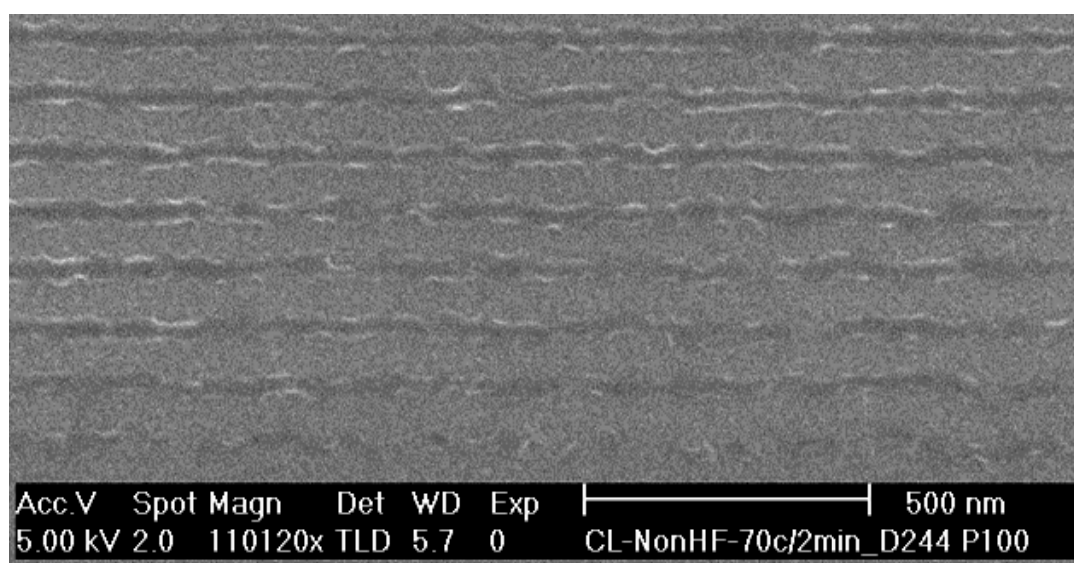


Figure 4.15: 100 nm half pitch lines in a ~28 nm CA film on non-HF cleaned Si at 0.24 nC/cm dose

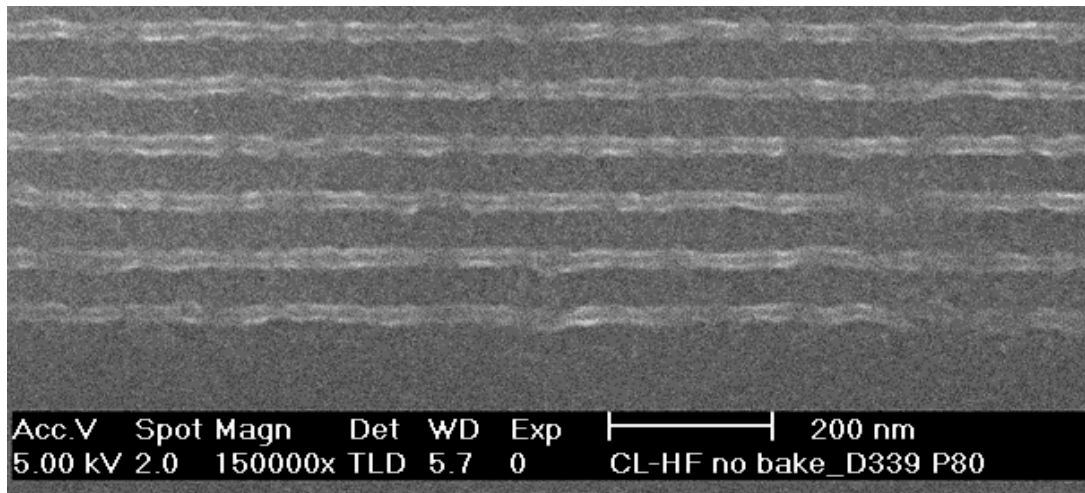


Figure 4.16: 80 nm half pitch lines in a ~28 nm CA film on non-HF cleaned Si at 0.34 nC/cm dose

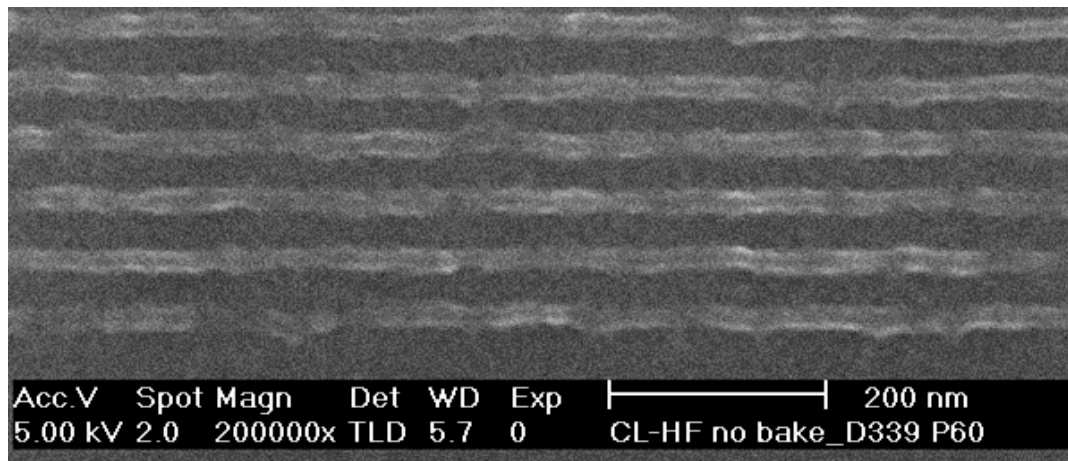


Figure 4.17: 60 nm half pitch lines in a ~28 nm CA film on non-HF cleaned Si at 0.34 nC/cm dose

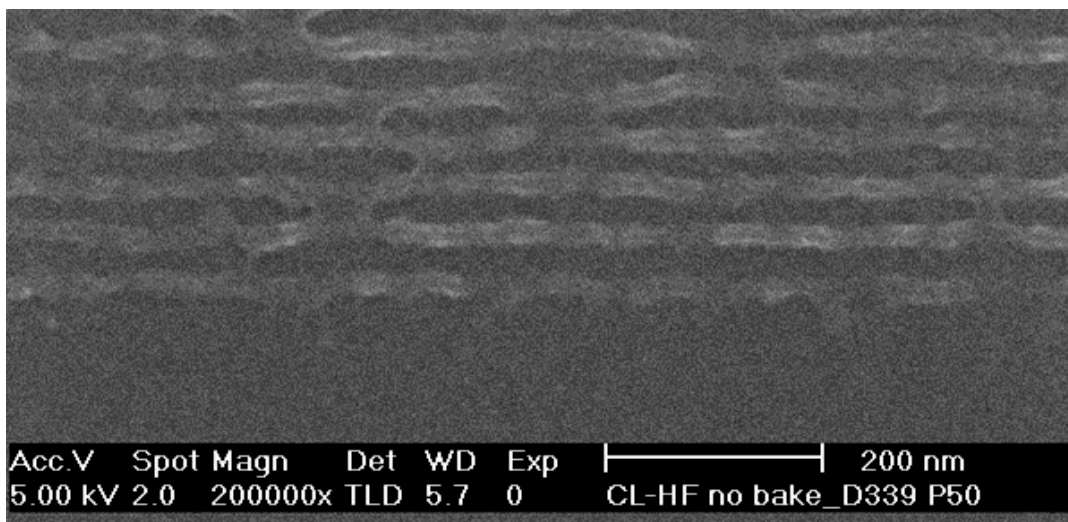


Figure 4.18: 50 nm half pitch lines in a ~28 nm CA film on non-HF cleaned Si at 0.34 nC/cm dose

4.5.2.2 CAR in chloroform on glass

About ~80 nm thick CAR film was prepared on a glass sample (spin speed to 500 rpm for 5 seconds; 1800 rpm for 60 seconds). The sample was baked at 50 °C for 2 minutes before exposure.

For patterning the ebeam energy was set to 30 keV with 0.038 nA beam current (spot size 2), the applied area doses were 20 – 650 $\mu\text{C}/\text{cm}^2$ and 50 – 1625 $\mu\text{C}/\text{cm}^2$; line doses were 1 – 32.5 nC/cm. After exposure the samples were baked for 1 minute at 100 °C and then developed in MCB for 10 seconds.

For images in the SEM, ~4 nm of gold was sputtered on top of the developed patterns to prevent the charging. The lithographic results are shown in figures 4.19 and 4.20.

Whilst these results are the highest resolution ebeam patterning on glass without a charge dissipation layer, the thickness of the film probably prevented even better results. It was difficult to produce a sub 30 nm film with the CA resist form 10 g/L chloroform as the chloroform evaporates very fast during the spinning process, even with the spin speed raised up to 8000 rpm it produced around ~68 nm film.

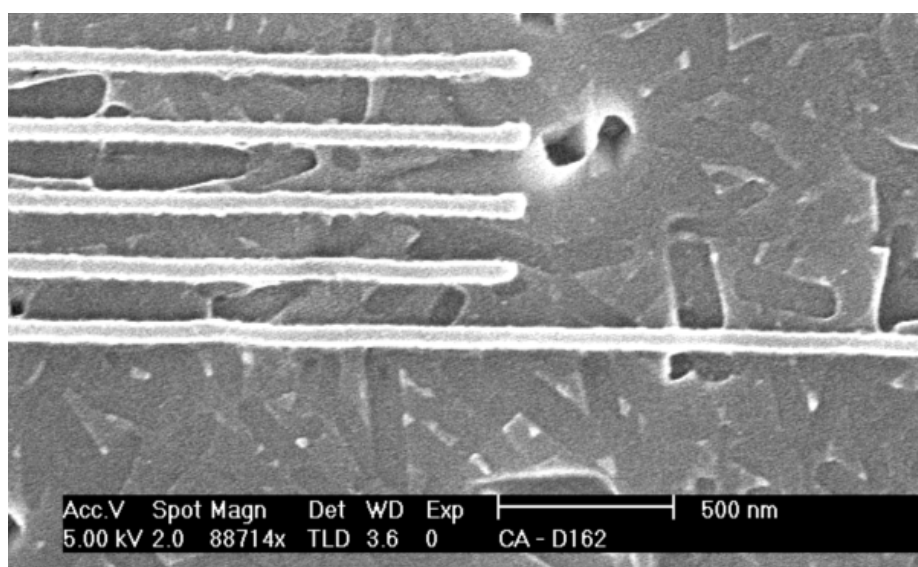


Figure 4.19: At 20 $\mu\text{C}/\text{cm}^2$ dose, 76 nm features on a pitch of 200 nm on glass

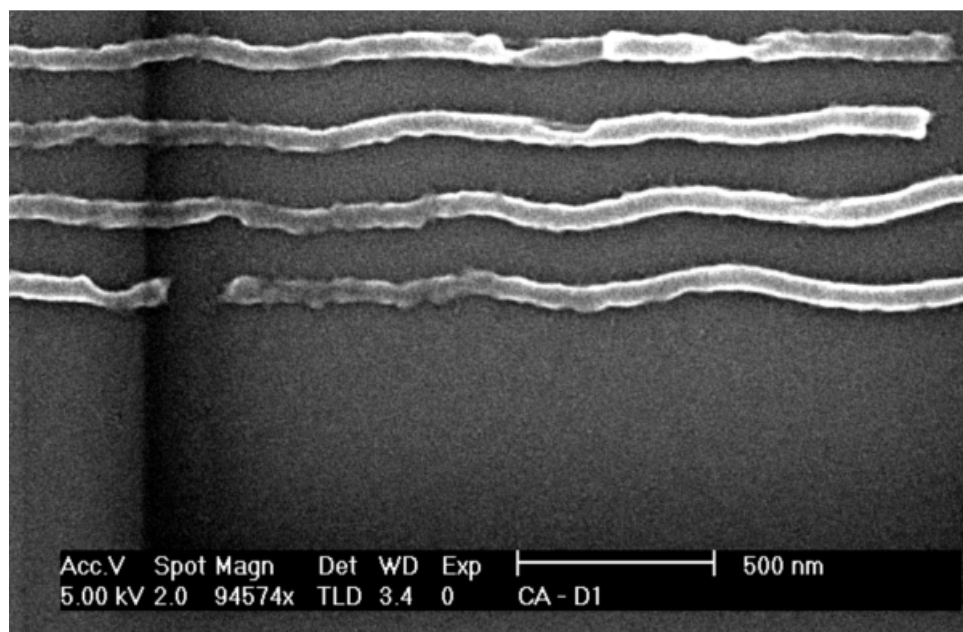


Figure 4.20: At $50 \mu\text{C}/\text{cm}^2$ dose, 55 nm features on a pitch of 200 nm on glass

Thus the CAR solution concentration was reduced to 5 g/L in chloroform. To achieve ~30 nm thick CAR film on glass spin speed was set to 500 rpm for 5 seconds and then 1000 rpm for 60 seconds. The sample was then baked at 50 °C for 2 minutes before the exposure. Beam energy was set to 30 keV with 0.038 nA beam current (spot size 2). An area dose range of 15 – 488 $\mu\text{C}/\text{cm}^2$ and 10 – 325 $\mu\text{C}/\text{cm}^2$; line dose range of 0.15 – 4.88 nC/cm was set. After exposure the samples were baked for 1 minute at 100 °C, and then developed in MCB for 10 seconds. For imaging with SEM, around ~4 nm gold was sputtered on top of the developed patterns.

In figure 4.21, 200 nm and 100 nm half pitch patterns were fully resolved at a dose of 116 $\mu\text{C}/\text{cm}^2$, however the 50 nm half pitch at dose 116 $\mu\text{C}/\text{cm}^2$ and single pixel lines with 1.16 nC/cm dose are not resolved.

In figure 4.22, at 360 $\mu\text{C}/\text{cm}^2$ dose the 200 nm half pitch patterns looks promising, but evidence of crystallization is seen which is probably limiting the higher resolutions. Further work to optimize for thin film formation on glass is required.

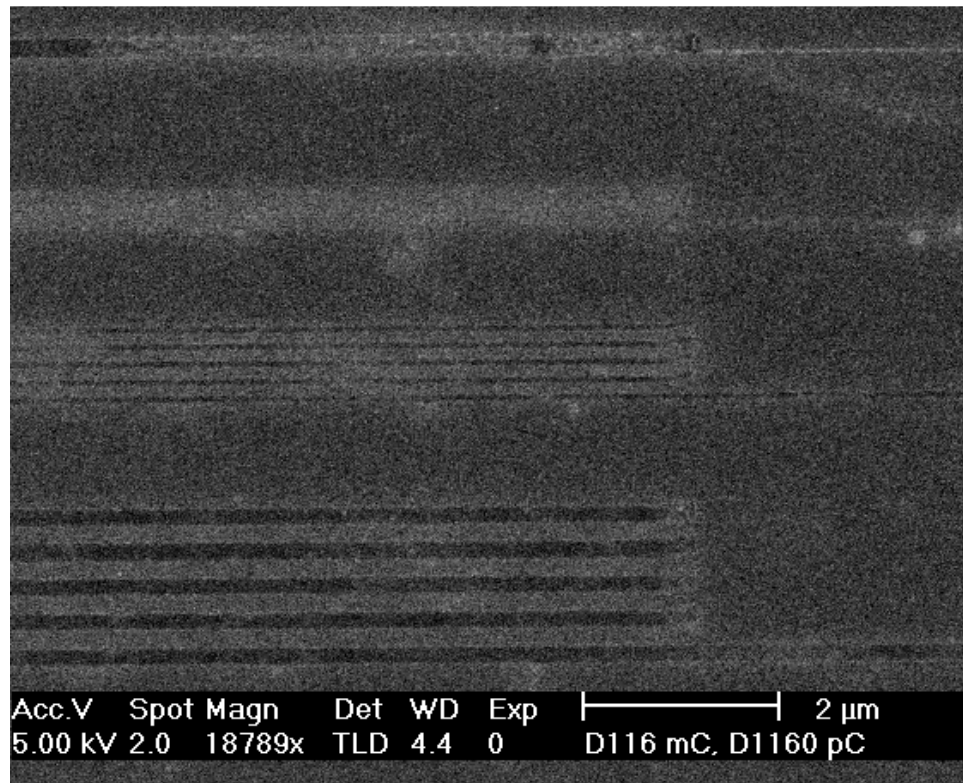


Figure 4.21: Area dose $116 \mu\text{C}/\text{cm}^2$ and line dose $1.16 \text{ nC}/\text{cm}$ on glass

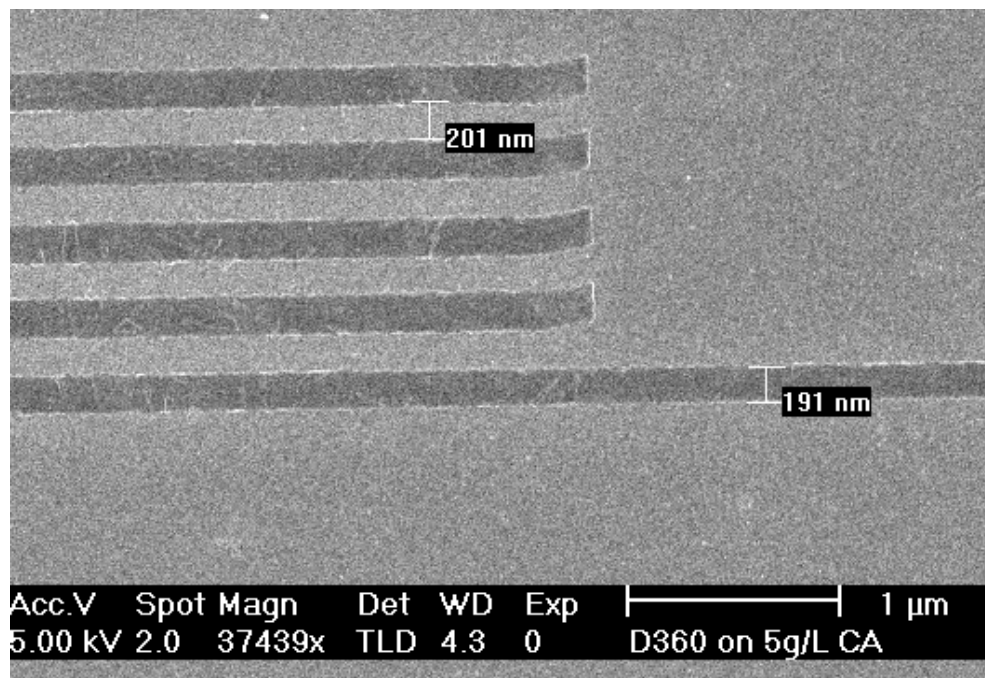


Figure 4.22: 200 nm half pitch and $\sim 200 \text{ nm}$ line at $360 \mu\text{C}/\text{cm}^2$ on glass

4.5.2.3 Comparing PMMA on glass

Whilst it is clear that the resolution can be achieved on glass in the CAR is not as good as that which can be achieved on silicon, it is nonetheless promising. For comparison films of PMMA were also patterned on glass. On a conductive substrate such as silicon, PMMA is one of the highest resolution ebeam resist.[110, 175] For comparing high resolution patterns with CAR in chloroform a ~30 nm PMMA (950 A2) film was therefore prepared on glass.

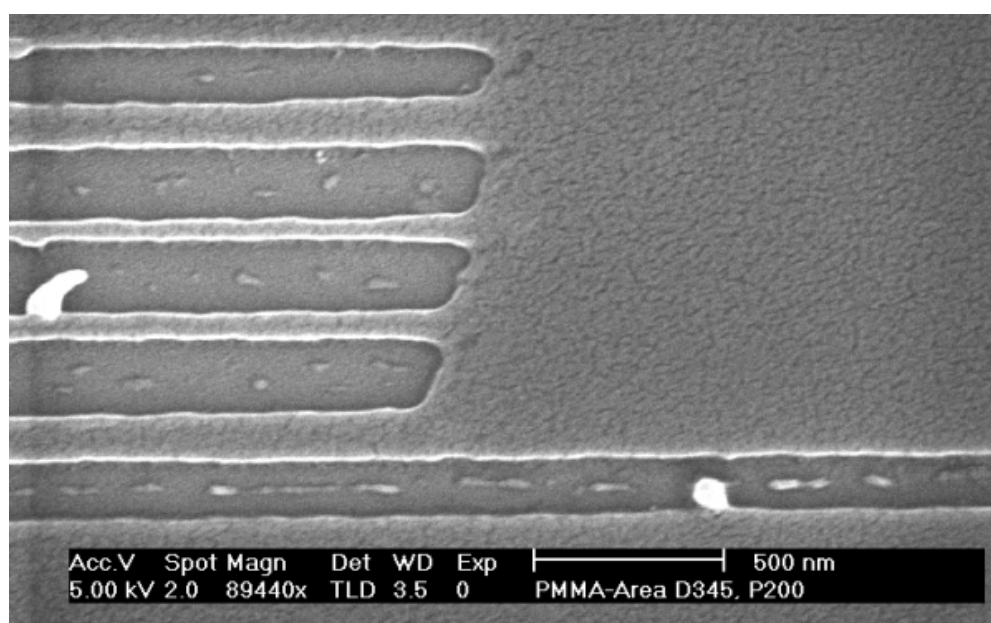


Figure 4.23: PMMA (950 A2) at dose $345 \mu\text{C}/\text{cm}^2$ and pitch 200 on glass

A beam acceleration of 30 keV was set, with 0.038 nA beam current (spot size 2). The applied area dose range was $10 - 325 \mu\text{C}/\text{cm}^2$ and line dose range was $0.1 - 3.25 \text{ nC}/\text{cm}$. After exposure the sample was developed in MIBK:IPA (1:3) for 2 seconds.

For imaging with the SEM, around ~3 nm gold was sputtered on top of the developed pattern. The PMMA sample's patterns showed strong and distortion, see figure 4.23.

4.6 Lithography at Chalmers

For further investigation, pure C5C5 and CAR (C5EPX:C5OH: TAS SbF₆ = 1:0.67:1), both are in 10 g/L in chloroform were tested in the MC2 lab at Chalmers University of Technology, Sweden.

Five different types of substrates - silicon, quartz (QZ), borosilicate glass (BS), fused silica (FS), and atomically flat glass (AFG); were selected for high resolution and sensitivity tests.

All substrates were treated with acetone and IPA, and then oxygen plasma at 25W 250mTorr was used for 30 seconds to clean any residue. Both resists were spin coated at 1000rpm for 60 seconds, and then C5C5 was baked at 70 °C for 5 minutes, and CAR was baked at 50 °C for 2 minutes. Both resists were exposed at 100 keV and 50 keV, and then developed in n-Amylacetate for 15 seconds instead of MCB, because chlorinated solvents are not allowed for general use in the MC2 lab for health and safety reasons.

Several exposure conditions were used initially, in order to find the most suitable setup, both at 100keV and 50keV acceleration voltages. For 100 keV exposures - 1, 2 and 10nA beam currents were used, with approximate beam diameters of 5, 7 and 25 nm, respectively. For 50 keV exposures – 1 and 10nA beam currents were used, with approximate beam diameters of 100 and 500 nm, respectively.

For sensitivity tests, a series of 250µm × 250µm squared patterns was selected. The dose was increased for each square from the base dose [$\mu\text{C}/\text{cm}^2$] in a logarithmic manner, so that the subsequent square was exposed with 10% more dose than the previous. As a total, twelve different doses were exposed in the series:

No.	1	2	3	4	5	6	7	8	9	10	11	12
Dose Factors	1.00	1.10	1.21	1.33	1.46	1.61	1.77	1.95	2.14	2.36	2.59	2.85

These square patterns were large enough to avoid edge and corner proximity effects. Film coating was not entirely successful under MC2 lab condition with variable film thickness up to ~100 nm.

For high resolution tests, equal width line and space grid patterns were used, e.g. 1 μm line/space means - 1 μm lines with a gap of 1 μm in between. The following patterns were exposed, one per exposure dose in the series: 2 μm , 1 μm , 500 nm and 250 nm line/space. As a rule, the line/space patterns were exposed with a dose two times the nominal solid area dose.

Initially, the ebeam exposures were performed at 100keV (10nA) using a JEOL JBX-9300FS. This worked well for silicon, but when the first insulating sample (quartz) severe charging was observed, even when the current was reduced to 2nA.

Therefore, it was chose to perform the exposures at 50 keV with 1 nA using a JEOL JBX-5D2 ebeam system. Some discharge was still observed. However, exposing 2 μm line/space patterns took about 4 hours for pure C5C5 samples, and it was decided not to reduce the current further due to the excessive exposure time.

4.6.1 Sensitivity of pure C5C5

For this test around ~160 nm C5C5 film was spin coated on a Si wafer. It was exposed at 50 keV with 10 nA current. The base dose was 5 mC/cm^2 . The sensitivity was found to be ~5.9 mC/cm^2 , and contrast 6.73 (see figure 4.24). However, no pattern was achieved at 100 keV with 10 nA exposure.

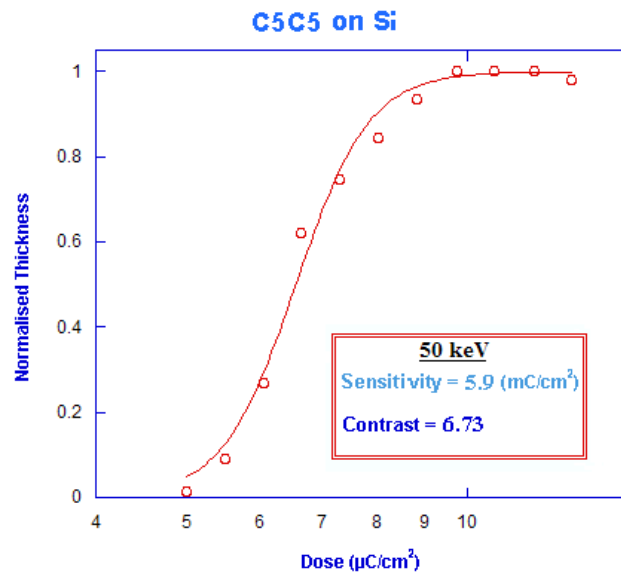


Figure 4.24: Pure C5C5 on Si, at 50 keV with 10 nA

4.6.2 Sensitivity of CAR

Two CAR films were spin coated one at ~ 130 nm thickness and the other at ~ 90 nm, on a Si wafer. They were exposed at 100 keV with 10 nA current. The base dose applied was $16 \mu\text{C}/\text{cm}^2$.

The sensitivity of the thick film was $21 \mu\text{C}/\text{cm}^2$, and contrast 3.89 (figure 4.25), and for the thin film the sensitivity was $43 \mu\text{C}/\text{cm}^2$, and contrast 2.47 (figure 4.26).

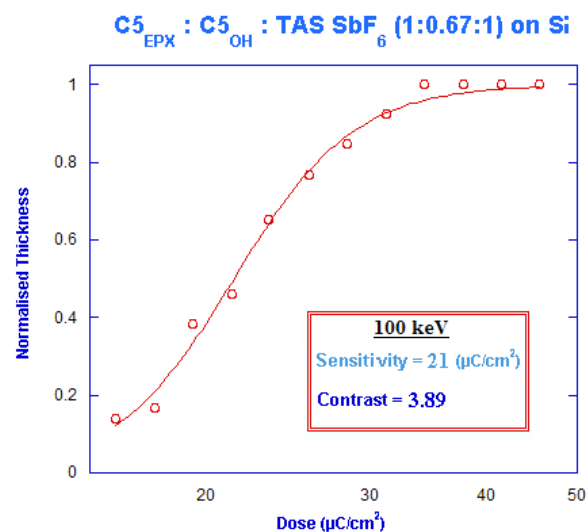


Figure 4.25: CAR on Si, at 100 keV with 10 nA on ~ 130 nm film

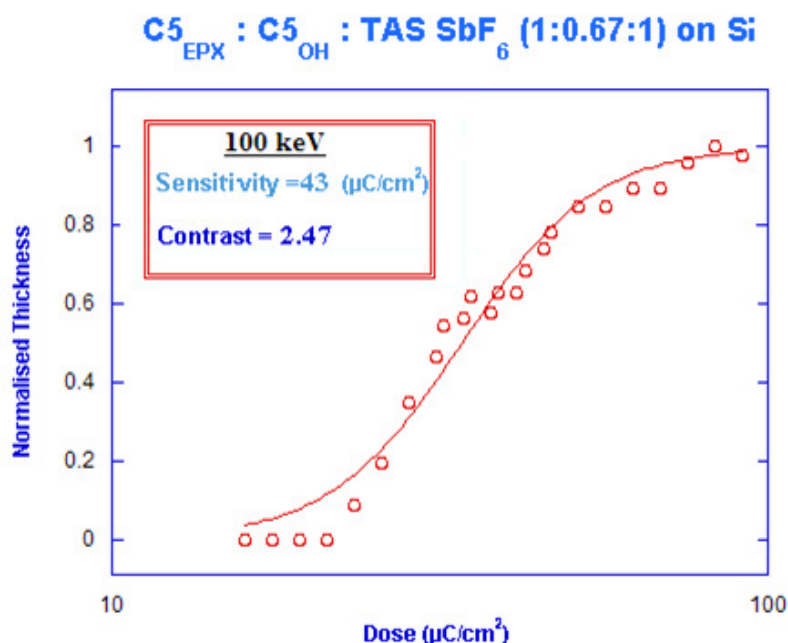


Figure 4.26: CAR on Si, at 100 keV with 10 nA on ~90 nm film

Next two thinner CAR films were spin coated; both were around ~70 nm on a Si wafer. They were exposed at 100 keV with 2 nA and 50 keV with 1 nA current. The base dose was applied $16 \mu\text{C}/\text{cm}^2$.

For the 100 keV with 2 nA sample, the sensitivity was found to be $45 \mu\text{C}/\text{cm}^2$, and contrast 2.17, and for the 50 keV with 1 nA sample, the sensitivity was $25 \mu\text{C}/\text{cm}^2$, and contrast 4.58 (figure 4.27).

The relative difference in sensitivity between 50 keV and 100 keV was as expected, around 1.8 times. The difference in beam diameter in the 100 keV and 50 keV exposures can be seen in the difference in edge sharpness in the two exposures. The resist non-uniformity is clearly the same in both exposures.

Finally a series of tests was performed on 5 CAR films on Si, QZ, BS, FS and AFG substrates. They were exposed at 50 keV with 1 nA current. The base dose applied was $8 \mu\text{C}/\text{cm}^2$. Results are shown in figure 4.28 and table 4.1.

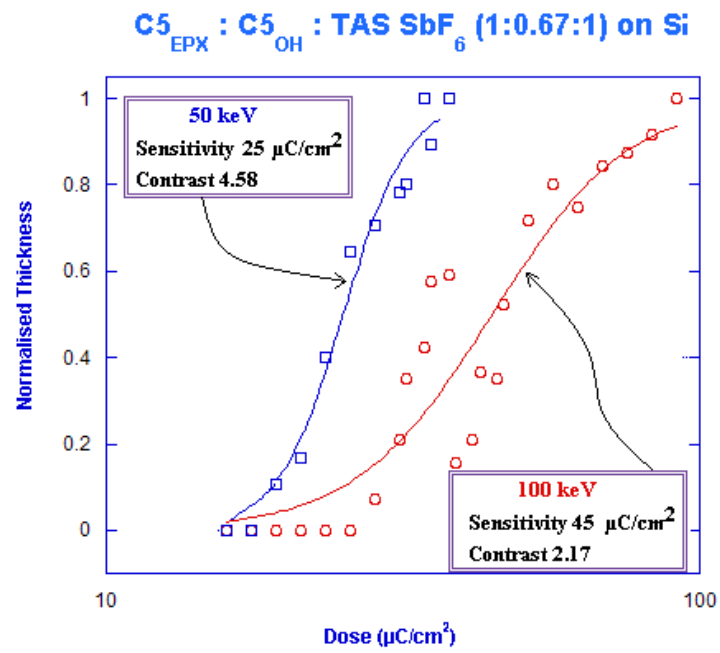


Figure 4.27: CAR on Si, at 100 keV with 2 nA and at 50 keV with 1 nA on ~70 nm films

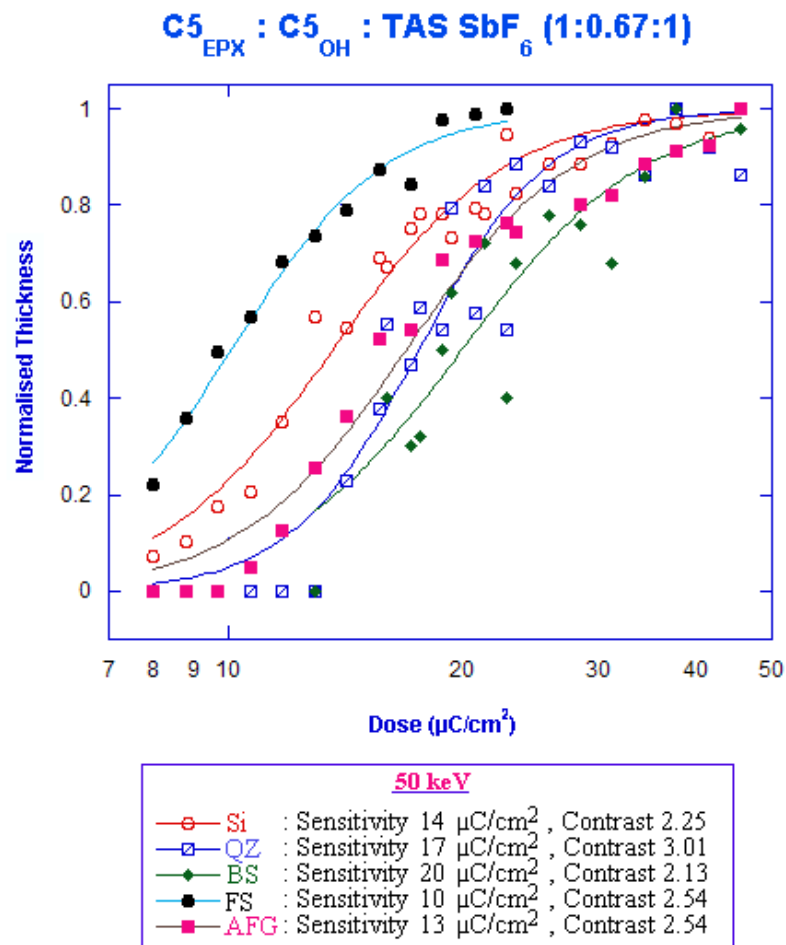


Figure 4.28: CAR on Si, QZ, BS, FS and AFG at 50 keV with 1 nA on ~100 nm film

Table 4.1: Sensitivity and Contrast at 50 keV for Si, QZ, BS, FS and AFG

Substrate	Sensitivity ($\mu\text{C}/\text{cm}^2$)	Contrast
Silicon (Si)	14	2.25
Quartz (QZ)	17	3.01
Borosilicate (BS)	20	2.13
Fused Silica (FS)	10	2.54
Atomically Flat Glass (AFG)	13	2.54

4.6.3 High resolution Patterning of CAR at 100 keV

At 100 keV with 10 nA exposures, dose range of 20 – 171 $\mu\text{C}/\text{cm}^2$ was applied for CAR on Si. At higher doses the patterns were over exposed. It was observed that at lower dose e.g. at 120 $\mu\text{C}/\text{cm}^2$ the 250 nm and 500 nm line/space patterns' were resolved, albeit with film quality varies, see figures 4.29 and 4.30.

Under the same exposure conditions at the lower dose range of 16 – 45.7 $\mu\text{C}/\text{cm}^2$ the non-uniform films become very obvious. The lines are perforated and broken by voids of size in the order of about 100nm, which makes it difficult to estimate the resolution, see figures 4.31 and 4.32.

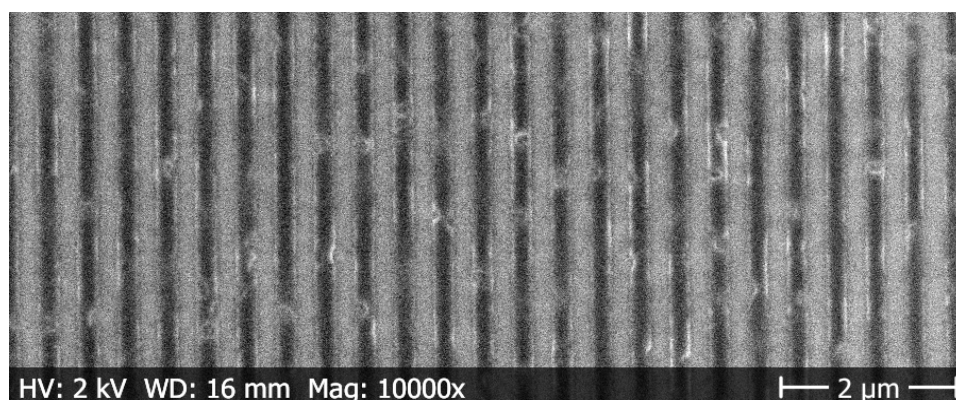


Figure 4.29: 250nm line/space patterns, at 120 $\mu\text{C}/\text{cm}^2$

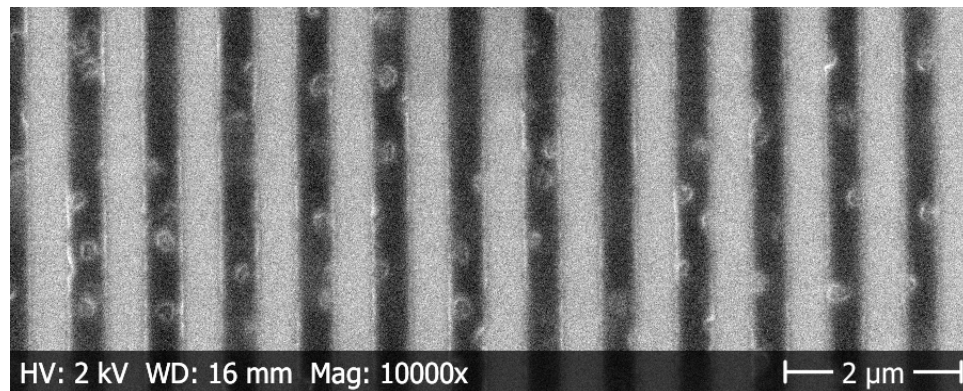


Figure 4.30: 500nm line/space patterns, at 120 $\mu\text{C}/\text{cm}^2$

It was observed that at 50 keV 1 nA exposures the resist also suffers from non-uniform composition, see figure 4.33. It is luckily that the change in sample preparation and developer required at the MC2 laboratory contributed to this.

Due to severe charging issue, none of the QZ, BS, FS and AFG samples were resolved to evaluate, see figures 4.34 and 4.35.

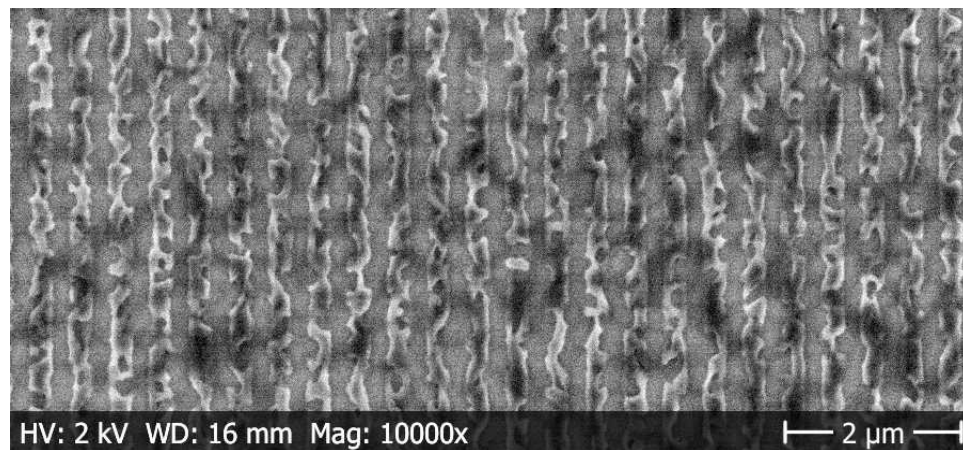


Figure 4.31: 250nm line/space patterns, 100 keV with 10 nA, at 39 $\mu\text{C}/\text{cm}^2$

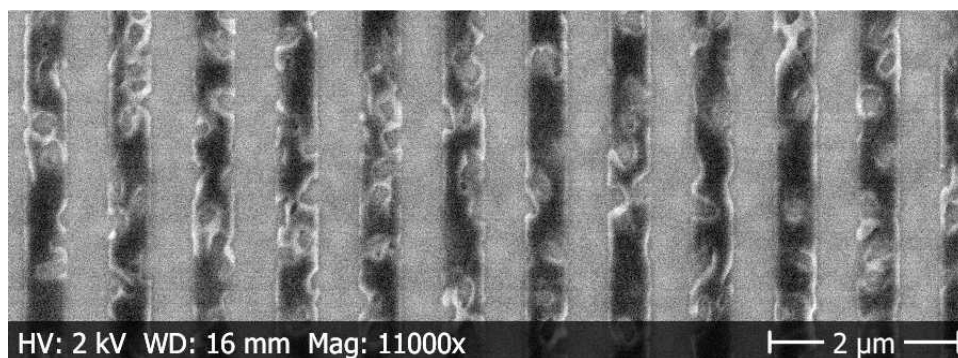


Figure 4.32: 500nm line/space patterns, 100 keV with 10 nA, at $39 \mu\text{C}/\text{cm}^2$

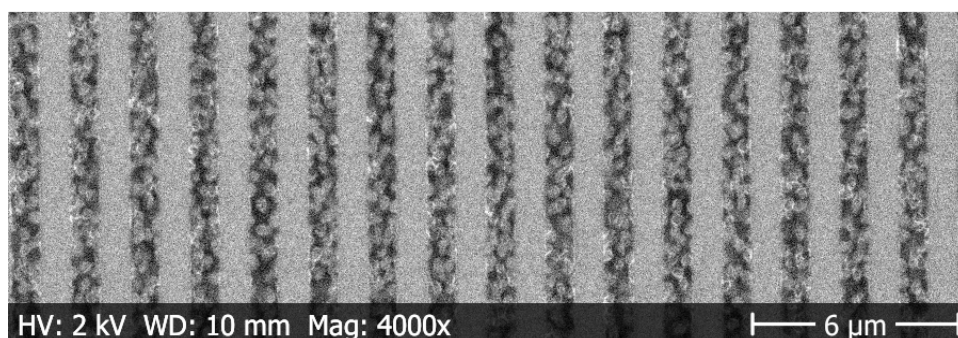


Figure 4.33: 2um line/space patterns, 50 keV with 1nA, at $52 \mu\text{C}/\text{cm}^2$



Figure 4.34: Discharge during exposure at 100 keV with 2nA.

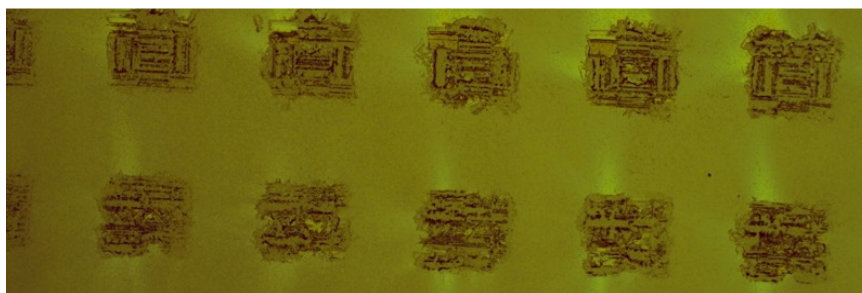


Figure 4.35: C5C5 on QZ after 50kV exposure and development. This behavior was typical for all insulating substrates.

4.7 Lithography in Leeds

An initial exposure test has been done on C5EPX on glass using 100 keV at the University of Leeds. For imaging purposes around ~1 nm gold was sputtered on top of the patterns after development. Figure 4.36 shows that, whilst there is some adhesions and pattern collapse presumably due to excessive film thickness, sub 30 nm lines were clearly achieved. More tests need to be done on 100 keV tool to optimize the patterning.

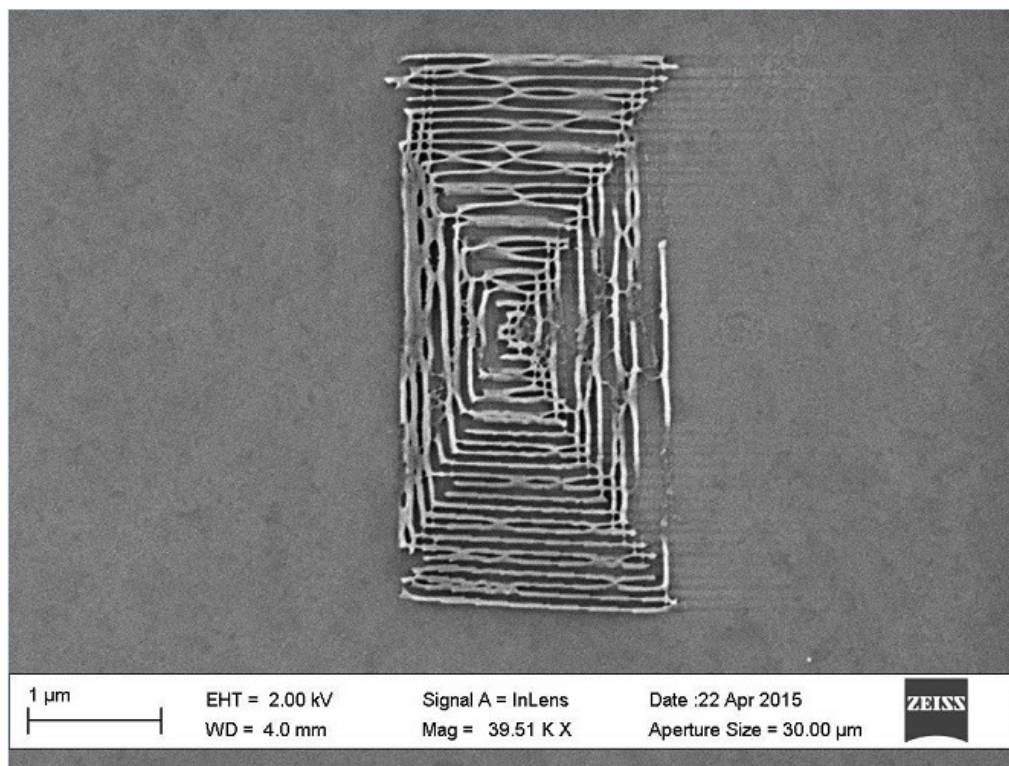


Figure 4.36: Pattern exposed at 100keV in Pure C5EPX film

4.8 Conclusion

Further work is clearly required to achieve optimal insulating substrate performance on all systems, although excellent results have been demonstrated at 30 keV and promising results on the University of Leeds 100 keV system.

Chapter 5

Conclusions and Future work

5.1 Conclusions

The project goal was to achieve high-resolution patterns on insulating substrates with the triphenylene derivative based ebeam resist. Various casting solvents were tested at and it was found that for both the pure C5C5, and the CAR, chloroform is the best solvent. However this solvent is not permitted for industrial use or in many research laboratories, because of its harmful effects on human organs. The second best casting solvent identified was PGMEA. This works to spin coat pure C5C5, but CAR films could not be cast from PGMEA. The pure C5C5 resist cast from PGMEA did not produced high-resolution patterning. Further work to investigate solvent systems, and if necessary modify the triphenylene resist for alternate solvents is clearly required.

Although chloroform is harmful, to evaluate resist performance further it was used here. The pure C5C5's sensitivity was found to be 4.3 mC/cm^2 at 20 keV, and 5.9 mC/cm^2 at 50 keV exposure on silicon substrates. The CAR sensitivity was $26 \text{ } \mu\text{C/cm}^2$ at 20 keV and $14 \text{ } \mu\text{C/cm}^2$ at 50 keV, and $21 \text{ } \mu\text{C/cm}^2$ with 100 keV exposure on silicon substrates.

The sensitivity of the CAR was evaluated on insulating materials – glass, quartz, fused silica, borosilicate and atomically flat glass. On glass the sensitivity of CAR at 30 keV was $45 \mu\text{C}/\text{cm}^2$. At 50 keV the sensitivity on quartz was $17 \mu\text{C}/\text{cm}^2$ on fused silica it was $10 \mu\text{C}/\text{cm}^2$, on borosilicate it was $20 \mu\text{C}/\text{cm}^2$, and on atomically flat glass it was $13 \mu\text{C}/\text{cm}^2$.

Various high-resolution tests have been done with both pure C5C5 and CAR samples. With pure C5C5, at 30 keV exposure, 20 nm half pitch lines in a 28 nm film at 62 nC/cm dose were achieved on silicon substrates. For CAR at 30 keV exposure, 80 nm half pitch lines in a 28 nm film at 0.34 nC/cm dose were achieved on silicon substrates. At 100 keV exposure 250nm line/space patterns at $120 \mu\text{C}/\text{cm}^2$ were achieved on a silicon substrate using the non-optimal MC2 sample preparation.

On glass, applying $50 \mu\text{C}/\text{cm}^2$ area dose, 55 nm features were achieved with pitch of 150 nm with CAR at 30 keV. A buckling effect was observed in the lines due to the penetration of the developer into the patterns, and subsequent swelling of the patterns. Further investigation to find a suitable developer is warranted, and thinner films may also improve performance.

These lithographic results lead to the conclusion that the CAR displays a very high sensitivity on both silicon and insulated substrates, and also showed high resolution patterns on both silicon and glass substrates. At 30 keV it works better than at 50 keV or 100 keV, although resist handling and sample preparation restrictions likely affected the results at 50 to 100 keV.

Further investigation is needed to optimized this system for more industrial compatibility in order to enable application to a wider range of tools, for instance to enable further 50 and 100 keV investigation.

Line edge roughness and etch resistance were not evaluated within this project and should be investigated in future.

It proved difficult to measure triphenylenes' conductivity for thin spin coated film. It has been observed that the conductivity of pure C5C5 decreases as the thickness increased. It has been speculated that the alignment of the molecular layers of triphenylene depends on thickness, and this is supported by initial polarizing microscopy. Further examination of this effect, for instance using small angle X-ray scattering (SAXS), is warranted.

The influence of temperature on conductivity was evaluated. It has been observed that when the temperature increases the conductivity also increases, which indicates that by increasing temperature the triphenylene molecules maybe oriented in such a way that hole-transfer mobility is increased for CAR. Alternatively ionic conduction (due to the PAG) may increase as the film softens at higher temperatures. Measuring single polarity conductivity over extended periods, to examine the films for ionic dopants depletion would be a useful extension.

Further investigation was done to understand if the I-V curve behaves the same for the individual resist components (C5OH and C5EPX) separately. By increasing and cooling the temperature, the conductivity was measured and I-V curve was recorded, and the behavior was the same for all cases, i.e. conductivity was low at low temperature and high at higher temperature.

A series of conductivity tests have been done at the University of Cambridge and Chalmers University of Technology, where both 2-probe and 4-probe VdP methods were applied. The conductivity of both pure C5C5 and CAR was found to be similar to that measured internally.

Overall, it proved exceptionally difficult to establish the conductivity of this thin film samples and many measurement techniques were investigated to gain consistent data. It appears clear that many aspects of the system can affect this. For

further study – molecular orientation of triphenylene, the effect of PAG in CA (ionic conduction), and environmental effects should all be examined.

5.2 Future Work

A new four point probe station has been designed, see figure 5.1. The whole probe station will be placed inside a Faraday box to minimize current leakage and EMF effects in the experiment. A new Keithley 4200 tool could be used to carry out measurements. New tokens (see figure 5.2) should be fabricated with various probe distances. By minimizing the measuring area, the effect of the high resistance will be reduced. Effects of various temperature and voltage conditions will be re-investigated.

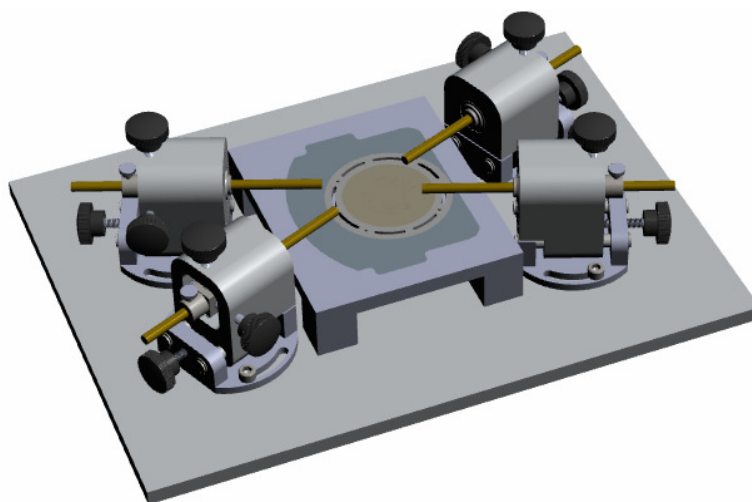


Figure 5.1: Four-probe station with heating stage and magnetic easy moveable probe holder

The token will be fabricated on insulating materials, such as – glass, quartz, fused silica, atomic smooth glass or borosilicate. All these substrates' conductivity should be tested prior the fabrication step. Figure 5.2 shows a schematic diagram of

the four-probe token fabrication recipe using glass. After substrate cleaning (with IPA/Acetone) around 100 nm of gold should be sputtered for the contact pads. About 2 μm PMMA will be spin coated. This thick layer of PMMA will prevent etching the gold layer where the unexposed pattern area is.

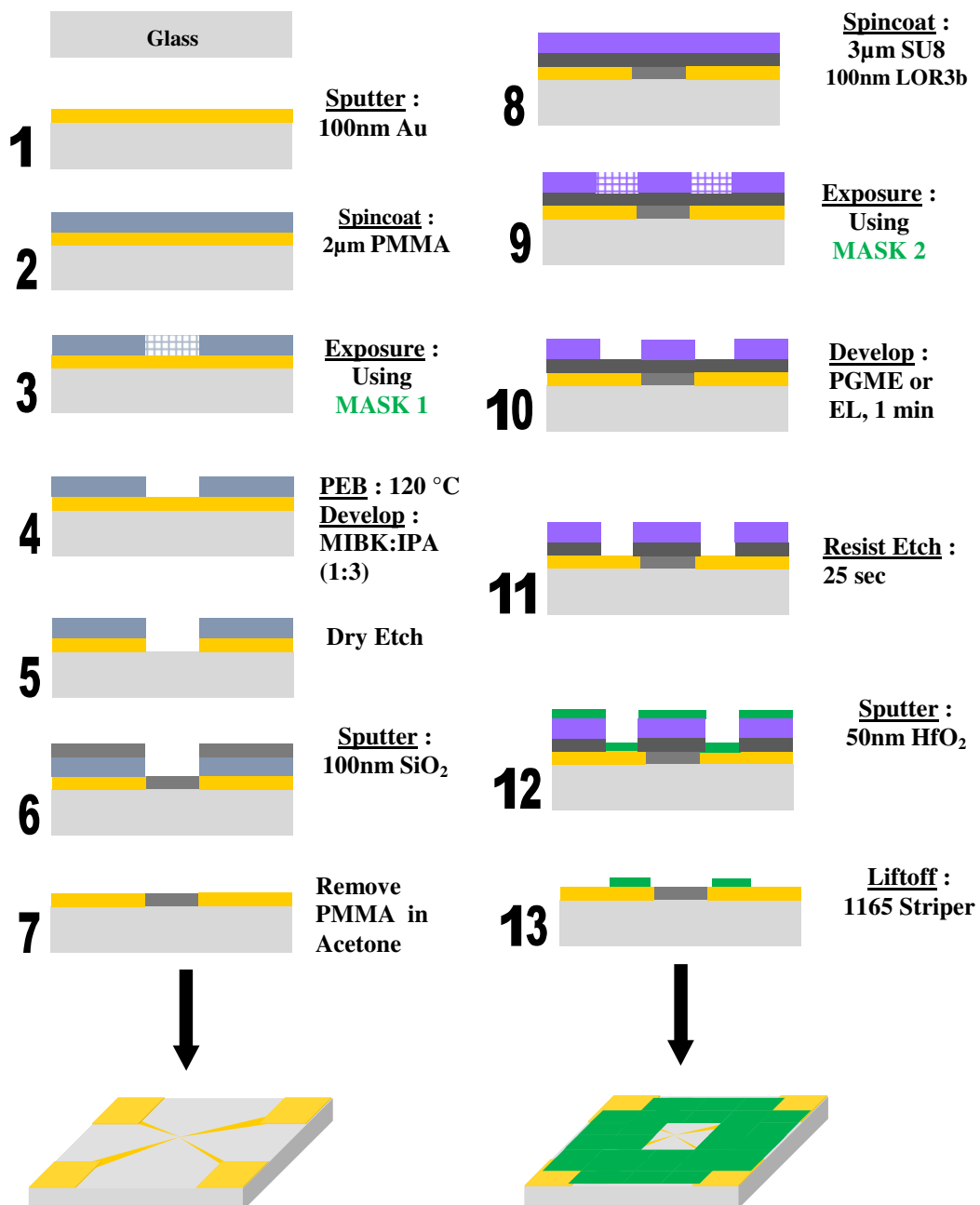


Figure 5.2: Schematic of four-probe token

A mask-aligner and a mask (see figure 5.3) should be used for exposing the pattern. After the exposure the sample will be baked at 120 °C for 5 minutes and then developed in MIBK:IPA (1:3) solution. After the development stage the exposed gold areas would be etched using a plasma etcher. A physical sputter etch using 30 sccm argon and 5 mTorr pressure for approximately 7 minutes will be required to etch the 100 nm gold layer. To make a very smooth surface 100 nm of SiO₂ will be deposited by sputtering process in-between the pad areas, which are etched after the etching step. After SiO₂ deposition, the PMMA layer will be removed using acetone. At this stage (figure 5.2 part 7) the sample will consist of gold pads and the electrodes on the glass substrate.

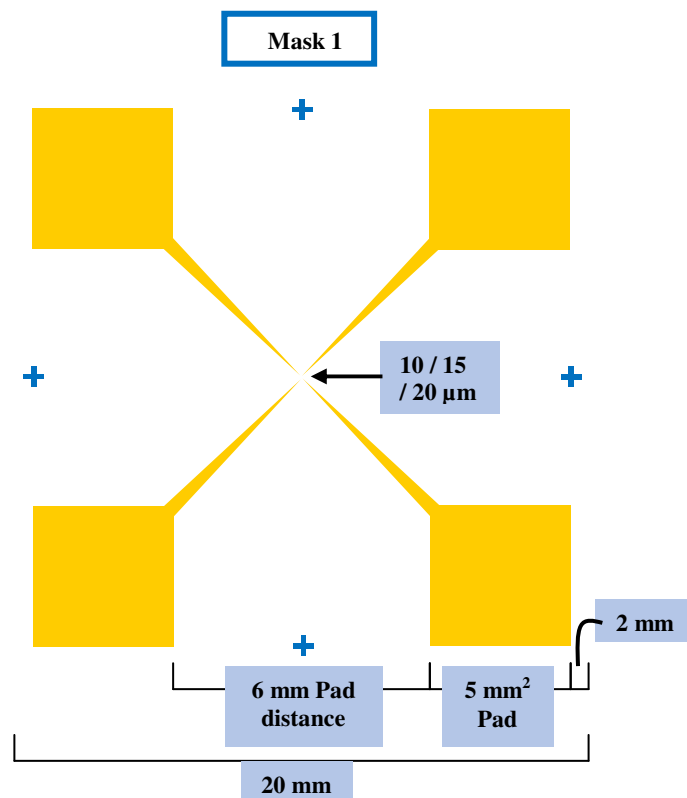


Figure 5.3: Mask 1, for creating gold pads

To create varied window sizes in center of the sample further lithography steps will be required. The gold pad sample will be cleaned using IPA/Acetone and about

100 nm of lift off resist LOR3b and 3 μm SU8 resist will be spin coated on top of each other. A second mask (see figure 5.4) and a mask aligner will be used for exposure. For developing exposed areas the sample will be developed by PGMEA or Ethyl Lactate for 1 minute. A very short (~ 25 sec) resist etch will be performed to etch the LOR3b resist. Around 50 nm of HfO_2 will be deposited by sputtering onto the sample. After this a lift-off step will be done using 1165 stripper for 10 minutes until the whole LOR3b resist layer is cleaned. This will open five windows, four on the gold pad areas (2.5 mm) and one in the center over the electrode tips (this window size will be varied).

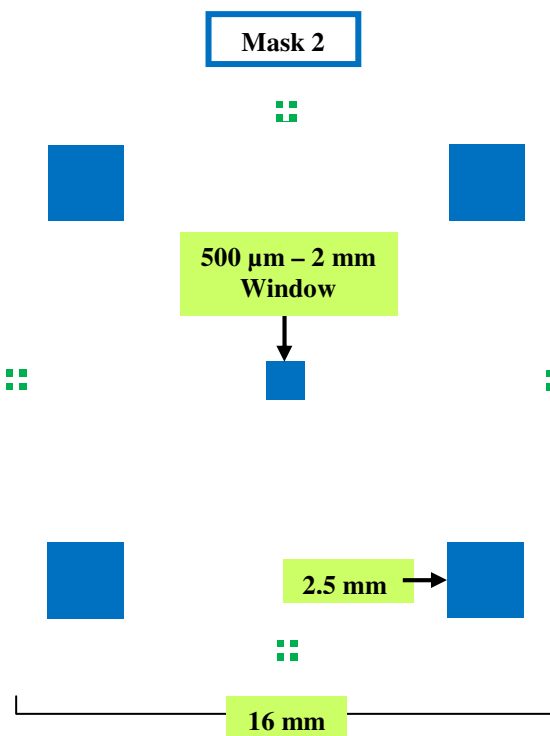


Figure 5.4: Mask 2, for creating opening windows

Various probe distances and window sizes in the center will allow us to control the amount and area of C5C5, CAR or any other resists to be measured. This will be more controllable than any of the ones using in the current work, as described in earlier chapters.

References

- [1] Meggs, Philip B. *A History of Graphic Design*. 1st Edition. New York: John Wiley & Sons, 1998. p. 146.
- [2] Carter R, Day B, Meggs PB. *Typographic design: form and communication*. 3rd ed. Hoboken, NJ: John Wiley & Sons, Inc.; 2002. p. 11.
- [3] Weaver, Peter. *The Technique of Lithography*. London: B.T. Batsford, 1964. p. 49.
- [4] Di Fabrizio E, Grella L, Baciocchi M, Gentili M, Ascoli C, Cappella B, Frediani C, Morales P. *Nanometer biodevice fabrication by electron beam lithography*. *Journal of Vacuum Science & Technology B: Microelectronics and Nanometer Structures Processing, Measurement, and Phenomena*. 1997;**15**(6):2892-6.
- [5] Peckerar M.C, Perkins FK, Dobisz EA, and Glembocki OJ. *Handbook of Microlithography, Micromachining and Microfabrication*. 1st edition. Edited by P. Rai-Choudhury; IEE, London, 1997, Vol. I, Chap. 8, p. 686.
- [6] Shoji H, Nakata Y, Mukai K, Sugiyama Y, Sugawara M, Yokoyama N, Ishikawa H. *Temperature dependent lasing characteristics of multi-stacked quantum dot lasers*. *Applied Physics Letters*. 1997;**71**(2):193-5.
- [7] Tang YS, Ni WX, Torres CS, Hansson GV. *Fabrication and characterization of Si-Si/sub 0.7/Ge/sub 0.3/quantum dot light emitting diodes*. *Electronics Letters*. 1995;**31**(16):1385-6.
- [8] Smith RA, Ahmed H. *A silicon Coulomb blockade device with voltage gain*. *Applied Physics Letters*. 1997;**71**(26):3838-40.

-
- [9] Ishikuro H, Hiramoto T. *Quantum mechanical effects in the silicon quantum dot in a single-electron transistor*. Applied Physics Letters. 1997;**71**(25):3691.
- [10] Mukherjee M, Roy SK. *Wide-Bandgap III–V nitride based avalanche transit-time diode in Terahertz regime: Studies on the effects of punch through on high frequency characteristics and series resistance of the device*. Current Applied Physics. 2010;**10**(2):646-51.
- [11] Shi J, Eastman LF, Xin X, Pophristic M..*High performance AlGaIn/GaN power switch with HfO₂ insulation*. Applied Physics Letters. 2009;**95**(4):042103.
- [12] Ümit Ö, Hofstetter D, Morkoc H..*ZnO devices and applications: a review of current status and future prospects*. Proceedings of the Institute of Electrical and Electronics Engineers (IEEE). 2010;**98**(7):1255-68.
- [13] Balmer RS, Brandon JR, Clewes SL, Dhillon HK, Dodson JM, Friel I, Inglis PN, Madgwick TD, Markham ML, Mollart TP, Perkins N. *Chemical vapour deposition synthetic diamond: materials, technology and applications*. Journal of Physics: Condensed Matter. 2009;**21**(36):364221.
- [14] Janner D, Tulli D, García-Granda M, Belmonte M, Pruneri V. *Micro-structured integrated electro-optic LiNbO₃ modulators*. Laser & Photonics Reviews. 2009;**3**(3):301-13.
- [15] Morkoç H, Strite S, Gao GB, Lin ME, Sverdlov B, Burns M..*Large-band-gap SiC, III-V nitride, and II-VI ZnSe-based semiconductor device technologies*. Journal of Applied Physics. 1994;**76**(3):1363-98.
- [16] Nakamura S, Mukai T, Senoh M. *Candela-class high-brightness InGaIn/AlGaIn double-heterostructure blue-light-emitting diodes*. Applied Physics Letters. 1994;**64**(13):1687-9.
-

-
- [17] Semiconductor Today. *Merchant substrate market for GaN to reach \$470m in 2013*. Available from: http://www.semiconductor-today.com/news_items/2009/MAY/STRATUNLIM_250509.htm
[Accessed 30th March, 2017].
- [18] Angelopoulos M, Shaw JM, Kaplan RD, Perreault S. *Conducting polyanilines: Discharge layers for electron-beam lithography*. Journal of Vacuum Science & Technology B: Microelectronics Processing and Phenomena. 1989;7(6):1519-23.
- [19] Moreau WM. *Semiconductor lithography: principles, practices, and materials*. New York: Plenum Press; 1988. p. 10.
- [20] Francis Gibbons. *Molecular Materials for Nanolithography*. University of Birmingham, UK. Doctoral Dissertation 2007.
- [21] Levinson HJ, Arnold WH. *Handbook of microlithography, micromachining, and microfabrication*. Volume 1, WA: Society of Photographic Instrumentation Engineers (SPIE) Press; 1997. p. 28.
- [22] Brainard RL, Barclay GG, Anderson EH, Ocola LE. *Resists for next generation lithography*. Microelectronic Engineering. 2002;61:707-15.
- [23] Levinson HJ, Arnold WH. *Handbook of microlithography, micromachining, and microfabrication*. Volume 1, WA: Society of Photographic Instrumentation Engineers (SPIE) Press; 1997. p. 57.
- [24] McCord MA, Rooks M.J. *Handbook of Microlithography, Micromachining and Microfabrication*. Volume 1. London: Institution of Electrical Engineers (IEE). 1997. p. 28.
- [25] Vieu C, Carcenac F, Pepin A, Chen Y, Mejias M, Lebib A, Manin-Ferlazzo L, Couraud L, Launois H. *Electron beam lithography: resolution limits and applications*. Applied Surface Science. 2000;164(1):111-7.
-

-
- [26] Wei Y, Back D. *193 nm immersion lithography: Status and challenges*. Society of Photographic Instrumentation Engineers (SPIE) Newsroom. doi. 2007;10(1117):2.
- [27] Sanders DP. *Advances in patterning materials for 193 nm immersion lithography*. Chemical Reviews. 2010;**110**(1):321-60.
- [28] Wei Y. *Extendibility of 193nm immersion lithography*. Society Of Photographic Instrumentation Engineers (SPIE) newsroom, doi. 2008;10(2.1200802):0974.
- [29] Dai H, Bencher C, Chen Y, Woo H, Ngai C, Xu X. *45nm and 32nm half-pitch patterning with 193nm dry lithography and double patterning*. Proc. Society of Photographic Instrumentation Engineers (SPIE) 2008; **6924**:21.
- [30] Bailey GE, Tritchkov A, Park JW, Hong L, Wiaux V, Hendrickx E, Verhaegen S, Xie P, Versluijs J. *Double pattern EDA solutions for 32nm HP and beyond*. Proc. Society of Photographic Instrumentation Engineers (SPIE) 2007; **6521**:1K.
- [31] Drapeau M, Wiaux V, Hendrickx E, Verhaegen S, Machida T. *Double patterning design split implementation and validation for the 32nm node*. Proc. Society of Photographic Instrumentation Engineers (SPIE) 2007; **6521**:09.
- [32] Bencher C, Chen Y, Dai H, Montgomery W, Huli L. *22nm half-pitch patterning by CVD spacer self alignment double patterning (SADP)*. Proc. Society of Photographic Instrumentation Engineers (SPIE) 2008; **6924**:4E.
- [33] Shiu W, Liu HJ, Wu JS, Tseng TL, Te Liao C, Liao CM, Liu J, Wang T. *Advanced self-aligned double patterning development for sub-30-nm DRAM manufacturing*. Proc. Society of Photographic Instrumentation Engineers (SPIE) 2009; **7274**:0E.
-

-
- [34] Carlson A, Liu TJ. *Negative and iterated spacer lithography processes for low variability and ultra-dense integration*. Proc. Society of Photographic Instrumentation Engineers (SPIE) 2008; **6924**:0B.
- [35] Wu B, Kumar A. *Extreme ultraviolet lithography: a review*. Journal of Vacuum Science & Technology B: Microelectronics and Nanometer Structures Processing, Measurement, and Phenomena. 2007;**25**(6):1743-61.
- [36] Wurm S. *Lithography perspective for the 22nm half-pitch*. Solid State Technology. 2010;**53**(2):16-9.
- [37] Wurm S. *Lithography Development and Research Challenges for the= 22 nm Half-pitch*. In Mask and Lithography Conference (EMLC), 2009 25th European 2009. p. 1-10.
- [38] Chou SY, Krauss PR, Renstrom PJ. *Nanoimprint lithography*. Journal of Vacuum Science & Technology B: Microelectronics and Nanometer Structures Processing, Measurement, and Phenomena. 1996;**14**(6):4129-33.
- [39] Chou SY, Krauss PR, Renstrom PJ. *Imprint of sub-25 nm vias and trenches in polymers*. Applied Physics Letters. 1995;**67**(21):3114-6.
- [40] Haisma J, Verheijen M, Van Den Heuvel K, Van Den Berg J. *Mold-assisted nanolithography: A process for reliable pattern replication*. Journal of Vacuum Science & Technology B: Microelectronics and Nanometer Structures Processing, Measurement, and Phenomena. 1996;**14**(6):4124-8.
- [41] Pan ZY, Chen CK, Gau TS, Lin BJ. *Influence of Shot Noise on CDU with DUV, EUV, and E-Beam*. Proc. Society of Photographic Instrumentation Engineers (SPIE) 2008; **6924**:1K.
- [42] Houli B, Umansky V, Heiblum M. *Low-energy electron beam lithography with 30 nm resolution*. Semiconductor Science and Technology. 1993;**8**(7):1490.
-

-
- [43] Gao B. *Patterning biomolecule at sub-30 nm resolution by electron beam lithography* University of Notre Dame, USA. Doctoral Dissertation. 2009
- [44] Hahmann P, Fortagne O. *50 years of electron beam lithography: Contributions from Jena (Germany)*. *Microelectronic Engineering*. 2009 Jun 30;**86**(4):438-41
- [45] Hu W, Sarveswaran K, Lieberman M, Bernstein GH. *Sub-10 nm electron beam lithography using cold development of poly (methylmethacrylate)*. *Journal of Vacuum Science & Technology B: Microelectronics and Nanometer Structures Processing, Measurement, and Phenomena*. 2004;**22**(4):1711-6.
- [46] Thompson LF, Wilson OG, Bowden MJ, Hennig H. *Introduction to microlithography—theory, materials, and processing*. Washington, DC: American Chemical Society, 1994.
- [47] Moreau WM. *Semiconductor lithography: principles, practices, and materials*. New York, NY: Springer Science & Business Media; 2012.
- [48] Ryan JM, Hoole AC, Broers AN. *A study of the effect of ultrasonic agitation during development of poly (methyl methacrylate) for ultrahigh resolution electron-beam lithography*. *Journal of Vacuum Science & Technology B: Microelectronics and Nanometer Structures Processing, Measurement, and Phenomena*. 1995;**13**(6):3035-9.
- [49] Langner GO. *The charging of dielectric layers by e-beam exposure*. *Proc. Microcircuit Engineering'79, RWTH (Aachen)*. 1979:261.
- [50] Cummings KD, Kiersh M. *Charging effects from electron beam lithography*. *Journal of Vacuum Science & Technology B: Microelectronics Processing and Phenomena*. 1989;**7**(6):1536-9.
-

-
- [51] Itoh H, Nakamura K, Hayakawa H. *Investigation of the charging effect on thin SiO₂ layers with the electron beam lithography system*. Journal of Vacuum Science & Technology B: Microelectronics Processing and Phenomena. 1989;7(6):1532-5.
- [52] Steenbrink SW, Kampherbeek BJ, Wieland MJ, Chen JH, Chang SM, Pas M, Kretz J, Hohle C, van Steenwinckel D, Manakli S, Le-Denmat J. *High throughput maskless lithography: low voltage versus high voltage*. Proc. Society of Photographic Instrumentation Engineers (SPIE) 2008; **6921**:1T.
- [53] Klein C, Platzgummer E, Loeschner H, Gross G, Dolezel P, Tmej M, Kolarik V, Klingler W, Letzkus F, Butschke J, Irmscher M. *Projection maskless lithography (PML2): proof-of-concept setup and first experimental results*. Proc. Society of Photographic Instrumentation Engineers (SPIE) 2008; **6921**:1O.
- [54] Loeschner H, Klein C, Platzgummer E. *Projection Charged particle Nanolithography and nanopatterning*. Japanese Journal of Applied Physics. 2010;49(6S):06GE01.
- [55] Klein C, Klikovits J, Szikszai L, Platzgummer E, Loeschner H. *Projection mask-less lithography (PML2)*. Microelectronic Engineering. 2010;87(5):1154-8.
- [56] Petric P, Bevis C, McCord M, Carroll A, Brodie A, Ummethala U, Grella L, Cheung A, Freed R. *New advances with REBL for maskless high-throughput EBDW lithography*. Proc. Society of Photographic Instrumentation Engineers (SPIE) 2011; **7970**:18.
- [57] McCord MA, Rooks M.J. *Handbook of Microlithography, Micromachining and Microfabrication*. Volume 1. London: Institution of Electrical Engineers (IEE), 1997. p. 144.
-

-
- [58] McCord MA, Rooks M.J. *Handbook of Microlithography, Micromachining and Microfabrication*. Volume 1. London: Institution of Electrical Engineers (IEE), 1997. p. 156.
- [59] Marrian CR, Tennant DM. *Nanofabrication*. Journal of Vacuum Science & Technology A: Vacuum, Surfaces, and Films. 2003;21(5):S207-15.
- [60] McCord MA, Rooks M.J. *Handbook of Microlithography, Micromachining and Microfabrication*. Volume 1. London: Institution of Electrical Engineers (IEE), 1997. p. 202.
- [61] McCord MA, Rooks M.J. *Handbook of Microlithography, Micromachining and Microfabrication*. Volume 1. London: Institution of Electrical Engineers (IEE), 1997. p. 203.
- [62] Constantoudis V, Patsis GP, Gogolides E. *Photoresist line-edge roughness analysis using scaling concepts*. Proc. Society of Photographic Instrumentation Engineers (SPIE) 2003; **5038**:901-909).
- [63] Scheckler EW, Ogawa T, Yamanashi H, Soga T, Ito M. *Resist pattern fluctuation limits in extreme-ultraviolet lithography*. Journal of Vacuum Science & Technology B: Microelectronics and Nanometer Structures Processing, Measurement, and Phenomena. 1994;**12**(4):2361-71.
- [64] Chandhok M, Datta S, Lionberger D, Vesecky S. *Impact of line-width roughness on Intel's 65-nm process devices*. Proc. Society of Photographic Instrumentation Engineers (SPIE) 2007; **6519**:1A.
- [65] Ban Y, Sundareswaran S, Pan DZ. *Electrical impact of line-edge roughness on sub-45-nm node standard cells*. Journal of Micro/Nanolithography, MEMS, and MOEMS. 2010;**9**(4):041206.

-
- [66] Yamaguchi T, Yamazaki K, Namatsu H. *Influence of molecular weight of resist polymers on surface roughness and line-edge roughness*. Journal of Vacuum Science & Technology B: Microelectronics and Nanometer Structures Processing, Measurement, and Phenomena. 2004;**22**(6):2604-10.
- [67] Leunissen LH, Ercken M, Patsis GP. *Determining the impact of statistical fluctuations on resist line edge roughness*. Microelectronic Engineering. 2005;**78**:2-10.
- [68] Patsis GP, Constantoudis V, Gogolides E. *Effects of photoresist polymer molecular weight on line-edge roughness and its metrology probed with Monte Carlo simulations*. Microelectronic Engineering. 2004;**75**(3):297-308.
- [69] Patsis GP, Gogolides E, Van Werden K. *Effects of photoresist polymer molecular weight and acid-diffusion on line-edge roughness*. Japanese Journal of Applied Physics. 2005;**44**(8R):6341.
- [70] Yoshimura T, Shiraishi H, Yamamoto J, Okazaki S. *Nano edge roughness in polymer resist patterns*. Applied Physics Letters. 1993;**63**(6):764-6.
- [71] Fedynyshyn TH, Pottebaum I, Astolfi DK, Cabral A, Roberts J, Meagley R. *Contribution of photoacid generator to material roughness*. Journal of Vacuum Science & Technology B: Microelectronics and Nanometer Structures Processing, Measurement, and Phenomena. 2006;**24**(6):3031-9.
- [72] Fedynyshyn TH, Astolfi DK, Goodman RB, Cann S, Roberts J. *Contributions of resist polymers to innate material roughness*. Journal of Vacuum Science & Technology B: Microelectronics and Nanometer Structures Processing, Measurement, and Phenomena. 2008;**26**(6):2281-9.

-
- [73] Hirayama T, Shiono D, Matsumaru S, Ogata T, Hada H, Onodera J, Arai T, Sakamizu T, Yamaguchi A, Shiraishi H, Fukuda H. *Depth profile and line-edge roughness of low-molecular-weight amorphous electron beam resists*. Japanese Journal of Applied Physics. 2005;**44**(7S):5484.
- [74] Kozawa T, Oizumi H, Itani T, Tagawa S. *Evaluation of chemical gradient enhancement methods for chemically amplified extreme ultraviolet resists*. Japanese Journal of Applied Physics. 2009;**48**(12R):126004.
- [75] Reynolds GW, Taylor JW. *Factors contributing to sidewall roughness in a positive-tone, chemically amplified resist exposed by x-ray lithography*. Journal of Vacuum Science & Technology B: Microelectronics and Nanometer Structures Processing, Measurement, and Phenomena. 1999;**17**(2):334-44.
- [76] Shin J, Han G, Ma Y, Moloni K, Cerrina F. *Resist line edge roughness and aerial image contrast*. Journal of Vacuum Science & Technology B: Microelectronics and Nanometer Structures Processing, Measurement, and Phenomena. 2001;**19**(6):2890-5.
- [77] Shin J, Ma Y, Cerrina F. *Depth dependence of resist line-edge roughness: Relation to photoacid diffusion length*. Journal of Vacuum Science & Technology B: Microelectronics and Nanometer Structures Processing, Measurement, and Phenomena. 2002;**20**(6):2927-31.
- [78] Yasin S, Khalid MN, Hasko DG, Ahmed H. *Influence of polymer phase separation on roughness of resist features in UVIII*. Microelectronic Engineering. 2004;**73**:259-64.

-
- [79] Yasin S, Hasko DG, Khalid MN, Weaver DJ, Ahmed H. *Influence of polymer phase separation on roughness of resist features*. Journal of Vacuum Science & Technology B: Microelectronics and Nanometer Structures Processing, Measurement, and Phenomena. 2004;**22**(2):574-8.
- [80] Flanagan LW, Singh VK, Willson CG. *Surface roughness development during photoresist dissolution*. Journal of Vacuum Science & Technology B: Microelectronics and Nanometer Structures Processing, Measurement, and Phenomena. 1999;**17**(4):1371-9.
- [81] Yoshizawa M, Moriya S. *Study of the acid-diffusion effect on line edge roughness using the edge roughness evaluation method*. Journal of Vacuum Science & Technology B: Microelectronics and Nanometer Structures Processing, Measurement, and Phenomena. 2002;**20**(4):1342-7.
- [82] Gokan H, Esho S, Ohnishi Y. *Dry etch resistance of organic materials*. *Journal of the electrochemical Society*. 1983;**130**(1):143-6.
- [83] Kunz RR, Palmateer SC, Forte AR, Allen RD, Wallraff GM, Di Pietro RA, Hofer DC. *Limits to etch resistance for 193-nm single-layer resists*. Proc. Society of Photographic Instrumentation Engineers (SPIE) 1996; **2724**:365-376.
- [84] Peckerar M.C, Perkins FK, Dobisz EA, and Glembocki OJ. *Handbook of Microlithography, Micromachining and Microfabrication*. 1st edition. Edited by P. Rai-Choudhury; IEE, London, 1997, p. 367.
- [85] Ito H. *Chemical amplification resists for microlithography*. Advances in Polymer Science, 2005;**172**:37-245.
- [86] Ito H. *Chemical amplification resists for microlithography*. Advances in Polymer Science, 2005;**172**:48.
-

-
- [87] Ito H. *Chemical amplification resists for microlithography*. Advances in Polymer Science, 2005;**172**:1012-1018.
- [88] Dektar JL, Hacker NP. Photochemistry of triarylsulfonium salts. Journal of the American Chemical Society. 1990;**112**(16):6004-15.
- [89] Crivello JV. *The discovery and development of onium salt cationic photoinitiators*. Journal of polymer science part A Polymer Chemistry. 1999;**37**(23):4241-54.
- [90] Ito H. *Chemical amplification resists: inception, implementation in device manufacture, and new developments*. Journal of Polymer Science Part A: Polymer Chemistry. 2003;**41**(24):3863-70.
- [91] Gallatin GM. *Resist blur and line edge roughness*. Proc. Society of Photographic Instrumentation Engineers (SPIE) 1996; **5754**:38-52.
- [92] Glezos N, Argitis P, Velessiotis D, Raptis I, Hatzakis M, Hudek P, Kostic I. *Aqueous base development and acid diffusion length optimization in negative epoxy resist for electron beam lithography*. Journal of Vacuum Science & Technology B: Microelectronics and Nanometer Structures Processing, Measurement, and Phenomena. 2000;**18**(6):3431-4.
- [93] Argitis P, Glezos N, Vasilopoulou M, Raptis I, Hatzakis M, Everett J, Meneghini G, Palumbo A, Ardito M, Hudek P, Kostic I. *Aqueous base developable epoxy resist for high sensitivity electron beam lithography*. Microelectronic Engineering. 2000;**53**(1-4):453-6.
- [94] Kadota T, Kageyama H, Wakaya F, Gamo K, Shirota Y. *Novel electron-beam molecular resists with high resolution and high sensitivity for nanometer lithography*. Chemistry Letters. 2004;**33**(6):706-7.
-

-
- [95] Kihara N, Saito S, Ushirogouchi T, Nakase M. EB Resist Materials Consist of Catechol Derivatives. *Journal of Photopolymer Science and Technology*. 1998;**11**(4):553-4.
- [96] Yoshiiwa M, Kageyama H, Shirota Y, Wakaya F, Gamo K, Takai M. *Novel class of low molecular-weight organic resists for nanometer lithography*. *Applied Physics Letters*. 1996;**69**(17):2605-7
- [97] Fujita JI, Ohnishi Y, Manako S, Ochiai Y, Nomura E, Sakamoto T, Matsui S. *Calixarene electron beam resist for nano-lithography*. *Japanese Journal of Applied Physics*. 1997;**36**(12S):7769.
- [98] Kretz J, Dreeskornfeld L, Ilicali G, Lutz T, Weber W. *Comparative study of calixarene and HSQ resist systems for the fabrication of sub-20nm MOSFET device demonstrators*. *Microelectronic Engineering*. 2005;**78**:479-83.
- [99] Tada T, Kanayama T. *Nanolithography using fullerene films as an electron beam resist*. *Japanese Journal of Applied Physics*. 1996;**35**(1A):L63.
- [100] Robinson AP, Palmer RE, Tada T, Kanayama T, Preece JA. *A Fullerene derivative as an electron beam resist for nanolithography*. *Applied Physics Letters*. 1998;**72**(11):1302-4.
- [101] Robinson AP, Palmer RE, Tada T, Kanayama T, Preece JA, Philp D, Jonas U, Deiderich F. *Electron beam induced fragmentation of fullerene derivatives*. *Chemical Physics Letters*. 1998;**289**(5):586-90.
- [102] Robinson AP, Palmer RE, Tada T, Kanayama T, Shelley EJ, Philp D, Preece JA. *Exposure mechanism of fullerene derivative electron beam resists*. *Chemical Physics Letters*. 1999;**312**(5):469-74.
- [103] Robinson AP, Zaid HM, Gibbons FP, Palmer RE, Manickam M, Preece JA, Brainard R, Zampini T, O'Connell K. *Chemically amplified molecular resists for electron beam lithography*. *Microelectronic Engineering*. 2006;**83**(4):1115.
-

-
- [104] Gibbons FP, Robinson AP, Palmer RE, Manickam M, Preece JA. *Ultrathin Fullerene Films as High-Resolution Molecular Resists for Low-Voltage Electron-Beam Lithography*. *Small*. 2006;**2**(8-9):1003-6.
- [105] Gibbons F, Zaid HM, Manickam M, Preece JA, Palmer RE, Robinson AP. *A Chemically Amplified Fullerene-Derivative Molecular Electron-Beam Resist*. *Small*. 2007;**3**(12):2076-80
- [106] Brainard RL, Barclay GG, Anderson EH, Ocola LE. *Resists for next generation lithography*. *Microelectronic Engineering*. 2002;**61**:707-15.
- [107] Robinson AP, Palmer RE, Tada T, Kanayama T, Allen MT, Preece JA, Harris KD. *10 nm scale electron beam lithography using a triphenylene derivative as a negative/positive tone resist*. *Journal of Physics D: Applied Physics*. 1999;**32**(16):L75.
- [108] Robinson AP, Palmer RE, Tada T, Kanayama T, Allen MT, Preece JA, Harris KD. *Polysubstituted derivatives of triphenylene as high resolution electron beam resists for nanolithography*. *Journal of Vacuum Science & Technology B: Microelectronics and Nanometer Structures Processing, Measurement, and Phenomena*. 2000;**18**(6):2730-6.
- [109] Tada T, Kanayama T, Robinson AP, Palmer RE, Allen MT, Preece JA, Harris KD. *A triphenylene derivative as a novel negative/positive tone resist of 10 nanometer resolution*. *Microelectronic Engineering*. 2000;**53**(1-4):425-8.
- [110] Cumming DR, Thoms S, Weaver JM, Beaumont SP. *3 nm NiCr wires made using electron beam lithography and PMMA resist*. *Microelectronic Engineering*. 1996;**30**(1-4):423-5.

-
- [111] Hu W, Sarveswaran K, Lieberman M, Bernstein GH. *Sub-10 nm electron beam lithography using cold development of poly (methyl methacrylate)*. Journal of Vacuum Science & Technology B: Microelectronics and Nanometer Structures Processing, Measurement, and Phenomena. 2004;**22**(4):1711-6.
- [112] Tseng AA, Chen K, Chen CD, Ma KJ. *Electron beam lithography in nanoscale fabrication: recent development*. Institute of Electrical and Electronics Engineers (IEEE) Transactions on Electronics Packaging Manufacturing. 2003;**26**(2):141-9.
- [113] Nishida T, Notomi M, Iga R, Tamamura T. *Quantum wire fabrication by e-beam lithography using high-resolution and high-sensitivity e-beam resist ZEP-520*. Japanese Journal of Applied Physics. 1992;**31**(12S):4508.
- [114] Medeiros DR, Aviram A, Guarnieri CR, Huang WS, Kwong R, Magg CK, Mahorowala AP, Moreau WM, Petrillo KE, Angelopoulos M. *Recent progress in electron-beam resists for advanced mask-making*. IBM Journal of Research and Development. 2001;**45**(5):639-50.
- [115] Society of Photographic Instrumentation Engineers (SPIE) *Handbook of microlithography, micromachining, and microfabrication*, Volume 1: Microlithography, Section 2.7.2.3.
Available from: www.cnf.cornell.edu/cnf_SPIE72.html
[Accessed 30th March, 2017]
- [116] Nakamura K, Shy SL, Tuo CC, Huang CC. *Critical dimension control of poly-butene-sulfone resist in electron beam lithography*. Japanese Journal of Applied Physics. 1994;**33**(12S):6989.

-
- [117] Tada T. *Highly Sensitive Positive Electron Resists Consisting of Halogenated Alkyl α -Chloroacrylate Series Polymer Materials*. Journal of the Electrochemical Society. 1983;**130**(4):912-7.
- [118] Society of Photographic Instrumentation Engineers (SPIE) *Handbook of microlithography, micromachining, and microfabrication*, Volume 1: Microlithography, Section 2.7.2.2.
Available from: http://www.cnf.cornell.edu/cnf_SPIE72.html
[Accessed 30th March, 2017]
- [119] Society of Photographic Instrumentation Engineers (SPIE) *Handbook of microlithography, micromachining, and microfabrication*, Volume 1: Microlithography, Section 2.7.3.2.
Available from: http://www.cnf.cornell.edu/cnf_SPIE73.html
[Accessed 30th March, 2017]
- [120] Zhou W, Wang ZL, editors. *Scanning microscopy for nanotechnology: techniques and applications*. New York, NY: Springer science & business media; 2007. p. 130 – 131.
- [121] Dobisz EA, Fedynyshyn TN, Ma D, Shirey LM, Bass R. *Electron-beam nanolithography, acid diffusion, and chemical kinetics in SAL-601*. Journal of Vacuum Science & Technology B: Microelectronics and Nanometer Structures Processing, Measurement, and Phenomena. 1998;**16**(6):3773-8.
- [122] Ocola LE, Tennant D, Timp G, Novembre A. *Lithography for sub-60 nm resist nanostructures*. Journal of Vacuum Science & Technology B: Microelectronics and Nanometer Structures Processing, Measurement, and Phenomena. 1999;**17**(6):3164-7.
-

-
- [123] Saint-Pol J, Landis S, Gourgon C, Tedesco S, Hanawa R, Suetsugu M, Akita M, Yamamoto S. *Negative tone chemically amplified resist formulation optimizations for ultra-high-resolution lithography*. *Microelectronic Engineering*. 2003;**67**:274-82.
- [124] Namatsu H, Yamaguchi T, Nagase M, Yamazaki K, Kurihara K. *Nano-patterning of a hydrogen silsesquioxane resist with reduced linewidth fluctuations*. *Microelectronic Engineering*. 1998;**41**:331-4.
- [125] van Delft FC, Weterings JP, van Langen-Suurling AK, Romijn H. *Hydrogen silsesquioxane/novolac bilayer resist for high aspect ratio nanoscale electron-beam lithography*. *Journal of Vacuum Science & Technology B: Microelectronics and Nanometer Structures Processing, Measurement, and Phenomena*. 2000;**18**(6):3419-23.
- [126] Matsui S, Igaku Y, Ishigaki H, Fujita J, Ishida M, Ochiai Y, Namatsu H, Komuro M. *Room-temperature nanoimprint and nano transfer printing using hydrogen silsequioxane*. *Journal of Vacuum Science & Technology B: Microelectronics and Nanometer Structures Processing, Measurement, and Phenomena*. 2003;**21**(2):688-92.
- [127] Junarsa I, Stoykovich MP, Nealey PF, Ma Y, Cerrina F, Solak HH. *Hydrogen silsesquioxane as a high resolution negative-tone resist for extreme ultraviolet lithography*. *Journal of Vacuum Science & Technology B: Microelectronics and Nanometer Structures Processing, Measurement, and Phenomena*. 2005;**23**(1):138-43.
- [128] Grigorescu AE, Van der Krogt MC, Hagen CW, Kruit P. *10nm lines and spaces written in HSQ, using electron beam lithography*. *Microelectronic Engineering*. 2007;**84**(5):822-4.
-

-
- [129] Henschel W, Georgiev YM, Kurz H. *Study of a high contrast process for hydrogen silsesquioxane as a negative tone electron beam resist*. Journal of Vacuum Science & Technology B: Microelectronics and Nanometer Structures Processing, Measurement, and Phenomena. 2003;**21**(5):2018-25.
- [130] Schmid GM, Carpenter LE, Liddle JA. *Nonaqueous development of silsesquioxane electron beam resist*. Journal of Vacuum Science & Technology B: Microelectronics and Nanometer Structures Processing, Measurement, and Phenomena. 2004;**22**(6):3497-502.
- [131] Hesketh PJ, editor. *Bionanofluidic Memes*. New York, NY: Springer Science & Business Media; 2007. p. 47.
- [132] van Delft FC. *Delay-time and aging effects on contrast and sensitivity of hydrogen silsesquioxane*. Journal of Vacuum Science & Technology B: Microelectronics and Nanometer Structures Processing, Measurement, and Phenomena. 2002;**20**(6):2932-6.
- [133] Society of Photographic Instrumentation Engineers (SPIE) *Handbook of microlithography, micromachining, and microfabrication*, Volume 1: Microlithography, Section 2.7.3.1.
Available from: http://www.cnf.cornell.edu/cnf_SPIE73.html
[Accessed 30th March, 2017]
- [134] Liu W, Ingino J, Pease RF. *Resist charging in electron beam lithography*. Journal of Vacuum Science & Technology B: Microelectronics and Nanometer Structures Processing, Measurement, and Phenomena. 1995;**13**(5):1979-83.

-
- [135] Lee Y, Lee W, Chun K. *Calculation of surface potential and beam deflection due to charging effects in electron beam lithography*. Journal of Vacuum Science & Technology B: Microelectronics and Nanometer Structures Processing, Measurement, and Phenomena. 2000;**18**(6):3095-8.
- [136] Leibold B, Butschke J, Bettin L, Beyer D, Irmischer M, Koepernik C, Plontke R, Vix A, Voehringer P. *Second-level imaging of advanced alternating phase-shift masks using e-beam lithography*. Proc. Society of Photographic Instrumentation Engineers (SPIE) 1996; **5256**: 1034-1044
- [137] Okai N, Yano T, Sohda Y. *Charge modeling for metal layer on insulating substrate*. Japanese Journal of Applied Physics. 2011;**50**(6S):06GC01.
- [138] Angelopoulos M, Patel N, Shaw JM, Labianca NC, Rishton SA. *Water soluble conducting polyanilines: applications in lithography*. Journal of Vacuum Science & Technology B: Microelectronics and Nanometer Structures Processing, Measurement, and Phenomena. 1993;**11**(6):2794-7.
- [139] Angelopoulos M, Shaw JM, Lecorre MA, Tissier M. *Conducting polyaniline: removable SEM discharge layer*. *Microelectronic Engineering*. 1991;**13**(1-4):515-8.
- [140] Angelopoulos M. *Conducting polymers in microelectronics*. IBM Journal of Research and Development. 2001;**45**(1):57-75.
- [141] Kakuchi M, Hikita M, Sugita A, Onose K, Tamamura T. *Electrically Conducting Two-Layer Resist System Using Amorphous Carbon Films*. Journal of The Electrochemical Society. 1986;**133**(8):1755-6.
- [142] Moreau WM. *Semiconductor lithography: principles, practices, and materials*. New York, NY: Springer Science & Business Media; 2012.P. 540-609.
-

-
- [143] Tan ZC, Sauer CA. *Application of charge-dissipation material in MEBES phase-shift mask fabrication*. Proc. Society of Photographic Instrumentation Engineers (SPIE) 1996; **2322**:141-148
- [144] Heeger AJ. *Semiconducting and metallic polymers: the fourth generation of polymeric materials (Nobel lecture)*. Angewandte Chemie International Edition. 2001;**40**(14):2591-611.
- [145] Pron A, Rannou P. *Processible conjugated polymers: from organic semiconductors to organic metals and superconductors*. Progress in Polymer Science. 2002;**27**(1):135-90.
- [146] Goldenberg LM, Lacaze PC. *Anodic synthesis of poly (p-phenylene)*. Synthetic metals. 1993;**58**(3):271-93.
- [147] Finch CA. *Encyclopedia of polymer science and engineering*. Volume 13, New York, NY:John Wiley & Sons, 1988. p. 42.
- [148] Chan HS, Ng SC. *Synthesis, characterization and applications of thiophene-based functional polymers*. Progress in Polymer Science. 1998;**23**(7):1167-231.
- [149] Gospodinova N, Terlemezyan L. *Conducting polymers prepared by oxidative polymerization: polyaniline*. Progress in Polymer Science. 1998;**23**(8):1443-84.
- [150] Abargues R, Nickel U, Rodriguez-Canto PJ. *Charge dissipation in e-beam lithography with Novolak-based conducting polymer films*. Nanotechnology. 2008;**19**(12):125302.
- [151] Todokoro Y, Kajiya A, Watanabe H. *Conductive two-layer resist system for electron-beam lithography*. Journal of Vacuum Science & Technology B: Microelectronics Processing and Phenomena. 1988;**6**(1):357-60.
-

-
- [152] Watanabe H, Todokoro Y. *E-beam direct wafer writing process using a water-soluble conductive layer*. Institute of Electrical and Electronics Engineers (IEEE) Transactions on Electron Devices. 1989;**36**(3):474-8.
- [153] Huang WS. *Synthesizing and processing conducting polythiophene derivatives for charge dissipation in electron-beam lithography*. Polymer. 1994;**35**(19):4057-64.
- [154] Hoang MH, Cho MJ, Kim KH, Lee TW, Jin JI, Choi DH. *Semiconducting 2, 3, 6, 7, 10, 11-Hexakis {[4-(5-dodecylthiophen-2-yl) phenyl] ethynyl} triphenylene and its discotic liquid crystalline properties*. Chemistry Letters. 2010;**39**(4):396-7.
- [155] Gupta SK. *Synthesis and characterization of some non-conventional discotic liquid crystals*. Doctoral Dissertation. Jawaharlal Nehru University, India;2012. p. 107.
- [156] Closs F, Siemensmeyer K, Frey T, Funhoff D. *Liquid crystalline photoconductors*. Liquid Crystals. 1993;**14**(3):629-34.
- [157] Allen MT, Diele S, Harris KD, Hegmann T, Kariuki BM, Lose D, Preece JA, Tschierske C. *Intermolecular organisation of triphenylene-based discotic mesogens by interdigitation of alkyl chains*X-Ray diffraction data, quantities of reagents used in the syntheses and spectroscopic data for C5Cn compounds are available as supplementary data. Journal of Materials Chemistry. 2001;**11**(2):302-11.
- [158] Inoue M, Monobe H, Ukon M, Petrov VF, Watanabe T, Kumano A, Schimizu Y. *Fast charged carrier mobility of a triphenylene-based polymer film possessing nematic order*. Optoelectronics Review. 2005;**13**(4):303.
-

-
- [159] Zaid HM, Manickam M, Preece JA, Palmer RE, Robinson AP. Anomalous acid diffusion in a triphenylene molecular resist with melamine crosslinker. *Microelectronic Engineering*. 2008;**85**(7):1540-4.
- [160] Kroto HW, Heath JR, O'Brien SC, Curl RF, and Smalley RE. *C60: buckminsterfullerene*. *Nature*. 1985;**318**(162):1236.
- [161] Schroder DK. *Semiconductor material and device characterization*. New York, NY:John Wiley & Sons, 2006. p. 2-34.
- [162] Sze SM. *Physics of Semiconductor Devices*. 2nd edition Wiley Inter-science. New York, NY:John Wiley & Sons, 1981. p. 30-35.
- [163] Runyan WR. *Semiconductor measurements and instrumentation*. New York, NY:McGraw Hill. 1975. p. 65-93.
- [164] *Low Level Measurements Handbook*. 7th Edition. Tektronix. Available from: www.tek.com/document/handbook/low-level-measurements-handbook
[Accessed 30th March, 2017]
- [165] Webster JG, Eren H, editors. *Measurement, instrumentation, and sensors handbook: electromagnetic, optical, radiation, chemical, and biomedical measurement*. New York CRC press; 1999. p. 43.
- [166] Van der Pauw method.
Available from: www.en.wikipedia.org/wiki/Van_der_Pauw_method
[Accessed 30th March, 2017]
- [167] *How Scanning Electron Microscopes Work*. Available from: <http://s.hswstatic.com/gif/scanning-electron-microscope-illustration.jpg>
[Accessed 30th March, 2017]
- [168] Chang TH. *Proximity effect in electron-beam lithography*. *Journal of vacuum science and technology*. 1975;**12**(6):1271-5.

-
- [169] Rubin SM. *Computer aids for VLSI design*. Reading, Massachusetts,, USA: Addison-Wesley; 1987 Jun.
Available from: www.rulabinsky.com/cavd/text/chapc.html
[Accessed 30thMarch, 2017]
- [170] *Sputter deposition of thin films*. Available from:
www.alacritas-consulting.com/sputter_deposition_for_thin_films.html
[Accessed 30thMarch, 2017]
- [171] Keithley 236-237-238 Source Measure Units Operator's Manual.
- [172] Keithley 236-237-238 Source Measure Unit Quick Reference Guide.
- [173] Bushby RJ, Donovan KJ, Kreouzis T, Lozman OR. *Molecular engineering of triphenylene-based discotic liquid crystal conductors*. Optoelectronics Review. 2005 Jan 1;**13**(4):269.
- [174] Tritto E, Chico R, Sanz-Enguita G, Folcia CL, Ortega J, Coco S, Espinet P. *Alignment of palladium complexes into columnar liquid crystals driven by peripheral triphenylene substituents*. Inorganic chemistry. 2014 Mar 17;**53**(7):3449-55.
- [175] *Keithley 4200*. Available from:
<http://nanoelec.usal.es/assets/img/facilities/9329Keihley-4200-parameter-analyzer1.jpg>
[Accessed 30thMarch, 2017]
- [176] Robinson AP, Palmer RE, Tada T, Kanayamat T, Allen MT, Preecel JA, Harris KD. *New High Resolution Liquid Crystal Electron Beam Resists*. In Materials Research Society Symposium (MRS) Proceedings 1999;**584**:129.
- [177] Material: Glass (SiO₂), bulk. Available from:
www.memsnets.org/material/glasssio2bulk
[Accessed 30thMarch, 2017]
-

- [178] Pradhan AA, Shah SI, Pakstis L. *Synthesis and Characterization of Metal Nanoparticles and the Formation of Metal-Polymer Nanocomposites*. In *Materials Research Society Symposium (MRS) Proceedings 2002*;740:6-10).